E.O. Paton Electric Welding Institute of the National Academy of Sciences of Ukraine

International Scientific-Technical and Production Journal

The Paton WELDING JOURNAL

February 2015
No.2

Published since 2000

English translation of the monthly «Avtomaticheskaya Svarka» (Automatic Welding) journal published in Russian since 1948

Founders
E.O. Paton Electric Welding Institute
of the NAS of Ukraine,
International Association «Welding»

Publisher
International Association «Welding»

Translators
A.A. Fomin, O.S. Kurochko,
I.N. Kutianova
Editor
N.A. Dmitrieva
Electron galley
D.I. Sereda, T.Yu. Snegiryova

Address
E.O. Paton Electric Welding Institute,
International Association «Welding»
11, Bozhenko Str., 03680, Kyiv, Ukraine
Tel.: (38044) 200 60 16, 200 82 77
Fax: (38044) 200 82 77, 200 81 45
E-mail: journal@paton.kiev.ua
www.patonpublishinghouse.com

State Registration Certificate
KV 4790 of 09.01.2001
ISSN 0957-798X

Subscriptions
$348, 12 issues per year,
air postage and packaging included.
Back issues available.

CONTENTS

CONCERNING REQUIREMENTS TO IMPACT TOUGHNESS OF JOINTS OF PIPELINES PRODUCED USING FLASH BUTT WELDING

V.I. KYRIAN, S.I. KUCHUK-YATSENKO and **B.I. KAZYMOV**
E.O. Paton Electric Welding Institute, NASU
11 Bozhenko Str., 03680, Kiev, Ukraine. E-mail: office@paton.kiev.ua

To provide serviceability of joints of pipelines produced using flash butt welding (FBW) alongside with the condition of strength the requirement to impact toughness *KCV* is set forth. Its level is established according to the requirements to the joints produced using arc welding methods, for which the probability of appearance of crack-like defects in them is peculiar. Absence of even preconditions to formation of cracks in the FB-welded joints allows initiating the review of requirements to impact toughness. As the standard level the *KCV* value is offered, which is reliably provided at optimum mode of FBW performance. The sufficiency of such *KCV* level is proved by reliable many-years practice in operation of different-purpose pipelines without fractures, including main pipelines of large diameter (up to 1420 mm). For the given *KCV* value at the working circumferential stresses in the pipeline and axial ones equal to half of their value, the critical sizes of hypothetic through longitudinal and circumferential cracks are calculated. Their sufficient sizes prove in appropriateness of such approach. 20 Ref., 3 Figures.

Keywords: *flash butt welding, typical defects of FBW, impact toughness, requirements, critical sizes of hypothetic cracks*

The main condition for serviceability of welded joints is the assurance of their strength, which is confirmed by the results of tensile tests of standard smooth (without stress concentrator) specimens, when fracture stress σ_f reaches ultimate strength σ_t:

$$\sigma_f = \sigma_t. \quad (1)$$

Except of condition (1) it is necessary also to guarantee the specified margin of toughness of metal to prevent fractures connected with possible formation of defects and fractures in welded joints. The required fracture toughness of metal depends on the type and size of a defect. The principal significance belongs to the sharpness of concentrator. If a defect is close to a crack-like one, then to eliminate cracking it is most perspective to use criteria of fracture mechanics, which reflect the ability of metal with a crack to plastic deformation without fracture initiating. Thus, the fracture mechanics allows reasonably evaluate the required level of fracture toughness, providing the serviceability of welded joints with crack-like defects of a certain size.

At the present time to establish the requirements to fracture toughness, the impact toughness *KCV* is used determined on the standard specimens with sharp notch, the radius of top of which is equal to 0.25 mm. This method found wide practical application due to the fact that quality relation between *KCV* value and character of fracture of ship-building steel (initiation of crack, its development and arresting) was established [1].

Later in the former USSR the requirements to pipe steels according to *KCV* values were introduced, which resulted in considerable reduction of fractures of pipelines manufactured of the best for that time low-alloyed steel 17G1S and its modifications [2]. Here, to provide the necessary level of impact toughness of metal of pipes of large diameter (> 620 mm) the transition to the new technology of manufacture of metal, i.e. controllable rolling, which obtained its large development abroad [3, 4], was required. And finally with the progress of fracture mechanics [5, 6] the impact toughness obtained some theoretical grounds for formation of requirements to the steel and welded joints according to *KCV* value with the purpose of elimination of fractures connected with crack-like defects.

From the given examples of use of impact toughness in practice it becomes obvious that the acceptable evaluation of toughness of metal fracture, suitable for prediction of serviceability of welded joints, can be obtained at the condition of proper grounds (theoretical, experimental or practical experience of service). However, today the impact toughness became so customary in practice that it started to be used without correcting of *KCV* values depending on the applied

technology of pipe welding and type of occurring defects. Moreover, the *KCV* values are used, established for electric arc methods of welding, for which the probability of formation of crack-like defects is high. It relates also for high-efficient automatic flash butt welding (FBW). At the same time, as was noted [7, 8], in the joints, made by FBW, there is no physical preconditions to formation of crack-like defects due to their formation without molten metal forced out from the fusion zone during upsetting. It is proved by non-destructive testing methods of welded joints (X-ray, ultrasonic) [9, 10] allowing detecting cracks with a high probability and also comprehensive investigations of quality of joints produced using FBW and reliable many-year practice of operation of great number of pipelines, including also those of a large diameter (1420 mm) [11].

It is a very important and principal moment, which allows putting a task for review of the requirements to impact toughness of joints produced by FBW. Moreover, today the requirements for arc-welded joints are used, for which cracks are the sufficiently obvious defect. These requirements without grounds are transferred to the joints produced by FBW.

The typical «defects» in the joining zone (JZ) in FBW at optimal modes, which were established experimentally according to the conditions of providing strength of joints and absence of inadmissible defects (decreasing strength by more than 5 %), are the zones of area of about 30 mm^2 with increased content of non-metallic inclusions similar by their composition to non-metallic inclusions of the similar zones in the metal of pipes being its heritage in fact (Figure 1) [12]. They are namely classified as the local structural heterogeneity (LSH).

The aim of this work is investigation of influence of LSH in welded joints of pipes on their mechanical properties and selection of grounded principle of formation of requirements to impact toughness of joints produced using FBW, which do not contain cracks.

Evaluation of mechanical properties of welded joints was carried out on a great number of full-scale pipes of 920–1420 mm diameter with wall thickness of 15.7–27 mm thickness of X60–X70 class of strength, produced at the optimal modes under the conditions of industrial production during construction of main pipelines and also at the testing area of the E.O. Paton Electric Welding Institute. For this purpose, the sections of plates of low-carbon low-alloyed pipe steels of modern production of up to 27 mm thickness

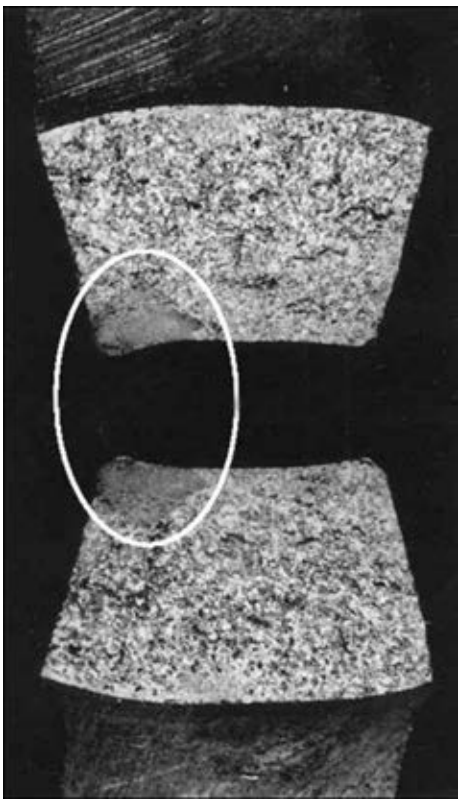

Figure 1. Fracture surface of specimen of joint, made by FBW, with LSH (*marked in oval*) tested for impact bending

of different classes of strength, including X80, were welded under the laboratory conditions.

The mechanical tests for rupture and impact bending, to which more than 60 butts of different pipes in the as-welded state were subjected, were carried out on standard specimens of welded joints in accordance with the requirements of API 1104 (USA) [13] and SP 105-34–96 (RF) [14].

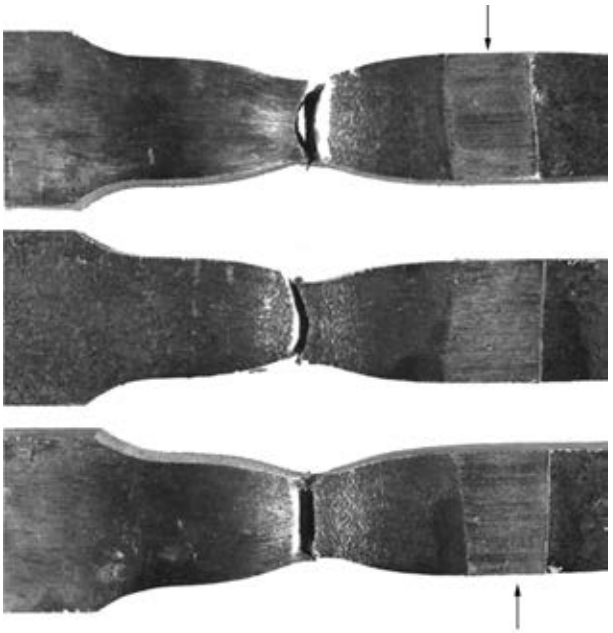

Figure 2. Standard specimens tested for tension. All fractures occurred across the base metal. JZ is shown by arrows

All the specimens, tested for rupture, were fractured across the base metal (Figure 2). The values of their strength, in spite of a high probability of presence of separate LSH areas in JZ, met the condition of strength (1). It was proved also by the results of tests of large-scale sectors of 300–500 mm elongation along the welded joint, cut out of pipes of large diameter with the specially produced areas, similar to LSH, in JZ of 10–70 mm^2 area [15]. The testing of large-scale sectors of pipes with such defects was carried out both at room temperature and also at –60 °C.

It was established that the test results on strength do not depend on structural heterogeneity of metal of pipes being welded, as a result of which LSH areas appear in the joints. For example, the joints of pipes with clearly expressed banding of metal, not less than 5 scale numbers (according to GOST 5640–68), i.e. the joints with the highest probability of formation of LSH areas in JZ showed the results meeting condition (1) as well as the joints of pipes, the metal of which had a lower banding (3–4 scale numbers).

The absence of influence of LSH on strength of joints, made by FBW, can be predetermined by the following. LSH does not create local critical stresses, which could lower the fracture stresses [16]. Besides, narrow JZ in FBW is ductile, it has the lowered strength as compared to the surrounding metal, however, it is located between the massive areas of heat-hardened metal. In loading due to contact hardening the mechanical properties of JZ are increased to the level of neighboring areas, which results in restricting the growth of deformations and manifesting of LSH. It should be also taken into account that probability of manifesting of LSH area in welded joint depends not only on properties of this single area, but also on neighboring ones [17]. It can be reflected by double integral from the function of stresses $\sigma(x, y)$ of two variables, spread to the area S of JZ with LSH:

$$\iint_S \sigma(x, y)ds, \tag{2}$$

where ds is the element of area; S is the area of integration. It represents the averaged total force F in JZ over the area of integration:

$$F = \sum_{n=1}^{N} \sigma(x_i, y_i)ds_i. \tag{3}$$

For convenience of practical application, formula (2) can be presented in Cartesian coordinates:

$$\iint_S \sigma(x, y)dxdy, \tag{4}$$

where $dxdy$ is the element of area.

Dependence (4) can be expressed in the form of repeated integrals:

$$\int_a^b dx \int_c^d \sigma(x, y)dy, \tag{5}$$

where a–b and c–d are the boundaries of integration, respectively along and across JZ.

The given data and the earlier performed investigations [8, 18] show that today requirements to impact toughness of joints, produced by FBW, are groundlessly overstated and need correcting. As far as in these welded joints the cracks are absent, then as the basis of the requirements to them the level of impact toughness should be taken, which is stably provided in FBW performed at optimum mode. The average KCV value of joints produced using FBW which are not subjected to heat treatment is equal to 20 J/cm^2 at testing temperature of 20 °C.

To prove the sufficiency of such KCV level, let us evaluate the critical sizes of hypothetical cracks (longitudinal and circumferential) in the pipeline of ∅1420 × 15.7 mm. For this purpose let us use the generalized correlation dependence between impact toughness KCV and critical values of stress intensity factor K_{1c} established in work [6]. This dependence based on the results of tests of great number of welded joints and steels of different classes with the yield strength of 200–1700 MPa and has the following form:

$$K_{1c} = \sqrt{\frac{\pi E\ KCV}{20 \cdot 10^2 (1 - \nu^2)}}, \tag{6}$$

where E is the elasticity modulus, MPa; ν is the Poisson coefficient; KCV is the impact toughness determined on the standard specimen with a sharp notch (Charpy), J/cm^2.

The results of K_{1c} calculations (formula(6)) according to KCV values for pipe steels and their welded joints are given in Figure 3.

The formula for determination of critical size of hypothetic through longitudinal crack of $2l$ length in the closed cylindrical shell depending on fracture toughness of metal K_{1c}, circumferential stress σ_θ determined by inner pressure P, pipe radius R and thickness of its wall l ($\sigma_\theta = PR/t$), can be written as follows [19]:

$$K_{1c} = \sigma_\theta \sqrt{\pi l} f_{\text{th.l}}(\xi). \tag{7}$$

The function $f_{\text{th.l}}(\xi)$ is plotted in the form of a series by degrees of parameter $\xi = l^2/Rt$ on

the basis of numerical solution of elastic problem for the pipe with the through longitudinal crack according to the general moment theory and is represented in the separate areas with the error of not more than 1 % in the wide range of change of parameter ξ(0–2812.5). At $0 < \xi \le 4.5$

$$f_{\text{th.l}}(\xi) = 1.005672 + 0.646787\,\xi - 0.12454\,\xi^2 + 0.12521\cdot10^{-1}\xi^3,$$

and at $4.5 \le \xi \le 55.125$

$$f_{\text{th.l}}(\xi) = 1.669865 + 0.208892\,\xi - 0.383589\cdot10^{-2}\xi^2 + 0.31666\cdot10^{-4}\xi^3.$$

According to formula (7) the critical size of hypothetic through longitudinal crack in the pipeline of 1420 mm diameter with the wall thickness of 15.7 mm at circumferential stress in the pipe wall determined by the inner pressure σ_θ = = 316 MPa which amounts to $0.7\sigma_y$ and fracture toughness K_{1c} = 84.6 MPa$\sqrt{\text{m}}$, established according to KCV = 20 J/cm^2 (formula (6)) (see Figure 3), is equal to 42.84 mm.

In the underground pipelines alongside with the main circumferential stress σ_θ the axial stresses σ_z also arise, which are not subjected to accurate calculation. They can be both tensile as well as compressive ones [2, 20]. In this case a great significance belongs to the temperature conditions of closing the main pipeline (welding of the last circumferential butt). Besides, the axial stresses σ_z are significantly influenced by the properties of soil, determining the level of jamming of pipeline, and also the presence of preweights, compensators and devices of water cooling. Therefore, for evaluation of critical size of hypothetic through circumferential crack in the circumferential butt, made by FBW, we supposed that $\sigma_z = 0.5\sigma_\theta$.

The limited state of pipeline with such a crack is expressed as follows [19]:

$$K_{1c} = \sigma_z\sqrt{\pi l}\,f_{\text{th.c}}(\xi). \qquad (8)$$

The function $f_{\text{th.c}}(\xi)$ was numerically determined similarly to $f_{\text{th.l}}(\xi)$ (7). Thus, at $0 < \xi \le 7.71$

$$f_{\text{th.c}}(\xi) = 1.00171 + 1.63983\cdot10^{-1}\xi - 1.92196\cdot10^{-2}\xi^2 + 1.27015\cdot10^{-3}\xi^3,$$

and at $7.71 \le \xi < 25$

$$f_{\text{th.c}}(\xi) = 1.38491 + 4.33069\cdot10^{-2}\xi - 2.32074\cdot10^{-4}\xi^2 + 1.47502\cdot10^{-6}\xi^3.$$

For the same parameters of pipeline (diameter, wall thickness, stress intensity factor), for which the critical size of longitudinal crack at axial stress σ_z = 158 MPa, the critical size of hypothetic through circumferential cracks in the circumferential butt, made by FBW, amounts to 155.1 mm.

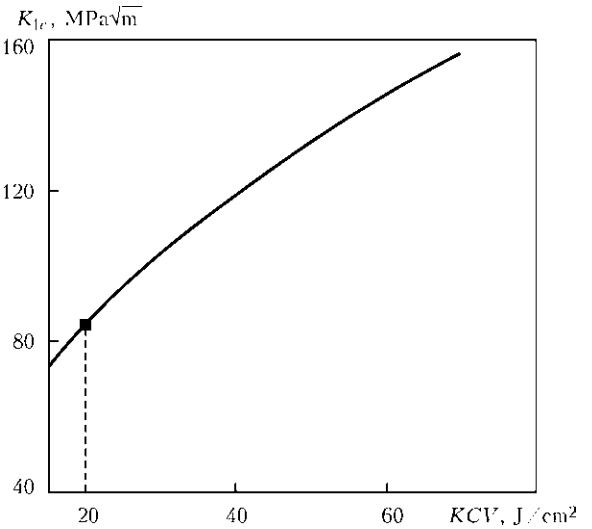

Figure 3. Dependence of critical value of stress intensity factor K_{1c} on impact toughness KCV at E = 210,000 MPa and ν = 0.28

Such established critical sizes of hypothetic through longitudinal and circumferential cracks explain a reliable (without fractures) service of main pipelines, manufactured using high-efficient FBW technology, observed during many years.

Conclusions

1. To prevent fractures connected with possible formation of technological defects in welded joints, the values of impact toughness (KCV), established on the standard specimens with a sharp notch, found the wide spreading.

2. The acceptable evaluation of impact toughness, suitable for prediction of the serviceability of welded joints, is given by KCV only at the condition of proper grounds (theoretic, experimental, practical experience of service).

3. To the joints, made by FBW, at the formation of which even physical preconditions to cracks formation (molten metal is forced out from the joint zone during upsetting) do not arise, today the requirement is also set forth to provide impact toughness at the level of welded joints produced using arc methods, for which the probability of cracks formation is peculiar.

4. For the joints, produced by FBW, as a standard KCV value it is most rationally to use the value, which is reliably provided at the optimal mode of welding. In the pipelines of large diameter it amounts to 20 J/cm^2 at 20 °C test temperature.

5. As the calculations showed, such level of impact toughness provides critical sizes of hy-

pothetic through longitudinal and circumferential cracks in the pipeline of 1420 mm diameter for detection of critical sizes at working circumferential stress $\sigma_\theta = 0.7\sigma_y$ and axial $\sigma_z = 0.5\sigma_\theta$. The length of longitudinal crack amounts to 42.84 and circumferential one is 155.1 mm.

6. The results of calculation allow meaningfully changing the attitude to the selection of *KCV* value for the joints, made by FBW, which will facilitate the wider application of the advanced high-efficient technology.

1. Nickols, R.U., Cowen, A. (1977) Selection of material and problems of design of large steel structures taking into account the strength of material to brittle fracture. In: *Fracture*. Vol. 5: Design of structures on brittle strength, 210–258. Moscow: Mashinostroenie.
2. Anuchkin, M.P., Goritsky, V.N., Miroshnichenko, B.I. (1986) *Pipes for main pipelines*. Moscow: Nedra.
3. Polyansky, R.P., Pasternak, V.I. (1979) *Pipes for oil and gas industry abroad*. Moscow: Nedra.
4. (1985) *Steels for gas pipeline pipes and fittings*: Proc. of Conf. Moscow: Metallurgiya.
5. *GOST 25.506–85*: Determination of characteristics of crack resistance (fracture toughness) under static loading. Introd. 01.01.86.
6. Girenko, V.S., Dyadin, V.P. (1985) Relation between impact toughness and fracture mechanics criteria δ_{1c} and K_{1c} of structural steels and their welded joints. *Avtomatich. Svarka*, **9**, 13–20.
7. Kuchuk-Yatsenko, S.I. (1992) *Flash butt welding*. Kiev: Naukova Dumka.
8. Kuchuk-Yatsenko, S.I., Kirian, V.I., Kazymov, B.I. et al. (2006) Methodology for control of fitness for purpose of flash butt welded joints in pipelines. *The Paton Welding J.*, **10**, 2–6.
9. Shcherbinsky, V.G., Alyokhin, N.P. (2000) *Ultrasonic testing of welded joints*. Moscow: N.E. Bauman MGTU.
10. *GOST 7512–82*: Non-destructive testing, welded joints, radiographic method. Introd. 01.01.98.
11. Kuchuk-Yatsenko, S.I., Kazymov, B.I., Radko, V.P. (1996) Complex testing of joints produced by automatic flash butt welding. *Tekhn. Diagnostika i Nerazrush. Kontrol*, **4**, 46–50.
12. Kuchuk-Yatsenko, S.I., Kazymov, B.I., Zagadarchuk, V.F. et al. (1984) Formation of «dead spots» in resistance butt welded joints. *Avtomatich. Svarka*, **11**, 23–26.
13. (1999) *API standard 1104*: Welding of pipelines and related facilities ASME boiler and pressure vessel. 19 ed.
14. *SP 105-34–96*: Fulfillment of welding jobs and testing of welded joints. Introd. 01.10.96.
15. Trufyakov, V.I., Mazur, V.G., Zhemchuzhnikov, G.V. et al. (1987) Influence of some defects on strength of butt joints produced by resistance welding. *Avtomatich. Svarka*, **2**, 7–9.
16. Finkel, V.M., Elesina, O.P., Fedorov, V.A. et al. (1971) Elastic stresses around nonmetallic inclusions. *Metallovedenie i Term. Obrab. Metallov*, **7**, 55–61.
17. Fridman, Ya.B. (1974) *Mechanical properties of metals*. Moscow: Mashinostroenie.
18. Kuchuk-Yatsenko, S.I., Kirian, V.I., Kazymov, B.I. et al. (2008) Peculiarities of impact toughness tests of automatic flash butt welded joints on pipes. *The Paton Welding J.*, **10**, 5–10.
19. Osadchuk, V.A. (1980) On criterion of propagation of longitudinal and transverse cracks in closed cylindrical shells. *Izvestiya AN SSSR. Mekhanika Tv. Tela*, **4**, 151–159.
20. Borodavkin, P.P., Sinyukov, A.M. (1984) *Strength of main pipelines*. Moscow: Nedra.

Received 13.11.2014

EFFECT OF WELDING THERMAL CYCLE ON STRUCTURE-PHASE TRANSFORMATIONS AND PROPERTIES OF HAZ METAL OF ALLOYED 30Kh2N2MF TYPE MEDIUM-CARBON STEEL

V.D. POZNYAKOV, V.A. KOSTIN, A.A. GAJVORONSKY, I.A. MOSSOKOVSKAYA, V.V. ZHUKOV and **A.V. KLAPATYUK**
E.O. Paton Electric Welding Institute, NASU
11 Bozhenko Str., 03680, Kiev, Ukraine. E-mail: office@paton.kiev.ua

Thermostrengthened alloyed medium-carbon and carbon steels of average, increased and high hardness are widely used in manufacture of welded metal structures for car bodies. HAZ metal should also have corresponding values of yield strength considering the requirements necessary for providing of welded joint full-strength. However, mechanical properties of HAZ metal obtained by means of formation of specific complex of microstructures, generated in process of its cooling (welding modes), in contrast to steel, which acquires necessary complex of mechanical properties as a result of initial heat treatment (quenching and tempering). Preferred formation of martensite structures in HAZ metal of welded joints from given steels and saturation of this area by diffusible hydrogen result in increase of their susceptibility to cold crack formation. In this connection, this work represents the results of investigations aimed at study of effect of welding thermal cycles on nature of structural transformations, hardness, static strength and cold crack resistance of HAZ metal of high-strength alloyed medium-carbon steel of the 30Kh2N2MF type with 0.31 and 0.36 % carbon content. Structure and kinetics of transformation of undercooled austenite was investigated using current methods of physical materials science by means of simulation of phase transformations on Gleeble 3800 machine. It is determined that austenite decomposition in the samples of 30Kh2N2MF steel HAZ, independent on carbon content in it, takes place mainly in area of martensite transformation at cooling rate $w_{6/5}$ = 2.5–30 °C/s. It is shown that hardness and static strength of HAZ metal in steel with 0.36 % C are provided for the whole studied range of cooling rates. Similar properties of HAZ metal in steel with 0.31 % C can be achieved under condition of cooling at 600–500 °C and rate not less than 10 °C/s. The results of investigations can be used for optimizing welding modes of special equipment and further improvement of modes of steel heat treatment. 15 Ref., 4 Tables, 7 Figures.

Keywords: *high-strength alloyed steels, heat-affected zone, welding thermal cycles, CCT diagram of austenite decomposition, metal structure, metal hardness*

At present time, thermostrengthened high-strength steels alloyed by chromium, nickel and molybdenum and containing 0.25–0.50 % carbon are widely used in manufacture of welded assemblies and bodies of special designation wheeled equipment. Sometimes vanadium, aluminum and boron are used for microalloying of such steels. Steels, depending on designation, can have average ($HB \geq 2850$ MPa), increased ($HB \geq 3350$ MPa) and high ($HB \geq 3630$ MPa) hardness. It is achieved after corresponding heat treatment consisting of quenching and tempering [1–4].

One of the main requirement made to such welded joints from given steels lies in the fact that hardness of HAZ metal should be not lower than that of base metal. It is obvious, considering the fact that structures from indicated steels are not quenched after welding and being subjected only to low-temperature tempering, that HAZ metal shall acquire necessary indices of hardness in as-welded condition.

It is known fact [5, 6] that mechanical properties of metal determine its structural composition. Besides, structure formation in HAZ metal of welded joints depends not only on steel chemical composition, but on welding thermal cycles as well. The metal can be soften under specific conditions if metal after heating is subjected to cooling with low rate. Its hardness and static strength rise, as a rule, with cooling rate increase.

Welded joints from high-strength alloyed medium-carbon steels are susceptible to cold crack formation. It is related with formation of hardening structures and residual tensile stresses in HAZ metal [7–10]. Presence of diffusible hydrogen in metal provokes for increase of possibility of cold crack formation and the process itself becomes more intensive [11, 12]. Heating of welded joints from medium-carbon high-strength steels is used

Table 1. Composition of samples of 30Kh2N2MF type steel, %

Sample type	C	Si	Mn	Cr	Ni	Mo	Cu	V	Al	Ti	S	P
X	0.31	1.16	0.74	1.66	2.26	0.30	0.080	0.20	0.040	0.024	0.010	0.016
H	0.36	1.32	0.81	1.65	2.34	0.50	0.062	0.20	0.037	0.025	0.010	0.019

for reduction of risk of cold crack formation. On the one hand, this allows regulating the kinetics of phase transformations and forming the structures with increased cold crack formation resistance, and, on the other hand, developing the conditions for active hydrogen desorption from the welded joint metal.

In this connection, aim of the present work lies in study of effect of welding thermal cycles on nature of structural transformations, hardness, static strength and cold crack formation resistance of HAZ metal of alloyed medium-carbon high-strength steel of 30Kh2N2MF type with 0.31 and 0.36 % carbon content.

Samples from medium-alloyed high-strength steel of 30Kh2N2MF type with total content of alloying elements approximately 4 % (Table 1) were taken as object for investigations.

Table 2 shows the mechanical properties of the samples in as heat-treated condition (quenching + low-temperature tempering).

Investigation procedures. Chemical analysis of the samples was carried out in accordance with GOST 18895–97 using optical emission spectrometer Spectrovak-1000 (Baird, USA).

Chemical etching in 4 % alcoholic nitric acid solution was used for determination of samples' microstructure. The samples for investigations were manufactured by standard procedures applying diamond pastes of different particle size.

Structural analysis was carried out with the help of light microscope «Neophot-32» at 200 and 500 magnification. Digital images were recorded using «Olympus» digital camera. Microhardness of structural constituents and HAZ metal integral hardness was measured on LECO hardness meter M-400 at 100 g ($HV0.1$) and 1 kg ($HV10$) loading, respectively, on GOST 2999–59.

Nature of structural transformations in HAZ metal of samples from 30Kh2N2MF steel were studied by simulation of thermal deformation welding cycle (TDWC) on Gleeble 3800 machine, equipped with fast-response dilatometer [13]. The investigations were carried out applying cylinder samples of 6 mm diameter and 80 mm length produced from rolled sheet of 12 and 20 mm thickness. In accordance with a procedure developed at the E.O. Paton Electric Welding Institute the samples were heated to 1250 °C in vacuum chamber and then cooled. At that, the parameters of welding thermal cycle (heat and time) were simulated with high accuracy in HAZ metal of joints in mechanized gas-shielded welding using 1.2 mm diameter solid wire and different modes of welding. Rate of sample heating from 20 to 1250 °C made 210 °C/s (heating time 6 s), and cooling rate in temperature range 600–500 °C was varied in $w_{6/5}$ 2.5–30 °C/s range.

Procedure, represented in work [14], was used for determination of temperatures of transformation beginning and ending in investigation of kinetics of austenite decay.

Mechanical properties of HAZ metal (yield strength, ultimate tensile strength, elongation and reduction in area) were determined on the results of static tension test at 20 °C of standard samples (type II on GOST 6996–66). The samples were produced from 12 × 12 × 150 mm steel preliminary subjected to treatment on welding thermal cycle. In process of heat treatment the workpieces were heated by passing current to 1250 °C (heating rate 150 °C/s) and then cooled in such a way as to provide 2.5–30 °C/s cooling rate, being regulated via change of intensity of workpiece argon purge, in 600–500 °C temperature interval.

Steel tendency to cold crack formation was studied on Implant method [15] using sample-inserts of 6 mm diameter without screw-shaped cut.

Critical stress σ_{cr}, at which the sample does not failure during 24 h, was taken as an index characterizing resistance of HAZ metal to cold crack formation.

Content of hydrogen in deposited metal was evaluated using «pencil probe» method. Mixture of distillated water with glycerin was applied as locking liquid.

Investigation results. Metal of sample X in as-delivered condition (without heat treatment)

Table 2. Mechanical properties of samples of 30Kh2N2MF type steel

Sample type	$\sigma_{0.2}$, MPa	σ_t, MPa	δ_5, %	ψ, %	KCU_{+20}, J/cm^2	KCU_{-40}, J/cm^2	HB, MPa
Requirements of TA	1470–1660	1750–1960	≥7	≥15	≥68.6	≥29.4	3880–4990
X	1426–1434	1673–1680	11.9–12.8	54.1–57.5	109–118	100–108	4150–4490
H	1470–1486	1787–1802	10.2–10.7	46.6–49.2	78–86	74–85	4400–4490

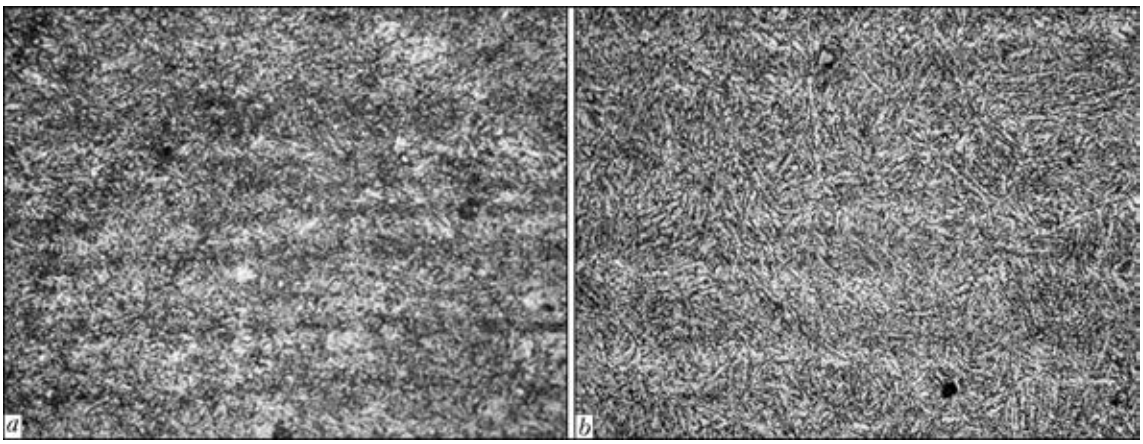

Figure 1. Structure (×500) of 30Kh2N2MF steel with 0.31 (*a*) and 0.36 (*b*) % C in as-delivered condition

has a structure consisting of mixture of upper and lower bainite with domination of upper bainite structure (Figure 1, *a*). Steel structure after heat treatment is transformed into martensite and lower bainite mixture (Figure 2, *a*). Light bands being observed in the structure of sample X are related with chemical micro-inhomogeneity (first of all, on carbon, sulfur and phosphor), forming in process of steel production. Used heat treatment provides some reduction of level of chemical inhomogeneity, but does not remove completely structure banding.

The investigations showed change of metal structure under TDWC effect. Figure 3, *a* shows CCT diagram of undercooled austenite decomposition, which characterizes effect of $w_{6/5}$ cooling rate on phase-structure transformations in HAZ metal of welded joints of steel X samples. Temperature of beginning of austenite decomposition A_{c3} for given metal makes 870–880 °C. Temperature of beginning of martensite (diffusion-free) transformation makes 350–355 °C and that of ending is 150–155 °C.

1.5 times increase of $HV0.1$ hardness of martensite matrix from 3680 (at 2.5 °C/s) to 5070 MPa (at 30 °C/s) should be related with reduction of size of martensite packages (Figure 4) due to increase of quantity of areas with crystallographic orientation favorable for development of martensite transformation. This is possibly an explanation of the fact that increase of cooling rate promotes for rise of static strength of HAZ metal, and its plastic properties redaction (Table 3). Figure 5 shows a change of microstructure of HAZ metal of steel 30Kh2N2MF with 0.31 % C. Microstructural investigations verified that transformations of undercooled austenite in HAZ metal take place only in martensite area at $w_{6/5}$ = 2.5–30 °C/s.

Martensite (M) is formed in area of HAZ metal overheating at $w_{6/5}$ = 2.5 °C/s. Martensite package size makes approximately h_M ~ 34 μm (Figures 4 and 5, *a*) with $HV0.1$ = 3360–3830 MPa microhardness. Internal hardness ($HV10$) of metal is approximately 3680 MPa, $\sigma_{0.2}$ = 1060 MPa, δ_5 = 14.7 %.

Increase of cooling rate from 2.5 to 20 °C/s provides no significant changes of HAZ metal structure in overheating area. However, at that, size of martensite packages reduce from 32.8 μm at $w_{6/5}$ = = 5 °C/s to 19 μm at $w_{6/5}$ = 20 °C/s (Figures 4 and 5). Integral hardness of metal during this rises from 4160 to 4670 MPa, and yield strength increases from 1127 to 1330 MPa. Its ductile properties at that decreases from 14.1 to 12.8 %.

Structure of metal in HAZ overheating area of 30Kh2N2MF steel with 0.31 % C also consists

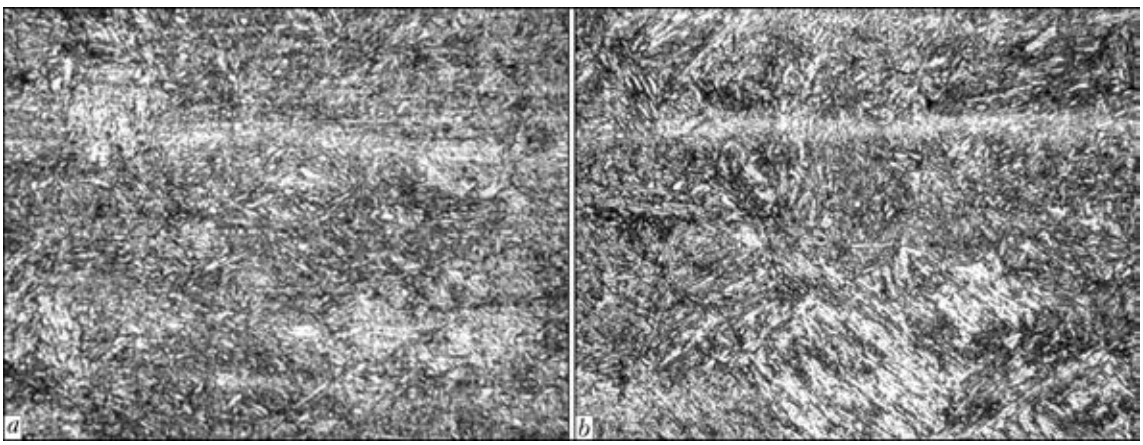

Figure 2. Structure (×500) of 30Kh2N2MF steel with 0.31 (*a*) and 0.36 (*b*) % C after quenching and low-temperature tempering

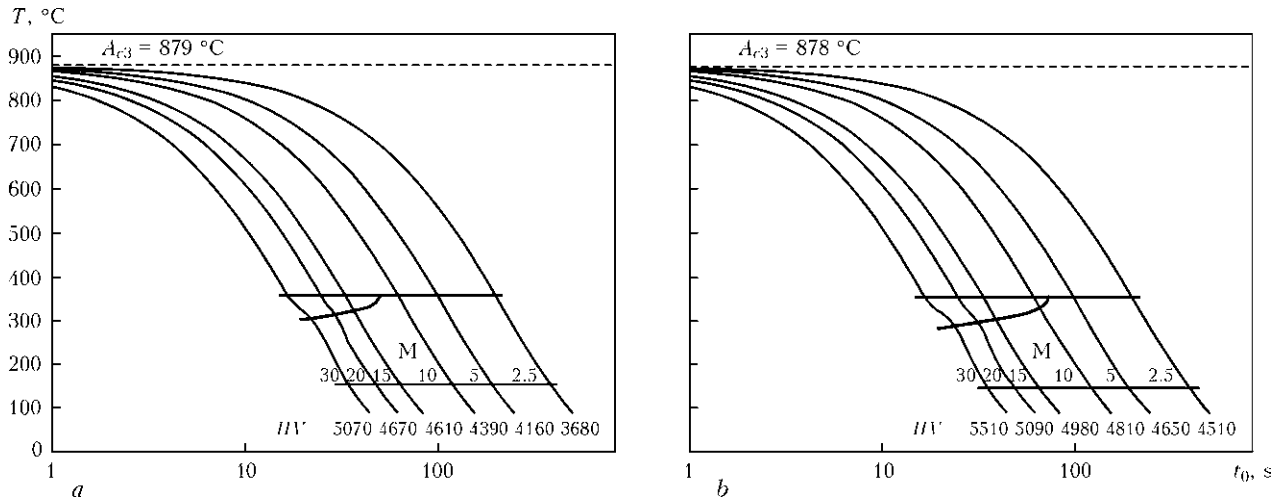

Figure 3. CCT diagrams of undercooled austenite decomposition in HAZ metal of joints from 30Kh2N2MF steel with 0.31 (*a*) and 0.36 (*b*) % C in arc welding: t_0 — cooling time

of martensite, size of packages of which does not exceed 12.5 μm at $w_{6/5}$ = 30 °C/s. At that, microhardness of martensite rises to $HV0.1$ = = 4170–4720 MPa and integral metal hardness increases to 5070 MPa (Figures 4 and 5, *f*). Due to this fact $\sigma_{0.2}$ of HAZ metal increases to 1534 MPa, and δ_5 and ψ (ductility) decrease to 11.7 and 48.8 %, respectively.

Set dependencies of metal structure change in sample X showed formation of martensite structure of increased hardness in HAZ metal of given steel at $w_{6/5} \geq 20$ °C/s. It is obvious that level of local internal stresses in metal structure at increase of cooling rate will also rise and its susceptibility to plastic deformation rapidly drop. In addition to rise of hydrogen content in HAZ metal, this develops the conditions at which indicated metal will have low cold crack resistance. It can be assumed based on mentioned above that cooling rate in HAZ metal should not exceed 20 °C/s in welded joints from steel with carbon content 0.31 % for prevention of cold crack formation.

Structure of metal of sample H, containing 0.36 % C, in-as delivered condition (without heat treatment) also consists of mixture of upper and lower bainite (see Figure 1, *b*). Heat treatment (quenching + low-temperature tempering) transforms the steel structure in the mixture of martensite, upper and lower bainite (see Figure 2, *b*).

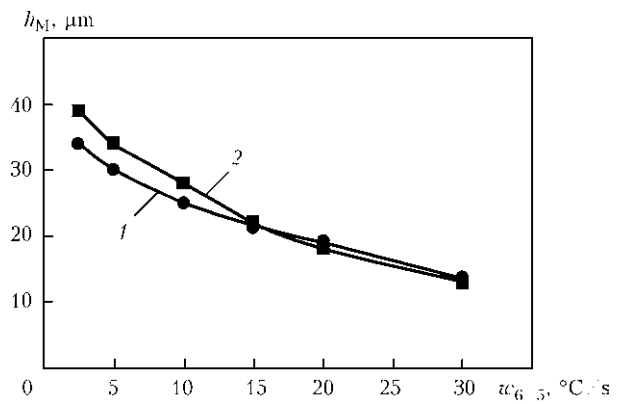

Figure 4. Effect of cooling rate on size of martensite packages h_M in structure of HAZ metal of 30Kh2N2MF steel with 0.31 (*1*) and 0.36 (*2*) % C

Structure of HAZ metal under TDWC effect is changed, size of structural constituents and metal hardness rise. Generalized results of investigations of effect of cooling rate on structure-phase transformations in HAZ metal are represented in Figure 3, *b* in form of CCT diagram of undercooled austenite decomposition. Figure 4 shows change of size of structural constituents, and Figure 5 represents typical microstructures, formed in area of overheating of HAZ metal under effect of TDWC. Data on change of mechanical properties of HAZ metal of 30Kh2N2MF type steel with 0.36 % C under effect of TDWC are given in Table 4.

Carried examinations showed that transformations of undercooled austenite in HAZ metal of steel with 0.36 % C in 2.5–30 °C/s cooling rate range take place exclusively in martensite area, the same as in steel with 0.31 % C. However, formation of martensite in it starts at lower (340–350 °C) transformation temperature and finishes at 140 °C (see Figure 3, *b*) in contrast to steel with 0.31 % C. Similar to previous case

Table 3. Mechanical properties of HAZ metal of samples of 30Kh2N2MF type steel with 0.31 % C

$w_{6/5}$, °C/s	$\sigma_{0.2}$, MPa	σ_t, MPa	δ_5, %	ψ, %	$HV10$, MPa
2.5	1060	1250	14.7	58.6	3680
5	1127	1330	14.1	58.0	4160
10	1200	1410	13.0	57.0	4390
15	1300	1510	12.4	55.1	4610
20	1330	1540	12.8	54.8	4670
30	1534	1684	11.7	48.8	5070

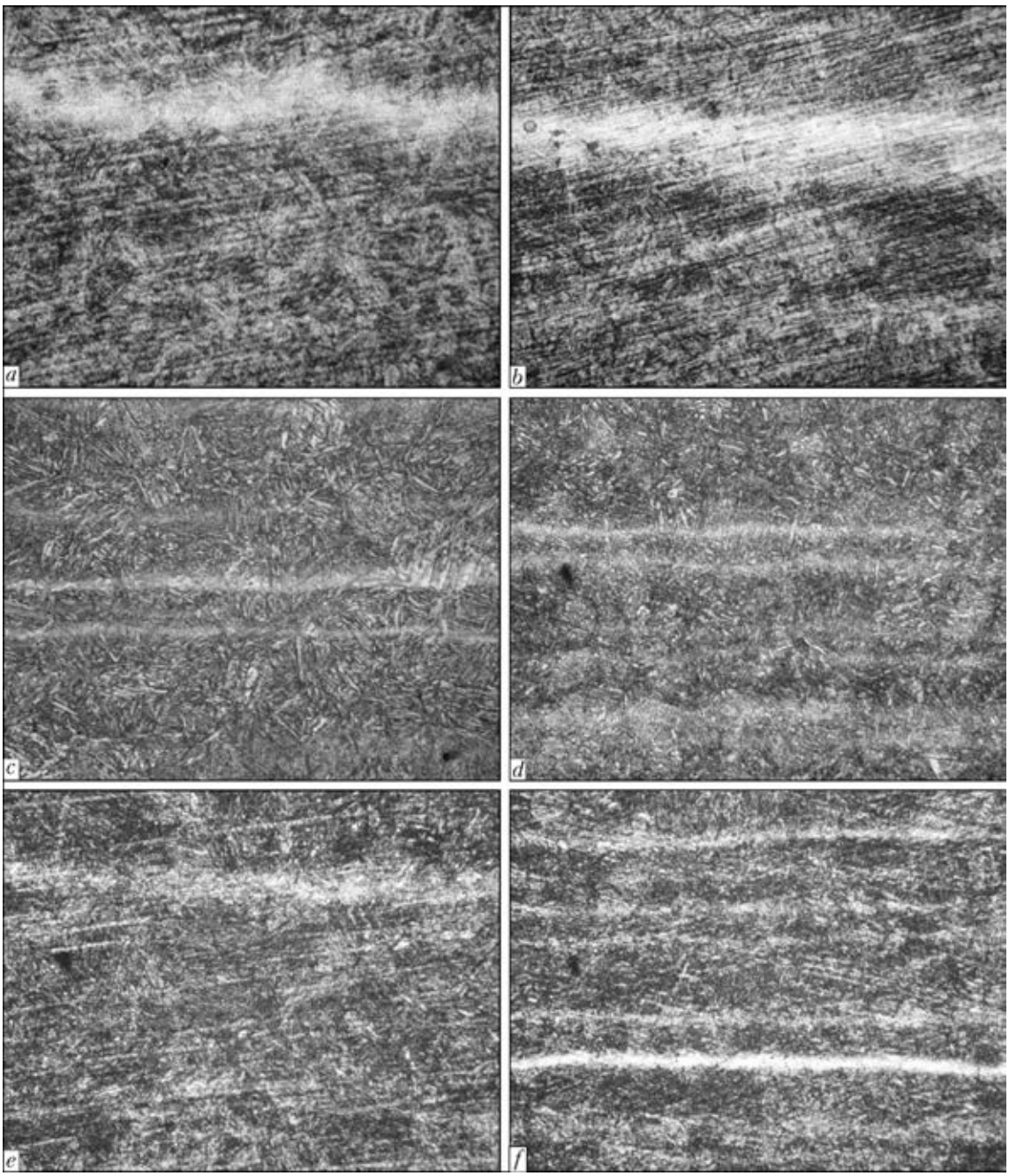

Figure 5. Microstructure (×500) of HAZ metal in overheating area of 30Kh2N2MF steel, containing 0.31 % C, at $w_{6/5}$ = = 2.5 (*a*), 5 (*b*), 10 (*c*), 15 (*d*), 20 (*e*) and 30 (*f*) °C/s

the cooling rate has noticeable effect on parameters of HAZ metal structure. Data on change of size of martensite packages, microstructure and integral hardness of HAZ metal in area of this steel overheating are presented in Figures 4, *b* and 3, *b*, respectively.

The results of metallograpy indicate that martensite (Figure 6, *a*), having approximately h_M ~ 37.1 μm (see Figure 4) size packages and $HV0.1$ = 3930–4730 MPa microhardness, is formed in structure of HAZ metal of steel with 0.36 % C at $w_{6/5}$ = 2.5 °C/s. Integral hardness of quenched HAZ metal under specified cooling conditions makes $HV10$ = = 4510 MPa, $\sigma_{0.2}$ = = 1240 MPa, δ_5 = 12.8 %.

Increase of cooling rate from 5 to 15 °C/s promotes for reduction of martensite packages from 33.8–22.5 μm and rise of its microhardness from 3810–4850 to 4470–5000 MPa (see Figure 6). At that, integral hardness of quenched HAZ metal increases from 4550 to 4980 MPa, $\sigma_{0.2}$ changes from 1262 to 1445 MP, and elongation indices drop from 12.7 to 11.2 %.

The most observable change of structure parameters in area of overheating of HAZ metal of steel with 0.36 % C was noticed in the samples being cooled at $w_{6/5}$ = 30 °C/s. At that, martensite structure with $HV0.1$ = 4460–5200 MPa microhardness and h_M ~ 12.5 μm size packages is formed in HAZ metal. Under such conditions of

Table 4. Mechanical properties of HAZ metal of samples from 30Kh2N2MF steel with 0.36 % C

$w_{6/5}$, °C/s	$\sigma_{0.2}$, MPa	σ_t, MPa	δ_5, %	ψ, %	$HV10$, MPa
2.5	1240	1460	12.8	55.8	4510
5	1262	1490	12.7	55.0	4550
10	1395	1615	12.1	53.6	4810
15	1445	1705	11.2	48.3	4980
30	1607	1896	10.4	46.8	5510

structure formation quenched HAZ metal acquires integral hardness at the level of $HV10$ = = 5510 MPa. At that, yield strength of metal increases to 1607 MPa, elongation and reduction in area reduce to 10.4 and 46.8 %, respectively.

Thus, it can be noted that martensite structure with increased hardness is formed in HAZ metal of steel with 0.36 % C at lower cooling rates (≥ 15 °C/s), in contrast to steel with 0.31 % C. It can be assumed, based on mention above, that prevention of cold crack formation in welded joints requires such technological parameters of welding modes for joints from 30Kh2N2MF steel with 0.36 % C, at which cooling rate of HAZ metal will not exceed 15 °C/s.

Quantitative estimation of susceptibility of 30Kh2N2MF type steel to cold crack formation

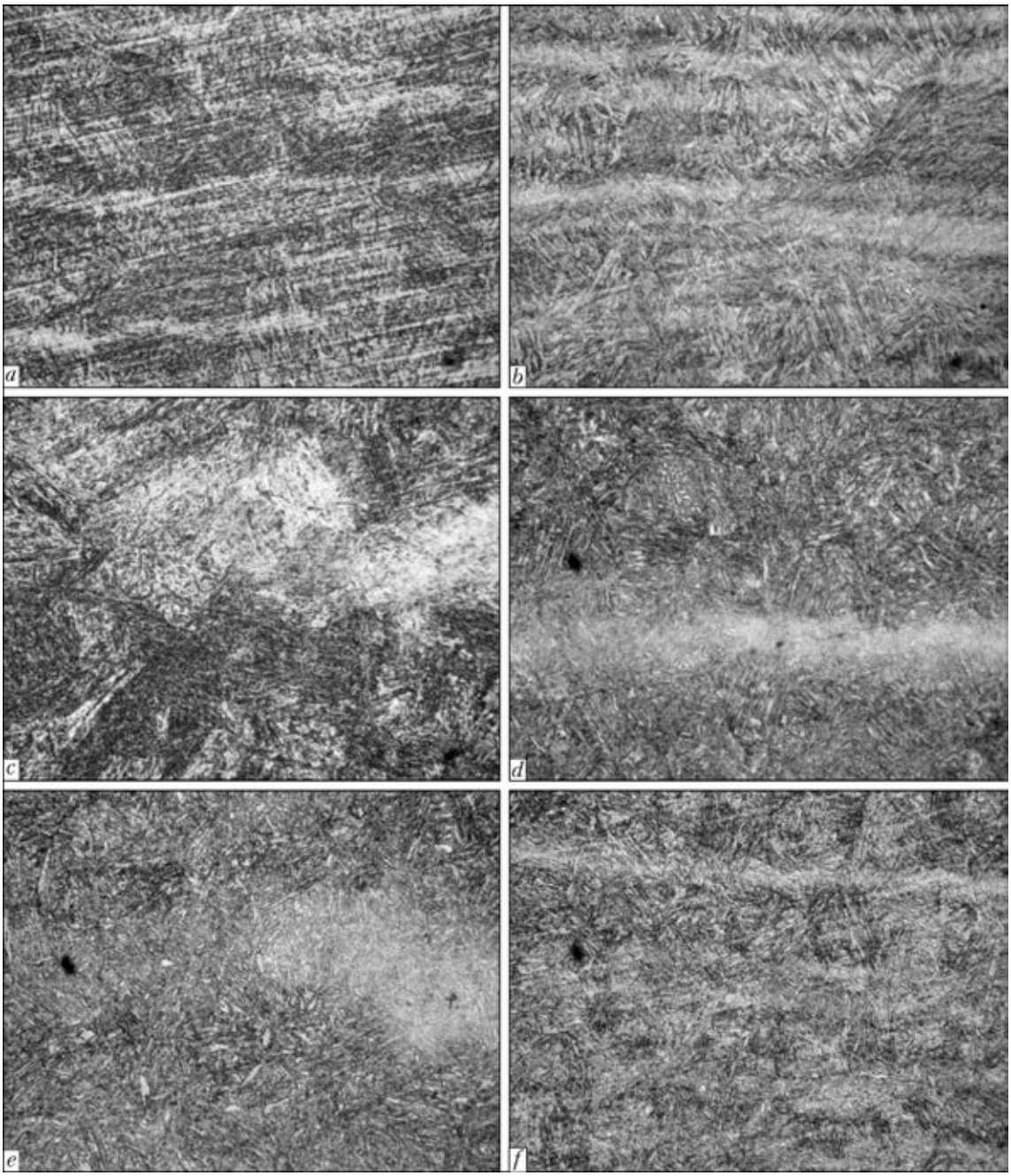

Figure 6. Microstructure (×500) of HAZ metal in overheating area of 30Kh2N2MF steel, containing 0.36 % C, at $w_{6/5}$ = = 2.5 (*a*), 5 (*b*), 10 (*c*), 15 (*d*), 20 (*e*) and 30 (*f*) °C/s

was carried out using samples-inserts produced from steel with 0.36 % C.

Deposition, joining sample-insert with support plate, was performed by mechanized welding in Ar + 20 % CO_2 gas mixture using solid Sv-08GSMT grade wire of 1.2 mm diameter. Content of diffusible hydrogen in metal deposited by indicated wire in as-delivered condition makes $[H]_{dif}$ = = 4.2 $cm^3/100$ g. Special treatment of wire before welding, which lied in its heating in furnace to 240 °C, holding at this temperature during 2 h, cooling in furnace to ambient temperature and further mechanical grinding, allowed reducing $[H]_{dif}$ content in the deposited metal to 1.1 $cm^3/100$ g. Figure 7 shows the results of tests on Implant method. They give characteristic of σ_{cr} change in HAZ metal of 30Kh2N2MF steel depending on temperature of sample pre-heating and content of diffusible hydrogen in the deposited metal.

Carried investigations indicated that increase of $[H]_{dif}$ in the deposited metal from 1.1 to 4.2 $cm^3/100$ g provides for virtually 2 times reduction of resistance of HAZ metal to cold crack formation. Preheating to 150–200 °C allows for significant increase of resistance of welded joints produced by Sv-08GSMT wire to given type of fracture.

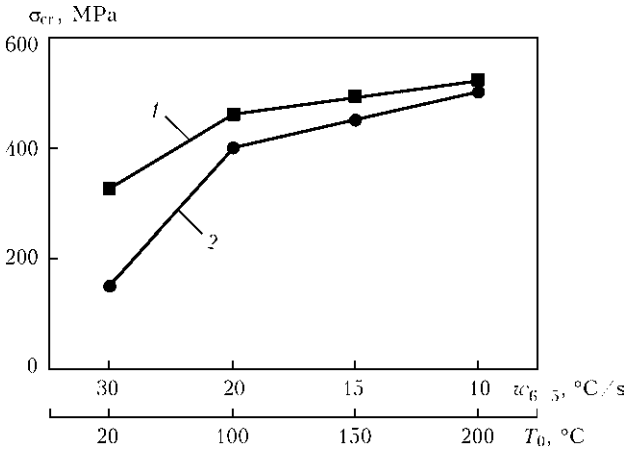

Figure 7. Effect of sample preheating temperature T_0 and content of diffusible hydrogen in deposited metal on susceptibility to cold crack formation of HAZ metal of 30Kh2N2MF type steel: *1* — $[H]_{dif}$ = 1.1; *2* — 4.2 $cm^3/100$ g

Conclusions

1. It is determined that transformations of undercooled austenite in HAZ metal of alloyed medium-carbon steel 30Kh2N2MF independent on content of carbon in it, take place in area of martensite transformation with formation of insignificant quantity of upper and lower bainite at $w_{6/5}$ = 2.5–30 °C/s.

2. Increase of sample cooling rate from 2.5 to 30 °C/s and content of carbon from 0.31 to 0.36 % provides for rise of HAZ metal hardness in overheating area from 3680 to 5070 and from 4390 to 5420 MPa, respectively. At that, its static strength also increases, whereas ductility reduces.

3. Prevention of cold crack formation in welded joints requires such technological parameters of welding modes for 30Kh2N2MF steel with 0.31–0.36 % C, at which HAZ metal cooling rates will not exceed 15 °C/s and diffusible hydrogen content in the deposited metal makes 1.5 $cm^3/100$ g.

4. Increase of $[H]_{dif}$ content in deposited metal from 1.1 to 4.2 $cm^3/100$ g provides for 2 times reduction of cold crack formation resistance of HAZ metal of 30Kh2N2MF type steel. Preheating to 150–200 °C can increase cold crack formation resistance of welded joints produced by Sv-08GSMT wire.

1. Tolten, G.T. (2006) *Steel heat treatment: Metallurgy and technologies*. Front cover. CRC Press (Technology & Engineering).
2. Kashirsky, Yu.V., Koloskov, M.M. (2000) Information bank on machine building materials and processing modes. *Tyazh. Mashinostroenie*, **4**, 12–19.
3. Goldshtejn, M.I., Grachev, S.V., Veksler, Yu.G. (1985) *Special steels*: Manual for higher education institutions. Moscow: Metallurgiya.
4. Bolshakov, V.I., Dolzhenkov, I.E., Dolzhenkov, V.I. (2002) *Technology of heat and combined treatment of metal products*: Manual for higher education institutions. Dnepropetrovsk: Gaudeamus.
5. Kuchuk-Yatsenko, S.I., Grigorenko, G.M., Novikova, D.P. et al. (2007) Effect of energy input on ductile properties of flash butt welded joints in steel X70. *The Paton Welding J.*, **6**, 2–6.
6. Medovar, L.B., Saenko, V.Ya., Polishko, A.A. et al. (2010) Effect of ESC LM thermal cycle on structure of model multilayer ingot. *Zbirnyk Nauk. Prats MUSB*, **1**, 75–83.
7. Seo, J.S., Kim, H.J., Ryoo, H.S. (2008) Microstructure parameter controlling weld metal cold cracking. *J. Achievements in Materials and Manufact. Eng.*, 27(Issue 2), 199–202.
8. Sterenbogen, Yu.A. (1986) Some factors determining the resistance of HAZ metal of martensitic steels to cold cracking. *Avtomatich. Svarka*, **6**, 5–8.
9. Skulsky, V.Yu. (2009) Peculiarities of kinetics of delayed fracture of welded joints of hardening steels. *The Paton Welding J.*, **7**, 12–17.
10. Gajvoronsky, A.A., Sarzhevsky, V.A., Gordonny, V.G. (1997) Weldability of medium-carbon alloyed steel 38Kh2MYuA. *Avtomatich. Svarka*, **4**, 20–24, 33.
11. Li, S., Akiyama, E., Yuuji, K. et al. (2010) Hydrogen embrittlement property of a 1700 MPa class ultrahigh strength tempered martensitic steel. *Sci. and Technol. Adv. Materials*, **11**, 1–6.
12. Wongpanya, P., Boellinghaus, Th., Lothongkum, G. (2008) Heat treatment procedures for hydrogen assisted cold cracking avoidance in S 1100 QL steel root welds. *Welding in the World*, **52**, 671–678.
13. Grigorenko, G.M., Kostin, V.A., Orlovsky, V.Yu. (2008) Current capabilities of simulation of austenite transformations in low-alloyed steel welds. *The Paton Welding J.*, **3**, 22–24.
14. Cherepin, V.T. (1968) *Experimental technique in physical metals science*. Kiev: Tekhnika.
15. Makarov, E.L. (1981) *Cold cracks in welding of alloyed steels*. Moscow: Mashinostroenie.

Received 17.12.2014

EFFECT OF TITANIUM-CONTAINING INOCULANTS ON STRUCTURE AND PROPERTIES OF WELD METAL OF HIGH-STRENGTH LOW-ALLOY STEELS

V.V. GOLOVKO, S.N. STEPANYUK and **D.Yu. ERMOLENKO**
E.O. Paton Electric Welding Institute, NASU
11 Bozhenko Str., 03680, Kiev, Ukraine. E-mail: office@paton.kiev.ua

There is a necessity in increase of toughness and ductility indices of weld metal of high-strength low-alloy steels. Effect of inoculants on process of solidification and formation of grains of primary structure is not studied enough. Possibility of regulation of grain size of primary weld metal structure by weld metal melt inoculation with refractory titanium compounds, included into flux-cored wire was considered. Distribution of non-metallic inclusions in weld metal on size and morphology was investigated. Examinations of primary and secondary weld metal structure were carried out. It is determined that entering of titanium refractory compounds into the weld pool allows changing the size of primary structure dendrites. It was found that presence of titanium compounds having poor wetting by liquid iron (TiN) at interface results in blocking of dendrite growth. At the same time, introduction of titanium compounds characterized by small liquid iron wetting angles (TiC), in the melt promotes for formation of coarser dendrites. It was shown that weld metal with bainite (TiN) or ferrite (TiC) secondary structures, which are close on strength indices but differ on ductility and toughness levels, can be obtained depending on inoculant structure. Obtained results are realized in technology for welding of HSLA steels using flux-cored wire with titanium-containing inoculants. Technology has passed experimental-industrial verification at Novo-Kramatorsk Machine-Building Works. 7 Ref., 5 Tables, 5 Figures.

Keywords: *arc welding, low-alloy steels, flux-cored wire, introduction of titanium-containing inoculants, weld metal, structure and properties*

In recent decades, significant widening of volumes of application of high-strength low-alloy (HSLA) steels is one of the typical peculiarities of production of welded metal structures. Their application allows reducing metal intensity of the parts and decreasing energy consumption for their manufacture. Complex of mechanical properties of welded structure is determined by structure indices of base metal as well as metal of welded joint. If structure of cold-rolled metal is formed as a result of complex metallurgical and thermomechanical influence, then possibility of regulation of weld metal microstructure is highly limited. Non-metallic inclusions (NMI) are one of the effective means of such regulation.

Scientific and technical literature has large number of works investigating effect of inclusions on conditions of ferrite structure formation and peculiarities of $\gamma \rightarrow \alpha$ transformations [1–3]. Significantly smaller amount of works is dedicated to investigation of role of NMI in processes of solidification and grain formation of the primary structure [4, 5]. It is known fact that nature of re-solidification process can significantly differ depending on primary austenite grain size [4], and refractory inclusions, which are present in the metal melt, can influence dendrite growth conditions [5].

Table 1. Melting temperature and angle of wetting by molten iron of titanium compounds at 1600 °C [6]

Inclusion	T_{melt}, °C	θ, deg	Lattice type
TiO_2	1750	78	FCC, a = 0.417 nm
TiN	2950	130	FCC, a = 0.423 nm
TiC	3150	49	FCC, a = 0.431 nm

The aim of present research lied in investigation of possibility of regulation of grain size in primary structure of weld metal on HSLA steels, produced by ($Ar + CO_2$)-shielded flux-cored wire arc welding. It can be done by weld pool melt inoculation with refractory titanium compounds, included in wire core. Titanium compounds with different liquid iron wetting value at 1600 °C (Table 1) were taken as inoculants.

Table 2 gives chemical composition of weld metal, produced in accordance with the requirements [7].

Sections for investigation of peculiarities of NMI distribution and microstructure content as well as samples for determination of mechanical properties in accordance with the requirements of GOST 6996–66 were manufactured from weld metal. Results of determination of weld metal mechanical properties, given in Table 3, showed that examined welds are close on strength indices (σ_t, $\sigma_{0.2}$), but differ on ductility (δ_5, ψ) and toughness (KCV) levels.

Table 2. Chemical composition of examined welds

Inoculant	Weight fraction in weld metal, %						
	C	Mn	Si	Ni	Mo	Ti	Al
TiO_2	0.032	1.32	0.30	2.14	0.26	0.013	0.038
TiC	0.046	1.39	0.34	2.10	0.24	0.011	0.033
TiN	0.035	1.40	0.32	2.19	0.26	0.011	0.036

Table 3. Mechanical properties of metal of examined welds

Inoculant	σ_t	$\sigma_{0.2}$	δ_5	ψ	*KCV*, J/cm^2, at *T*, °C			
	MPa		%		20	0	−20	−40
TiO_2	693	605	14	48	89	85	82	57
TiC	715	644	19	63	95	89	85	73
TiN	712	580	5	15	55	47	40	32

Examination of peculiarities of NMI distribution was carried out on unetched sections using optical microscope «Neophot-30» and further computer processing of images for obtaining information on their volume content (Figure 1). Metallographic and fractographic examinations of weld metal samples were performed in sharing centers of the E.O. Paton Electric Welding Institute. Analysis of weld metal microstructure was carried out on transverse sections after etching in 4 % HNO_3 solution in ethyl alcohol using scanning electron microscope JSM-35CF. Morphology and composition of NMI on fracture surfaces was examined with the help of Auger-microprobe JAMP 9500F, equipped by energy-dispersion X-ray spectrometer of INCA system (researcher L.M. Kapitanchuk).

Due to the fact that aim of the work lied in investigation of effect of introduction of refractory inoculants into the weld pool, the specific attention was paid to analysis of morphology and structure of NMI. It was determined that the inclusions in the studied samples can be divided on two main groups on morphological characteristics, namely single-phase and multi-phase. Single-phase inclusions of up to 0.3 μm size in weld metal consisted of refractory particles of titanium oxides (TiO_2), titanium carbides (TiC) and titanium nitrides (TiN). Inclusions of this type of more than 0.1 μm size were represented by silicate or manganese aluminum silicate compounds (Figure 2).

Analysis of morphological peculiarities of NMI of more than 0.5 μm size showed that their center, as a rule, contain refractory inclusions with more fusible constituent precipitating on their surface during weld metal cooling. As can be seen from data given in Table 4, the metal of examined welds contained approximately equal fraction of inclusions of up to 0.3 μm, the main part of which are presented by refractory titanium compounds. However, this metal was different in grain size of primary structure as well as composition of secondary microstructure.

Figure 3 shows the samples of weld metal primary structure, obtained on «Neophot-30» after etching in boiling solution of sodium picrate. It also gives the results of measurement of thickness of dendrites, formed in process of metal soliditication.

As can be seen from data presented, inoculation of refractory titanium compounds in the weld pool effects the size of dendrite structure, forming during solidification. Nature of this effect, shown in Figure 4, allows making a conclusion that inclusions with increased energy of interaction with den-

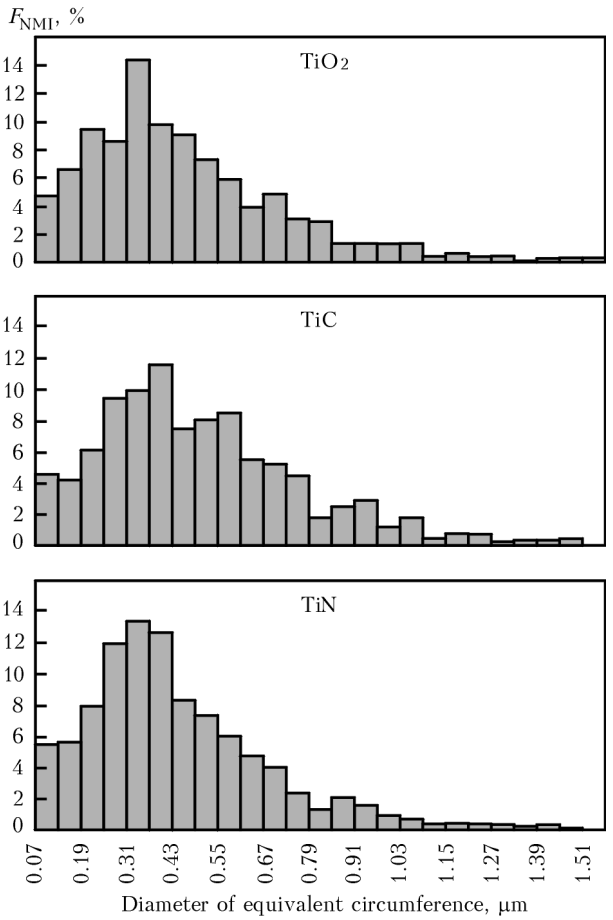

Figure 1. Distribution of NMI F_{NMI} in weld metal on their sizes

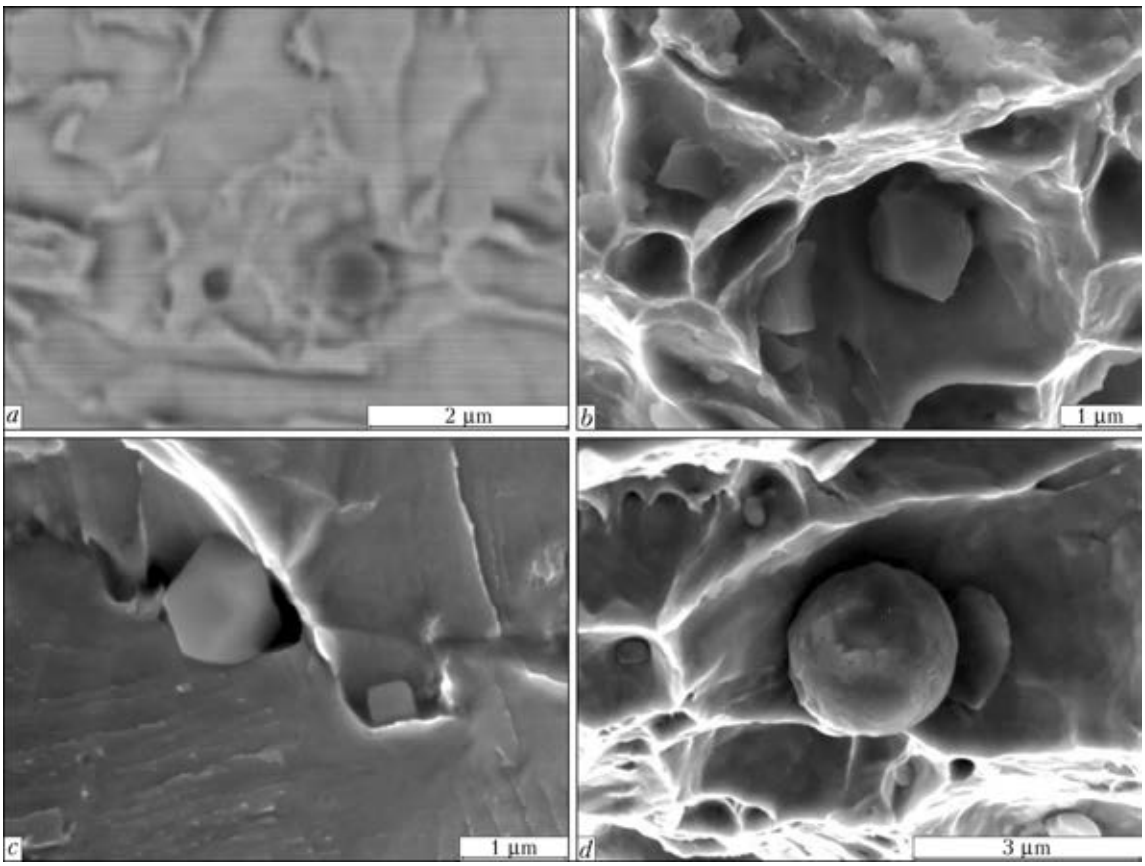

Figure 2. Morphology of NMI in weld metal: *a* — aluminum oxide; *b* — titanium carbide; *c* — titanium nitride; *d* — manganese aluminum silicate

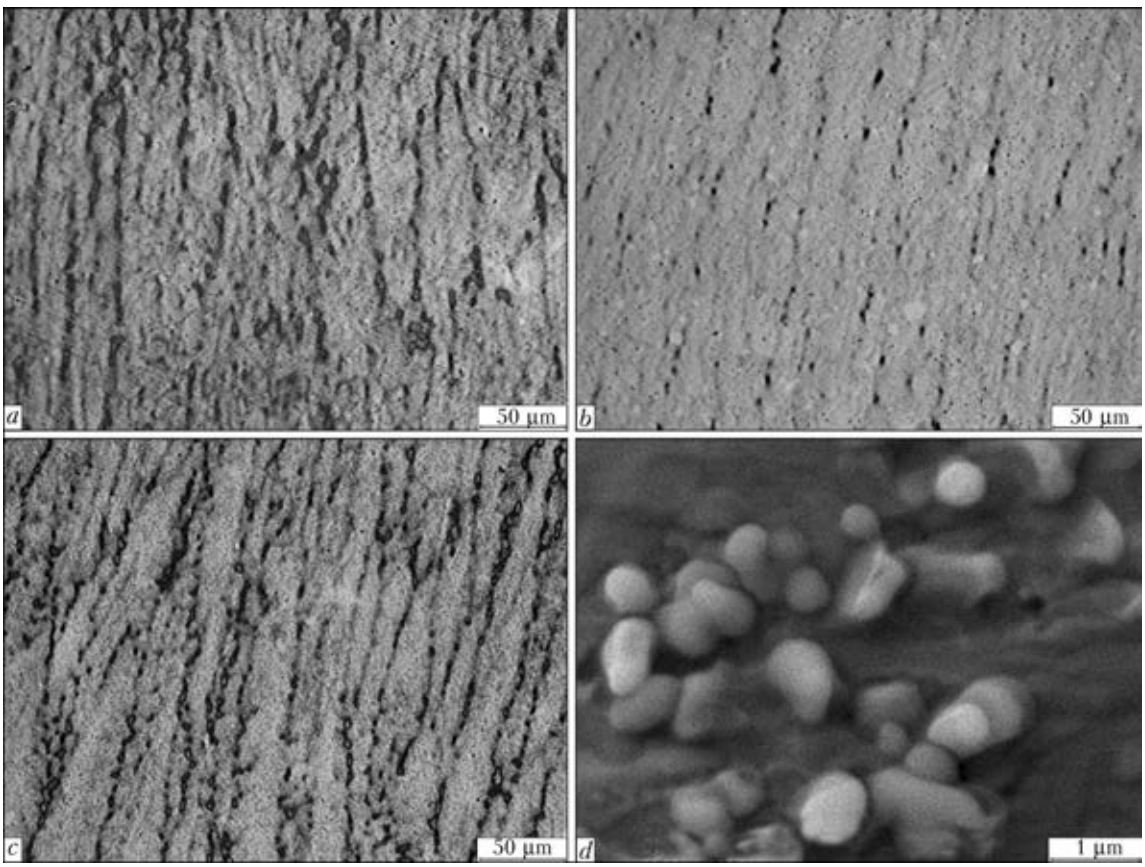

Figure 3. Primary structure of weld metal: *a* — TiO_2; *b* — TiC; *c* — TiN; *d* — nanoparticles of refractory inclusions on interface

Table 4. Fractional composition of NMI in examined weld metal

Inoculant	Volume fraction, %, of inclusions of size, μm		
	<0.3	0.3–0.8	>0.8
TiO_2	29.64	61.54	8.82
TiC	24.50	63.50	12
TiN	31.11	60.59	8.30

Table 5. Fraction of structural constituents in microstructure of weld metal, and results of determination of their hardness

Inoculant	Structural constituent	Hardness *HV*	Fraction in microstructure, %
TiO_2	Acicular ferrite	254–264	60
	Polyhedral ferrite	236–254	21
	Polygonal ferrite	250–254	12
	Lower bainite	274–297	8
TiC	Acicular ferrite	236–264	56
	Polyhedral ferrite	213–216	42
	Polygonal ferrite	224–228	2
TiN	Lower bainite	300–309	85
	Polygonal ferrite + bainite	274–276	9
	Polyhedral ferrite + bainite	270–276	6

drite surface (Figure 3, *d*), present in solidification front, promote for rise of rate of its growth. This can be an explanation for significant increase of dendrite size in the case of titanium carbide inoculation in comparison with two other researched variants (Figure 4).

It is known fact that grain size of primary structure effects the nature of $\gamma \rightarrow \alpha$ transformation processes. Weld metal secondary structure was investigated using optical and electron metallography. It was determined that microstructure of welds consists of mixture of ferrite and bainite structures. Figure 5 shows the microstructure samples, and Table 5 gives the results of determination of fraction of separate structural constituents in it.

Analysis of microstructure composition of weld metal, obtained after completion of re-solidification processes, showed change of fraction of ferrite and bainite constituents in it depending on grain size of primary structure, that can be explained by competitive nature of two main processes of ferrite phase nucleation in course of $\gamma \rightarrow \alpha$ transformation. If dendrites of up to 100 μm size are formed in the case of presence on solidification front of TiN inclusions, capable to suppress growth of solidifying γ-phase, then replacement of these inclusions to TiC particles promotes for increase of dendrite size to 150 μm.

In the fist case, boundaries of primary grains are the centers of α-phase nucleation. This is the place for formation of bainite structure in high-

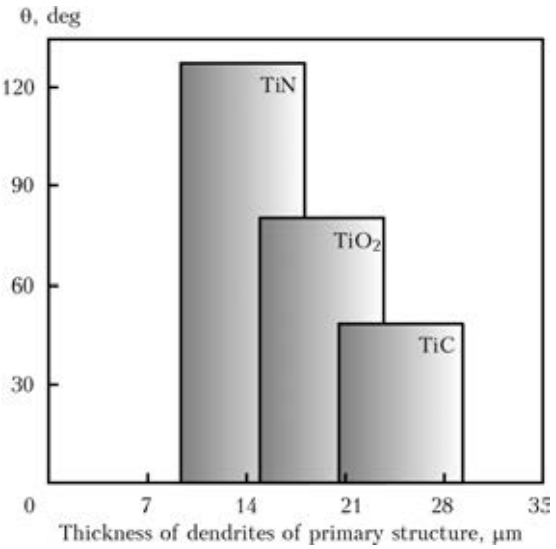

Figure 4. Relationship between angle of wetting of refractory compounds by liquid iron and thickness of dendrites of primary structure of investigated weld metal

temperature area of intermediate transformation. In the second case, with coarser austenite grains, nucleation of new phase on interface surface of some NMI with metallic matrix becomes more energy profitable. In this situation, process of bainite transformation is shifted in the area of lower temperatures, that promotes for formation of ferrite structures of acicular morphology. Such a conclusion about effect of titanium-containing inoculants on conditions of formation of weld metal microstructure in HSLA steels is verified by results of experiments carried in given work.

Complete understanding of effect of inoculants introduced into the weld pool on formation of weld metal primary structure requires detailed investigation of physical-chemical peculiarities of these processes. Results of such investigations will be stated in the next publications dedicated to this subject.

Conclusions

Effect of titanium-containing inoculants on conditions of structure formation in weld metal of high-strength low-alloy steels was investigated. It is determined that size of primary structure dendrites can be changed by introduction of refractory titanium compounds into the weld pool. Presence of titanium nitrides on interface results in blockage of dendrite growth, whereas introduction of titanium carbides into the melt promotes for formation of coarser dendrites. Change of primary structure size influences the nature of $\gamma \rightarrow \alpha$ transformation processes. If nucleation of α-phase in disperse dendrite structure is started at grain boundaries in upper area of bainite transformation, then nucleation of ferrite inside the

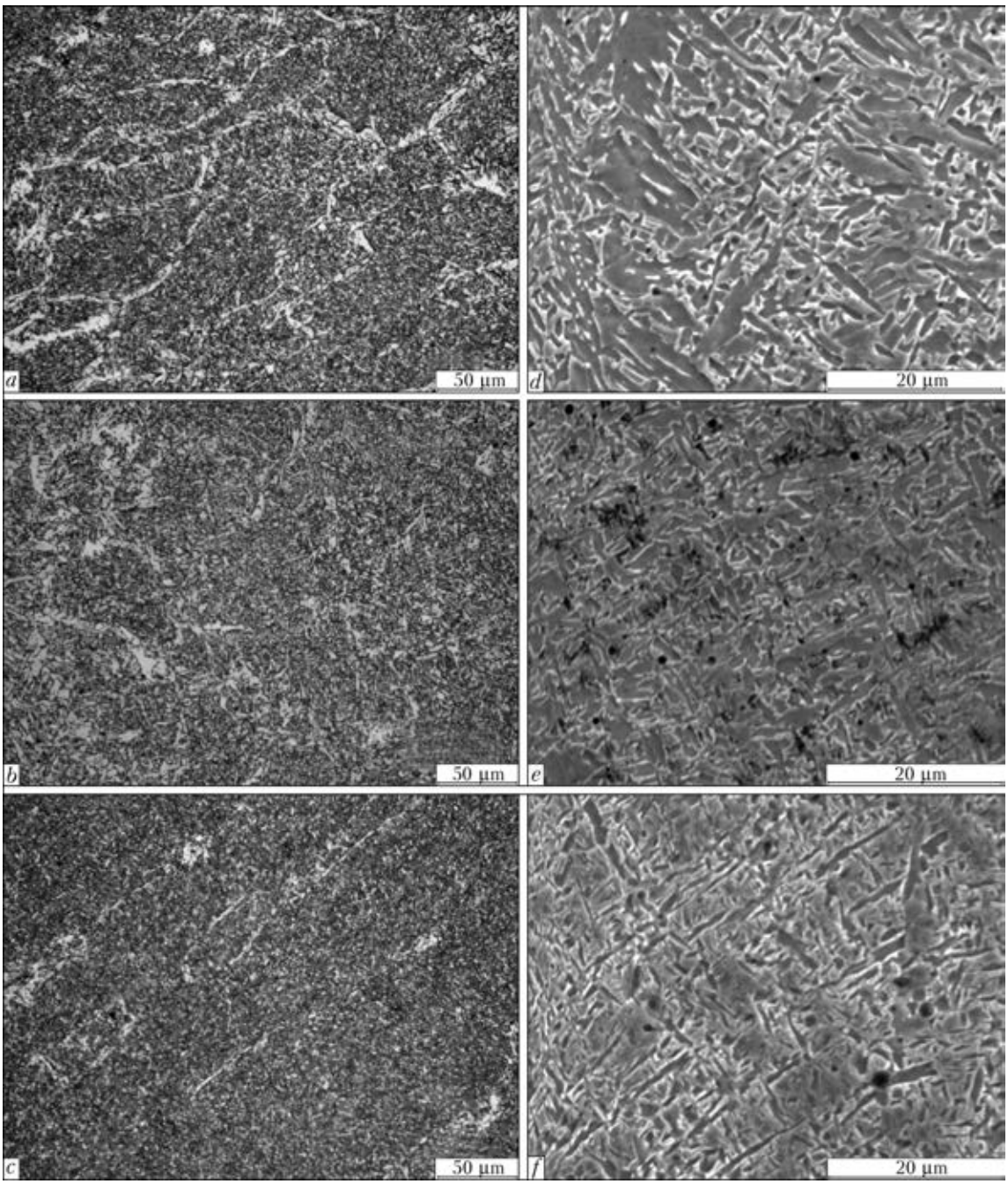

Figure 5. Microstructure of examined weld metal: *a*, *d* — TiO_2; *b*, *e* — TiC; *c*, *f* — TiN

primary grains at boundaries with non-metallic inclusions at temperatures close to ending of bainite transformation is typical for coarser dendrites. It is shown that weld metal with bainite (TiN) or ferrite (TiC) secondary structures, which are close on strength indices but differ on the level of ductility and toughness, can be obtained depending on inoculant composition.

1. Lee, T.-K., Kim, H.J., Kang, B.Y. et al. (2000) Effect of inclusion size on the nucleation of acicular ferrite in welds. *ISIJ Int.*, 40(**12**), 1260–1268.
2. Oh, Y.J., Lee, S.-Y., Byun, J.-S. (2000) Non-metallic inclusions and acicular ferrite in low carbon steel. *Materials Transact.*, 41(**12**), 1663–1669.
3. Babu, S.S. (2004) The mechanism of acicular ferrite formation in weld deposits. *Current Opinion in Solid State and Materials Sci.*, **8**, 267–278.
4. Zhang, L., Thomas, B. (2006) State of the art in the control of inclusions during steel ingot casting. *Metallurg. and Materials Transact.*, 37(**5**), 733–761.
5. Vanovsek, W., Bernhard, C., Fiedler, M. et al. Influence of alloying additions on the morphology of non-metallic inclusions in high-strength steel welds. *IIW Doc. II-1776–11* (II-C-421–11).
6. Lyakishev, N.P., Pliner, Yu.L., Lappo, S.I. (1985) *Alloys and steels doped with titanium*. Moscow: Metallurgiya.
7. *ISO 26304:2011*: Welding consumables. — Solid wire electrodes, tubular cored electrodes and electrode-flux combinations for submerged arc welding of high strength steels. — Classification.

Received 23.12.2014

SUPERSONIC PLASMA GAS AIR SPRAYING OF CERMET COATINGS OF THE (Ti, Cr)C–NiCr SYSTEM

Yu.S. BORISOV, A.L. BORISOVA, M.V. KOLOMYTSEV and **O.P. MASYUCHOK**
E.O. Paton Electric Welding Institute, NASU
11 Bozhenko Str., 03680, Kiev, Ukraine. E-mail: office@paton.kiev.ua

Effect of plasma gas air spraying (PGAS) factors (plasmatron power, consumption of plasma gas, spraying distance, anode diameter) of mechanical mixture from double titanium-chromium carbide and nichrome powders on characteristics of produced coatings (structure, microhardness, porosity, chipping resistance) was investigated. Program of experiments was composed using mathematical planning method. Regression equations, determining quantitative dependence of values of average and maximum microhardness, stability of microhardness indices and level of chipping on spraying process factors, were received based on data processing results. Indices of heat content in plasma jet and duration of powder particle passing through plasma jet were used for analysis of the results. It is determined that mode of plasma jet outflow and value of its heat content have the largest effect on structure and properties of produced coatings. Using 10 mm diameter anode, providing supersonic jet outflow mode at 5.6 kW·h/m^3 heat content index, for PGAS of coatings from mechanical mixture of titanium-chromium carbide and nichrome powders (3:1) promotes for formation of dense coatings (porosity <1 %) with cermet structure (titanium-chromium carbide and nichrome). Such coatings have average microhardness 12.6 GPa that 1.5 times exceeds microhardness of thermal coatings from mechanical mixture of chromium carbide and nichrome powders (8.6 GPa). 20 Ref., 6 Tables, 2 Figures.

Keywords: *cermets, double titanium-chromium carbide, supersonic plasma gas air spraying, coating properties, microhardness, experiment planning*

The most wide-spread class of coatings, protecting surface of the parts from different types of wear [1–3], is the thermal coatings with cermet structure, consisting from metallic matrix, mainly based on nickel, cobalt or iron alloys with strengthening phase principally of tungsten, chromium or titanium carbides. In recent times they receive specific attention due to possibility of their application as alternative to solid chromium coatings. This allows for solving one the current tasks of environment protection [4–6].

WC–Co and Cr_3C_2–NiCr [3, 6, 7] cermet systems received the widest practical application. The leading world companies Starck (Germany), Sulzer (USA) and Praxair (USA) had developed compositions and mastered series of technologies for manufacture of powders of these materials, being special in their properties for application at plasma, detonation and high-velocity oxy-fuel spraying units [8–10]. These materials are delivered in form of mechanical mixtures of carbide powders and matrix alloy or conglomerate powders of cermet components, preliminary subjected to sintering–grinding of mechanical mixture or its conglomeration–sintering. Properties of produced coatings depend to significant extent on powder production method [11].

Compositions of WC–Co cermets for thermal spraying differ on cobalt content (12–17 wt.%), and additional chromium alloying (4–8 wt.%) is used for increase of corrosion resistance. Microhardness of produced coatings depends on cobalt content and makes *HV*0.3-1200 at 12 % Co and *HV*0.3-900–1000 at 17 % Co [8].

Content of NiCr in compositions of cermets for thermal spraying of Cr_3C_2–NiCr system lies in 15–25 wt.% range, and average microhardness significantly varies depending on NiCr amount (*HV*0.3-1035 for Cr_3C_2–15 % NiCr; *HV*0.3-865 for Cr_3C_2–25 % NiCr), as well as method of powder production. It rises in the case of Cr_3C_2–25 % NiCr to *HV*0.3-1100 at transfer from application of mechanical mixture of powders to powder produced by method of preliminary agglomeration of mixture of fine powder components with further sintering [11]. A reason of such change is more uniform distribution of components and presence of product of carbide and alloy interaction during sintering.

Important service property of studied cermet coatings, determining area of their practical application, is the maximum temperature of their operation. In air it makes 480–500 °C for WC–Co and 870–900 °C for Cr_3C_2–NiCr cermets [8–10] according to passport data, represented by companies-manufacturers of special powders for thermal spraying. However, safe protection of coat-

Table 1. Characteristics of powder-components of (Ti, Cr)C–NiCr mechanical mixture

Material	Composition, wt.%	Melting temperature, °C	Density, g/cm^3	Particle size, μm
Double titanium-chromium carbide	TiC — 70, Cr_3C_2 — 30	~2750	5.35	15–40
Nichrome	Ni — 80, Cr — 20	1400	8.40	40–63

ing from oxidation in the case of Cr_3C_2–NiCr cermet is provided due to formation of dense Cr_3C_2 film on its surface that takes place in 600–700 °C temperature area [12].

In this connection, development of thermal cermet coating, providing surface protection from wear at operating temperatures of 500–700 °C, is of current importance. Double titanium-chromium carbide can be referred to carbide materials with such property. It has high oxidation resistance at up to 1100 °C, and at the same time exceeds titanium carbide (32 GPa) and chromium carbide (22.8 GPa) on microhardness value (up to 40 GPa) [13].

Experiments on deposition of cermet coatings, containing double titanium-chromium carbide (Ti, Cr)C were based on application of composite powders (Ti, Cr)C, clad by nickel [14–16] or nickel–molybdenum [17]. The coatings were produced by plasma spraying method using argon-hydrogen mixture [14–17] as working gas as well as under conditions of plasma gas air spraying (PGAS) at subsonic and supersonic mode of plasma jet outflow [17].

The structure of plasma coatings, produced using Ar/H_2 plasma jet and 30–35 kW plasmatron power [17], consists of carbide phase of HV 25–30 GPa microhardness, metallic phase with HV 1.8 GPa as well as phase having HV 15–16 GPa and, apparently, being a product of interaction of (Ti, Cr)C with shell metal of particles (Ni) [14, 15].

Analysis of phase and structure transformations in powders of pure and clad (Ti, Cr)C, which take place under PGAS conditions, showed that supersonic mode provides for reduction of level of sprayed material oxidation and increase stability of clad shell on carbide core.

Table 2. Matrix of fractional factorial experiment 2^{3-1}

Number of experiment	X_1	X_2
1	+	+
2	+	–
3	–	+
4	–	–

Examination of heat resistance of plasma coatings from Ni(Ti, Cr)C composite powders with 30–35 wt.% Ni showed that they have sufficiently high oxidation resistance at 800 °C in air [15, 18].

Aim of the present work lies in experiments on deposition of coatings from mechanical mixture of (Ti, Cr)C and NiCr powders under conditions of supersonic PGAS for determination of effect of its main parameters on structure and properties of coatings being produced.

Materials and equipment. Mechanical mixture of powders of double titanium-chromium carbide with 7:3 proportion of TiC:Cr_3C_2 and in 3:1 proportion of nichrome were used as spraying material. Table 1 gives the characteristics of (Ti,Cr)C and NiCr.

Coating deposition was carried out on «Kiev-S» machine for supersonic PGAS, developed together with Gas Institute and E.O. Paton Electric Welding Institute of NASU [19]. Air was applied as a plasma gas.

Experiment procedure. Method of mathematical planning of experiment was applied for development of research program. Plan of experiments on coating spraying was compiled using the blocks of matrix of fractional factorial experiment 2^{3-1} for different diameter size of anode nozzle d_a = 10 and 11 mm (Table 2). Fundamental difference in conditions of spraying process with 10 and 11 mm anode diameters lies in nature of plasma jet outflow.

In the first case (d_a = 10 mm) it has supercritical nature, i.e. a jet is supersonic. In the second case (d_a = 11 mm) it can lie in pre-critical as well as critical area depending on electric power and consumption of plasma gas, i.e. the jet should be considered subsonic. Plasmatron electric power W, kW (X_1), consumption of plasma gas (air) G, m^3/h (X_2) and spraying distance L, mm (Table 3) were taken as variables. Consumption of spray material (6 kg/h) remained constant for all experiments.

Table 4 shows the working plan, composed in accordance with matrix of fractional factorial experiment planning.

Analysis of process of plasma spraying of coatings with cermet structure using mechanical mixtures of powders from carbides and alloy, which is metallic matrix of structure, in the case of their mutual feed in the jet requires consideration of series of fundamental peculiarities of such a process [20]:

• separation of traveling path of particles of carbide and metal and appearance of inhomogeneity of their concentration in jet volume are possible at the initial stage of the process during entering of gas-

Table 3. Intervals of variation and values of factors of PGAS of coatings

Variation parameters	Factors		
	W, kW	G, m^3/h	L, mm
Upper level +	90	24	200
Lower level –	70	16	160
Base level 0	80	20	180
Variation interval	10	4	20

powder mixture in plasma jet at difference of density values and component part size;

• difference in value of melting difficulty parameter of metal and carbide particle material [1, 2] and sizes of their particles results in inhomogeneity of their melting conditions at heating in plasma jet, which can be aggravated in the case of mentioned above separation of particles of cermet components in jet volume;

• one of the main requirements to selection of parameters of plasma spraying of carbide material coatings is minimizing of carbon loss, taking place at movement of particles in the jet oxygen-containing zones, which depend on level of carbide particle overheating above the melting temperature, spraying distance, speed and path of powder particle flying.

As long as providing wear resistance is one of the main tasks of technology of plasma spraying of carbide-containing cermet coatings, then the following was used as response functions in experiment plan:

• H_{μ}^{av} — average microhardness of coating (GPa) as characteristic of its structure and index of its possible wear resistance;

• H_{μ}^{max} — maximum microhardness of coating (GPa), characterizing the level of preservation of carbide microhardness, i.e. value of carbon loss;

• $\Delta X/H_{\mu}^{av}$ — relationship of confidence interval to average coating microhardness, reflecting the level of structure homogeneity of produced coating;

• B — level of coating chipping as index of coating cohesion strength related with particle heating inhomogeneity;

• phase composition and coating porosity.

Two complexes of spraying process parameters were developed for analysis of relationship of obtained results with conditions of spraying process, in particular, characteristics of plasma jet and time of staying in jet volume of particle of spray material effecting heat transfer development as well as level of particle interaction with ambient atmosphere:

• $K_h = W/G$, kW·h/m^3 — index of heat content of plasma jet, received by it during passing through arc discharge;

Table 4. Plan of experimental work on PGAS of 75(Ti, Cr)C + + 25NiCr powder

Number of experiment	W, kW	G, m^3/h	L, mm
d_a = 10 mm			
1/1	90	24	200
2/1	90	16	160
3/1	70	24	160
4/1	70	16	200
d_a = 11 mm			
1/2	90	24	200
2/2	90	16	160
3/2	70	24	160
4/2	70	16	200

• $K_{\tau} = 2.82Ld_a^2/G$, s — index of duration of process of powder particle movement in jet volume up to the moment of collision to base surface.

The coatings were deposited on surface of steel samples, preliminary subjected to jet-abrasive machining using corundum powder. Consumption of transporting gas was selected in such a way that flying path of particles of (Ti, Cr)C and NiCr powders was located in plasma jet axial zone.

Methods of metallography («Neophot-32»), X-ray-phase analysis (DRON-3M, CuK_{α} with nickel filter) and microhardness gage PMT-3 were use for examination of coating structure and properties. Coating porosity was determined in dark background of section image and amount of chipping was measured using ImagePro program.

Results of experiment and discussion. Table 5 shows the results of examination of structure and properties of the coatings, produced during performance of experiment plan in accordance with Table 4. Figure 1 represents microstructure of coatings, deposited using the modes corresponding to working plan. Coating thickness lied in 150–250 μm range.

Microstructures of coatings, presented in Figure 1, can be divided on two groups:

• 2/1, 4/1, 1/2 and 2/2, which differ by high density (porosity <1 %) with low chipping level (5–10 %) and absence of inclusions of unmelted particles at the largest thickness of produced layer (to 250 μm);

• 1/1, 3/1, 3/2, and 4/2, where porosity is increased to 3 %, the inclusions of unmelted particles and increased chipping level (to 13–15 %) are observed, and layer thickness makes 100–150 μm.

Presence of such microstructure peculiarities can be explained by difference in conditions of their deposition and, first of all, different value of K_h index, characterizing plasma jet heat content. As for the first group it makes 4.4–5.6, and that for the second group is 2.9–3.75 kW·h/m^3.

Table 5. Characteristics of structure and properties of PGAS (Ti, Cr)C–NiCr coatings produced in accordance with experiment plan (acc. to Table 4).

d_a, mm	Number of experiment	Microhardness $HV0.05$, GPa		$\Delta X/H_\mu^{av}$	Chipping B, %	Phase composition	Porosity, %	Structure peculiarity	K_h, kW·h/m^3	$K_\tau \cdot 10^{-3}$, s
		H_μ^{av}	H_μ^{max}							
10	1/1	5.70	8.86	0.2	12	NiCr, (Ti, Cr)C, Ti_2O_5, $CrTiO_3$	<3	Unmelted particles	3.75	2.35
	2/1	12.60	19.14	0.208	5	(Ti, Cr)C, NiCr, $CrTiO_3$, NiCrO	<1	Same	5.6	2.82
	3/1	3.36	6.43	0.214	15	NiCr, (Ti, Cr)C, Ti2O5, $CrTiO_3$	<3	»	2.9	1.88
	4/1	6.20	10.78	0.303	10	(Ti, Cr)C, NiCr, $CrTiO_3$, NiCrO	<1	»	4.4	3.70
11	1/2	6.98	8.86	0.251	12	NiCr, (Ti, Cr)C, $CrTiO_3$	<1	»	3.75	2.84
	2/2	7.45	13.36	0.204	8	NiCr, (Ti, Cr)C, $CrTiO_3$, $Cr_{23}C_6$	<1	»	5.6	3.41
	3/2	6	10.23	0.218	10	NiCr, (Ti, Cr)C, $CrTiO_2$, TiO	<3	Coarse unmelted particles	2.9	2.27
	4/2	5.30	10.23	0.166	13	NiCr, (Ti, Cr)C, $CrTiO_3$, NiCrO	<3	Same	4.4	4.48

This in combination with the first group with increased index of heating time ((2.82–3.7)·10^{-3} s) provides for efficient particle heating and formation of dense coating structure with increased cohesion strength.

Similar conclusion was made during analysis of indices of coating microhardness, where coatings from the first group have higher values of average (6.2–12.6) and maximum microhardness (10.78–19.14 GPa) then coatings of the second group (3.36–6.98 and 6.43–10.23 GPa, respectively). Data on phase composition of coatings can explain these results.

Since (Ti, Cr)C–NiCr coating is cermet on its structure, then it consists of phase of NiCr metallic binder and (Ti, Cr)C carbide phase, varying by significantly different hardness. In this connection, obtained data on measurement of average microhardness reflect a relationship of these phases in coating volume. (Ti, Cr)C and NiCr volume fractions in accordance with their weight proportion 3:1 and material density (see Table 1) make 82 and 18 %, respectively, in initial sprayed material. Difference of component melting temperature in process of spraying firstly provokes for melting of NiCr, and participation of (Ti, Cr)C in coating formation depends on development of heat exchange processes. According to condition mentioned above, they are more favorable for carbide melting in experiments 2/1 and 4/1, that is verified by phase composition of these coatings (see Table 5). Conditions of experiments 2/1 and 2/2 are virtually the same on K_h and K_τ indices, however, composition and microhardness are different. Leading phase is NiCr in the case of 2/2. This can be related with deviation of (Ti, Cr)C particle path to colder zone of plasma jet at transfer from supersonic to subsonic mode of jet outflow.

Regression equations were composed for determination of level of effect of different factors of spraying process modes on coating characteristics using data, obtained during performance of experiment plan according to Tables 4 and 5.

In use of 10 mm diameter anode:

$$H_\mu^{av} = 7.04 + 0.021W - 0.024G - 0.011L;$$

$$H_\mu^{max} = 11.3 + 0.027W - 0.037G - 0.015L;$$

$$\Delta X/H_\mu^{av} = 0.213 - 0.014W - 0.0145G + 0.008L;$$

$$B = 7 - 0.2W + 0.75G + 0.025L.$$

In use of 11 mm diameter anode:

$$H_\mu^{av} = 6.4 + 0.008W + 0.001G - 0.003L;$$

$$H_\mu^{max} = 10.7 + 0.011W - 0.004G - 0.011L;$$

$$\Delta X/H_\mu^{av} = 0.182 - 0.0083W - 0.0047G + 0.0069L;$$

$$B = 9.5 - 0.15W + 0.25G + 0.05L.$$

Data of given above regression equations were used for plotting the diagrams of trends, reflecting intensity of effect of separate process factors on coating characteristics (Figure 2).

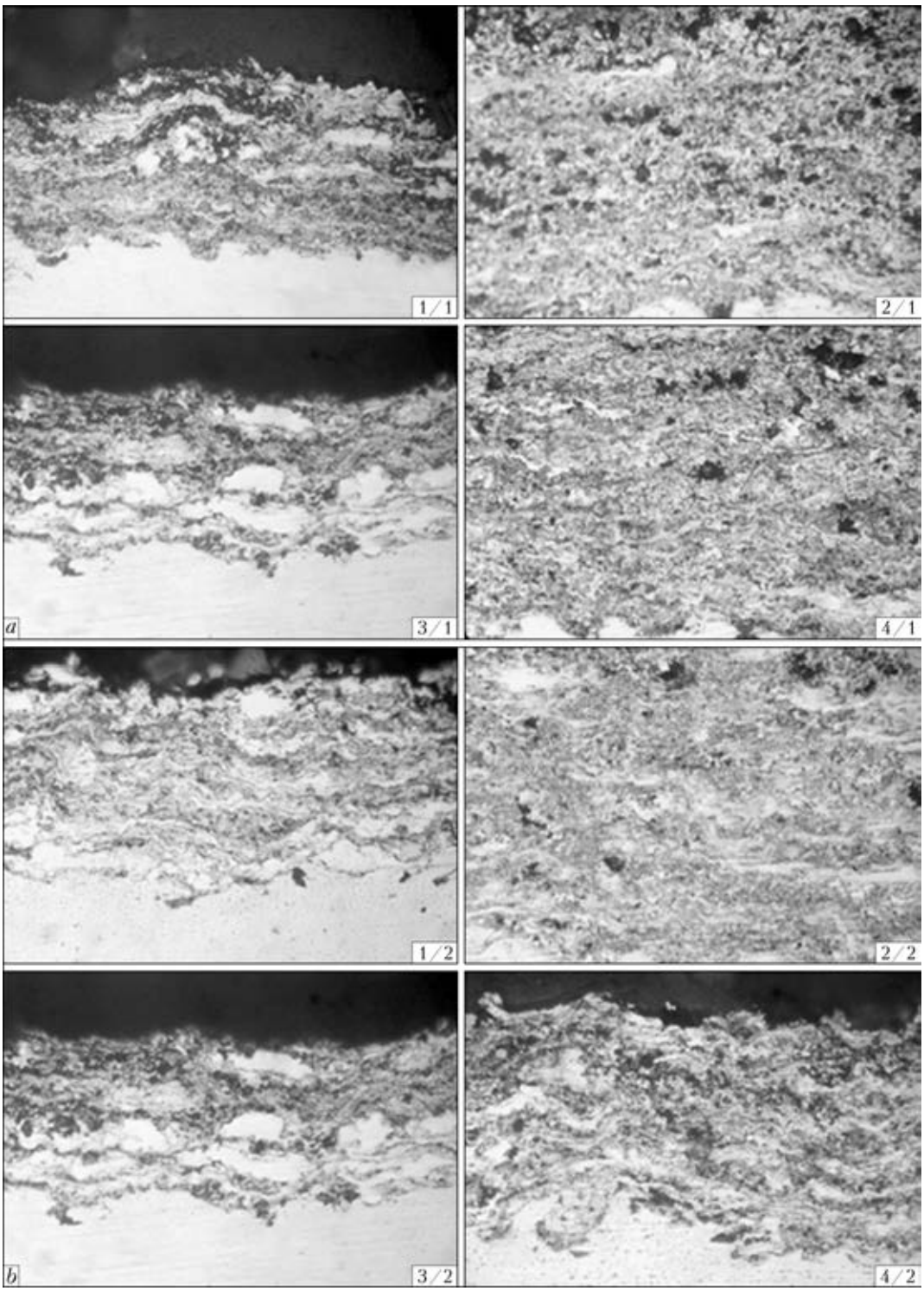

Figure 1. Microstructure (×400) of (Ti, Cr)C– NiCr coatings PGA-sprayed using modes acc. to Table 4: *a* — anode diameter 10 mm; *b* — 11 mm

Table 6 gives the correlation of nature and intensity of effect of different factors on properties of produced coatings (in selected experiment area), performed based on trend indices (see Figure 2).

It follows from Table 6 that trends of d_a = 10 and 11 mm are unidirectional for W and L factors. Increase of W results in increase of H_{μ}^{av} and H_{μ}^{max}, as well as reduction of $\Delta X / H_{\mu}^{av}$ and B, and inverse effect is observed in rise of F factor. In whole it can be considered as relationship of quality of (Ti, Cr)C–NiCr coating by indices of its hardness and cohesion strength with condition of particle heating, caused by plasma jet temperature. The difference lies in intensity of effect of these factors at different mode of plasma jet outflow. Level of change of coating properties at increase of plasmatron power and reduction

Table 6. Character of effect of PGAS factors on properties of (Ti, Cr)C–NiCr coating

Properties	PGAS factors at d_a, mm					
	W		*G*		*L*	
	10	11	10	11	10	11
H_μ^{av}	↑↑	↑	↓	~	↓↓	↓
H_μ^{max}	↑↑	↑	↓	~	↓↓	↓
$\Delta X/H_\mu^{av}$	↓↓	↓	↓	~	↑↑	↑↑
B	↓↓	↓	↑	~	~	↑

Note. ↑↑, ↓↓ — strong; ↑, ↓ — moderate; ~ — weak effect.

of spraying distance is more significant in the case of supersonic mode.

Difference between effect of spraying factors on properties under conditions of subsonic and supersonic modes is observed for plasma gas consumption *G*. If tendency to some deterioration of coating quality on microhardness as well as chipping level is found in the first case at increase of plasma gas consumption, then this effect is considerably insignificant in the second case.

Formation of coatings under PGAS conditions is certainly related with conditions of heating of cermet particles, which are described to significant extent by K_h and K_τ values. The values of coating characteristics are matched in Table 5 with value of these indices for each of eight experiment conditions. It follows from data of Table 5 that change of K_h value from 2.9 to 5.6 kW·h/m^3 under conditions of supersonic jet application is inseparably associated with phase composition of coatings, exceed of microhardness indices (H_μ^{av}, H_μ^{max}) and reduction of level of its chipping and porosity. K_h = 5.6 kW·h/m^3 and

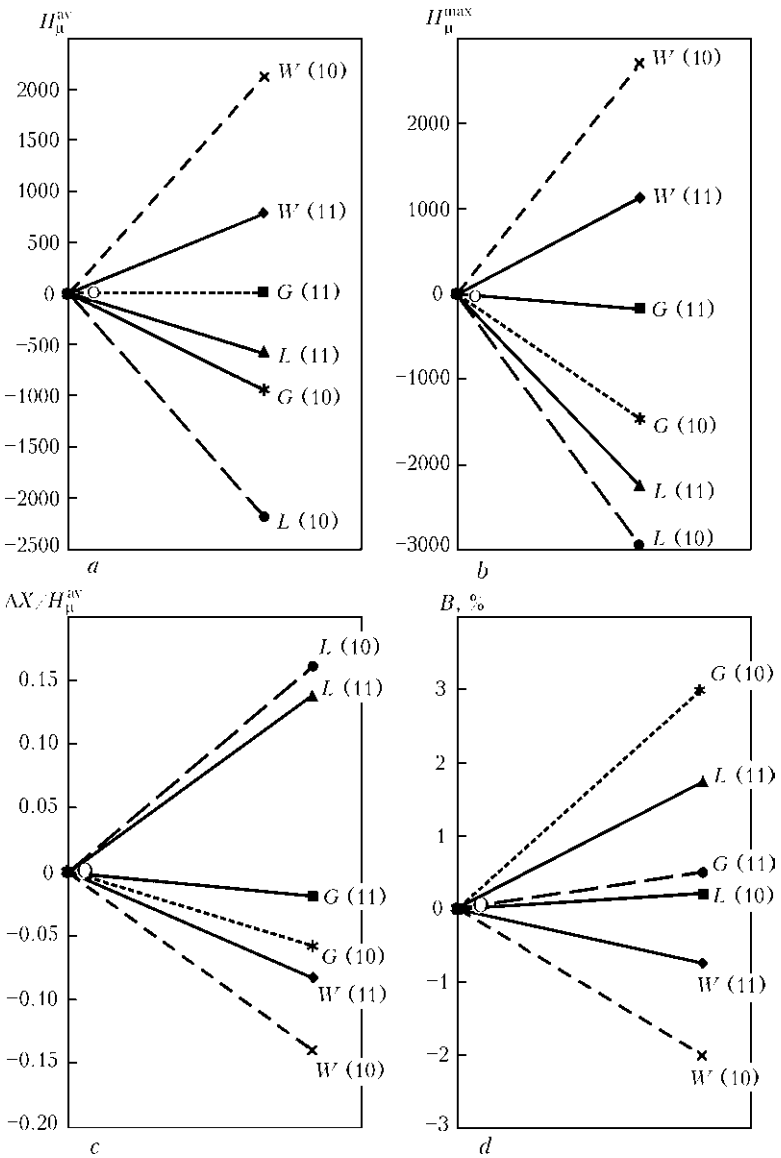

Figure 2. Effect of factors of PGAS process H_μ^{av} (*a*), H_μ^{max} (*b*), $\Delta X/H_\mu^{av}$ (*c*) and *B* (*d*) on coating characteristics; (10) and (11) — data of experiments carried at d_a = 10 and 11 mm, respectively

$K_\tau = 2.82 \cdot 10^{-3}$ s provide for formation of coating with prevailing (Ti, Cr)C content in the structure, that promotes for maximum indices of average (H_μ^{av} = 12.60 GPa) and maximum (H_μ^{max} = = 19.14 GPa) microhardness at minimum porosity (< 1 %) and chipping level (5 %). This can be explained by heating of particles in plasma jet with high heat content at increased duration of heating time. Obtained microhardness of cermet coating (Ti, Cr)C–NiCr, produced from mechanical mixture of powders in 3:1 proportion by means of supersonic PGAS, is 1.5 times higher than microhardness of Cr_3C_2–NiCr coating from similar mechanical mixture of components, sprayed by HVOF method (8.6 GPa) [12].

Effect of K_h index is weaker in the case of subsonic mode of plasma jet outflow, however, maximum values of coating characteristics (7.45 and 13.36 GPa, respectively) are also achieved at its 5.6 kW·h/m^3 value, but structure mainly includes NiCr phase.

Conclusions

1. Results of complex of experiments, carried using mathematical planning method, were used as a basis for performance of analysis of effect of plasma jet outflow mode (subsonic and supersonic) and parameters of plasma gas air spraying (plasmatron electric power, consumption of plasma gas and spraying distance) of mechanical mixture of (Ti, Cr)C–NiCr powders on structure and properties of produced coatings (microstructure, phase composition, microhardness, porosity, chipping resistance).

2. Analysis of received regression equations, reflecting quantitative relationship of value of coating characteristics with values of PGAS parameters, showed that plasmatron power and spraying distance have the largest effect on (Ti, Cr)C–NiCr microhardness, moreover, the level of this effect is significantly more under conditions of spraying by supersonic jet.

3. Indices of heat content K_h in plasma jet and relative duration of process of particle staying in the jet K_τ were proposed for analysis of conditions of spraying process. Change of K_h from 2.9 to 5.6 kW·h/m^3 results in increase of microhardness and porosity of the coatings, rise of (Ti, Cr)C content in phase structure and reduction of chipping level under supersonic mode of spraying.

4. The best indices of (Ti, Cr)C–NiCr coating are received at plasmatron power 90 kW, 24 m^3/h consumption of plasma gas and 200 mm spraying distance. In this case, average microhardness of the coating makes HV0.05 12.6 GPa, maximum one is 19.14 GPa, porosity <1 % and chipping level makes 5 % at prevailing (Ti, Cr)C phase in the structure.

1. Borisov, Yu.S., Borisova, A.L. (1986) *Plasma powder coatings*. Kiev: Tekhnika.
2. Borisov, Yu.S., Kharlamov, Yu.A., Sidorenko, S.L. et al. (1987) *Thermal coatings from powder materials*: Refer. Book. Kiev: Naukova Dumka.
3. Toma, D., Brandtt, W., Marginean, G. (2001) Wear and corrosion of thermoalloy sprayed cermet coatings. *Surface and Coatings Technology*, **138**, 149–158.
4. Espallargas, N., Berget, J., Guilemany, J.M. et al. (2008) Cr_3C_2–NiCr and WC–Ni spray coatings as alternatives to hard chromium for erosion-corrosion resistance. *Ibid*., **202**, 1405–1417.
5. Fedrizzi, L., Rossi, S., Cristel, R. et al. (2004) Corrosion and wear behavior of HVOF cermet coatings used to replace hard chromium. *Electrochimica Acta*, **49**, 2803–2814.
6. Guilemany, J.M., Espallargas, N., Suegama, P.H. et al. (2006) Comparative study of Cr_3C_2–NiCr coatings obtained by HVOF and hard chromium coatings. *Corrosion Sci*., **48**, 2998–3013.
7. Sahoo, P., Raghuraman, R. (1993) High temperature chromium carbides reinforced metal matrix composite coatings for turbomachinery application. In: *Proc. of Thermal Spray Conf.* (Aachen, Germany, 1993), 296–300.
8. Takeuchi, J., Nakahira, A. (1993) Cr_3C_2–NiCr cermet coatings using some HVOF, APS and UPS process. *Ibid*., 11–14.
9. Beczkowiak, J., Fisher, J., Schwier, Y. (1993) Cermet materials for HVOF processes. *Ibid*., 32–36.
10. (2000) Powder solutions catalog. In: *Praxair Surface Technologies.*
11. (2011) Thermal spray materials. In: *Sulzer Metco Guide*.
12. Keller, H., Pross, E., Schwier, G. (2000) Influence of the powder type on the structure and the properties of chromium carbide. In: *H.C. Starck Nickel, Chromium Alloys. Specialist for Specialties*.
13. Vojtovich, R.F., Pugach, E.A. (1973) Peculiarities of high temperature oxidation of carbides of VI group transition metals. *Poroshk. Metallurgiya*, **4**, 59–64.
14. Gorbatov, I.N., Ilchenko, N.S., Terentiev, A.E. et al. (1991) Effect of cladding of double Ti-Cr carbide on properties of plasma coatings. *Fiz.-Khimich. Obrab. Materialov*, **3**, 81–85.
15. Gorbatov, I.N., Shkiro, V.M., Terentiev, A.E. et al. (1991) Examination of properties of thermal coatings from composite powders of nickel-titanium and chromium carbide. *Ibid*., **4**, 102–106.
16. Gorbatov, I.N., Panasyuk, A.D., Shvedova, L.K. et al. (1991) Thermal coatings on the base of titanium-chromium carbide. *Zashch. Pokrytiya na Metallakh*, Issue 25, 22–25.
17. Borisova, A.L., Chernets, A.I. (1993) Phase and structural transformations in powders of pure clad double titanium-chromium carbide in plasma jet. *Problemy Spets. Elektrometallurgii*, **3**, 63–72.
18. Rajtses, V.B., Litvin, V.M., Rutberg, V.P. et al. (1986) Wear-resistant plasma coatings based on Ti-Cr double carbide. *Poroshk. Metallurgiya*, **10**, 46–47.
19. Borisov, Yu.S., Petrov, S.V. (1993) Application of supersonic jets in technology of thermal spraying. *Avtomatich. Svarka*, **1**, 24–34.
20. Borisov, Yu.S., Fishman, S.L., Yushkov, V.I. et al. (1975) Cermet plasma coatings. In: *Inorganic and organic-silicate coatings*. Leningrad: Nauka.

Received 21.11.2014

FEATURES OF CHROMIUM FILLER MELTING DEPENDING ON LASER RADIATION PULSE SHAPE IN WELDING AND SURFACING PROCESSES

G.A. BAEVICH, V.N. MYSHKOVETS and **A.V. MAKSIMENKO**
Gomel Fr. Skorina State University
104 Sovetskaya Str., 246019, Gomel, Belarus. E-mail: rector@gsu.by

Laser technologies are becoming ever wider applied in modern industry in welding and surfacing of metals. Here control of filler material heating and melting, its transfer and formation on the item is important. Laser radiation shapes for filler material melting and transfer with its minimum evaporation have been established with application of mathematical modeling of thermal processes. Pulse front parameters are determined, which ensure minimum energy consumption for heating and melting of chromium filler. Obtained results can be used in development of procedures of pulsed laser welding and surfacing of metals and alloys. 8 Ref., 1 Table, 9 Figures.

Keywords: *laser surfacing, pulse shape, power density, pulse duration, filler material, chromium, thermodeformational melting, solidification, weld pool, energy consumption, temperature fields*

Extensive application of lasers in modern industry for metal welding and surfacing depends on solving a number of problems, which may include the need for development of high quality and efficient processes with the capability of their further automation.

Laser welding and surfacing of metals is accompanied by a set of concurrent processes, the main of which are thermal impact on the metal surface, thermodeformational melting and solidification of metal in weld pool volume. Development of technological processes, which use pulsed laser radiation and filler material in the form of wire, should take into account several features, influencing the nature of formation and dynamics of the melt in weld pool zone.

It is experimentally established that under the conditions of laser welding [1], ensuring reliable contact between the filler and base promotes transfer of molten filler metal to the base and welded joint formation. Problems in welded joint formation develop, when there is no contact between the filler and base. In this case, the formed melt stays on the filler and after the laser impact stops, it solidifies in the form of a sphere. This kind of problems are the most common in those technological processes, where an automatic machine is used to feed the filler wire. This leads to interruption of the surfacing process and deterioration of the produced coating quality.

One of the variants of solving such problems can be application of laser radiation pulses of a special shape, providing not only heating and melting of the filler, but also molten metal transfer to the base. The transfer process can be implemented due to formation of a section with higher radiation intensity in the pulse, the impact of which on the filler initiates the process of

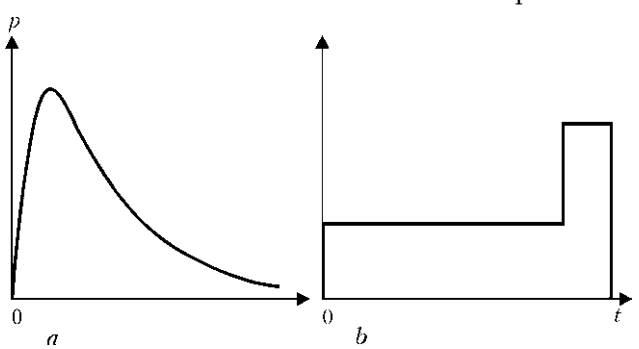

Figure 1. Laser pulses shaped in time (for *a* and *b* see the text)

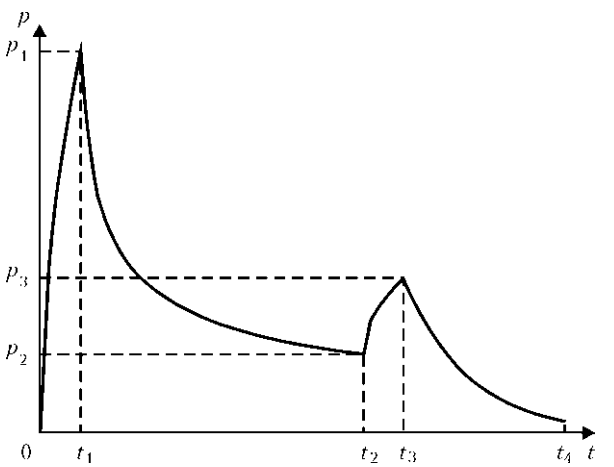

Figure 2. General view of time dependence of laser pulse power density

metal evaporation and generates the vapour recoil force, promoting molten metal separation from the filler wire.

Many batch-produced laser process systems use a pulse, the shape of which is shown in Figure 1, *a*. In this case, the maximum of laser radiation intensity fall to the pulse first part, and the decreasing trailing edge of this pulse does not create the conditions for molten metal separation from the filler wire.

Work [1] suggests using for filler material melting a pulse, the shape of which is given in Figure 1, *b*. Filler melting is performed by the pulse first part, and separation of the formed melt drop from the wire is provided by its second part. However, the nature of the dependence of power density on time imposes certain limitations at selection of the technological modes of the melting process.

The objective of this work was determination of the time and energy parameters of laser radiation pulse, ensuring filler material melting and transfer to the base with minimum metal evaporation in welding and surfacing processes.

It is proposed to use for this purpose a pulse, the shape of which is given in Figure 2. Pulse power density distribution in time can be presented as follows:

$$p(t) = \begin{cases} \dfrac{2T_{\text{m}}\lambda}{t_1\sqrt{\alpha\pi}}\sqrt{t}, \ 0 < t \le t_1, \\ \dfrac{2T_{\text{m}}\lambda}{t_1\sqrt{\alpha\pi}}(\sqrt{t} - \sqrt{t - t_1}), \ t_1 < t \le t_2, \\ \dfrac{2T_{\text{m}}\lambda}{(t_3 - t_2)\sqrt{\alpha\pi}}\sqrt{t - t_2 + q(t_2)}, \ t_2 < t \le t_3, \\ q(t_3)e^{\frac{t - t_3}{\tau}}, \ t_2 < t \le t_4, \end{cases}$$

where α is the filler material temperature conductivity; λ is the specific heat conductivity of filler material; T_{m} is the filler material melting temperature; $t_1 - t_4$ is the time of completion of the first-fourth pulse front, respectively; τ is the time of pulse front decrease.

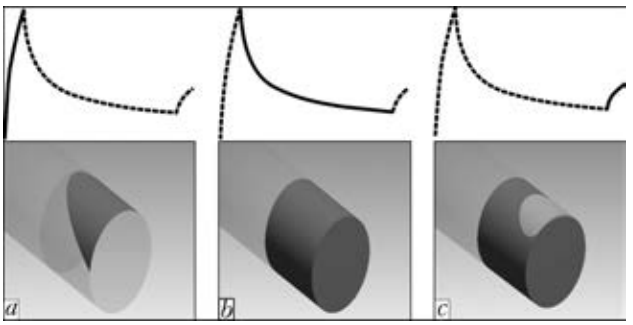

Figure 3. Schematic of laser radiation impact on filler material (for *a*–*c* see the text)

The pulse has a steep first front, reaching maximum value, which corresponds to power density, required for filler material surface melting in the zone of laser radiation impact (Figure 3, *a*), and decreasing second front, which ensures melting of the entire filler material volume (Figure 3, *b*) [2]. With steep third front, separation of molten filler material occurs under the impact of the recoil force, generated at metal evaporation from the melt surface (Figure 3, *c*). The fourth pulse front (see Figure 2), as a result of relatively slow decrease of radiation intensity, promotes the molten metal filling a recess, formed in the pulse initial part, as well as formation of the deposited bead before the moment of the start of metal solidification [3].

To determine the parameters of a pulse, ensuring melting and transfer of filler material to the base with minimum evaporation of metal, it is necessary to synchronize the time of initiation of the evaporation process and time to complete melting of filler material in the area of laser radiation impact. During investigations modeling of the process of laser surfacing with chromium filler wire of 0.2–0.4 mm diameter of base a of the same material, was performed. Temperature

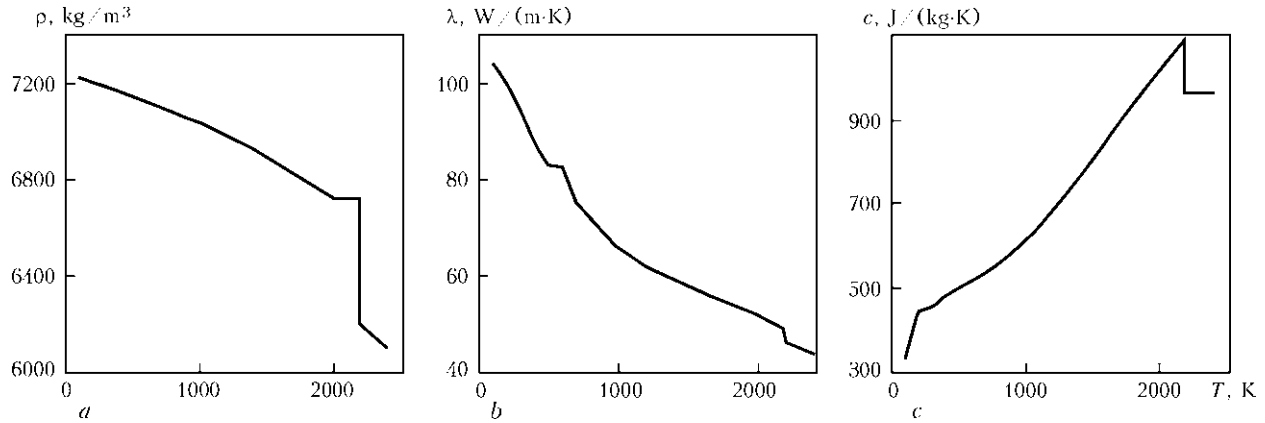

Figure 4. Temperature dependence of chromium thermophysical properties: *a* — density; *b* — specific heat conductivity; *c* — specific heat capacity

Time energy parameters of pulse first and second front

Filler surface temperature, °C	Peak power density $p_1 \cdot 10^{10}$, W/m^2	Duration of pulse second front$\cdot 10^{-3}$, s	Pulse energy$\cdot 10^{-3}$, J		Total energy of the first two fronts$\cdot 10^{-3}$, J
			First front	Second front	
2000	7.88	22.5	13.5	129.5	143.0
2100	8.27	16.5	14.2	108.9	123.1
2200	8.67	11.2	14.9	91.8	106.7
2300	9.06	7.7	15.5	77.4	92.9
2400	9.46	5.7	16.2	67.7	83.9
2500	9.85	4.0	16.9	16.9	77.7

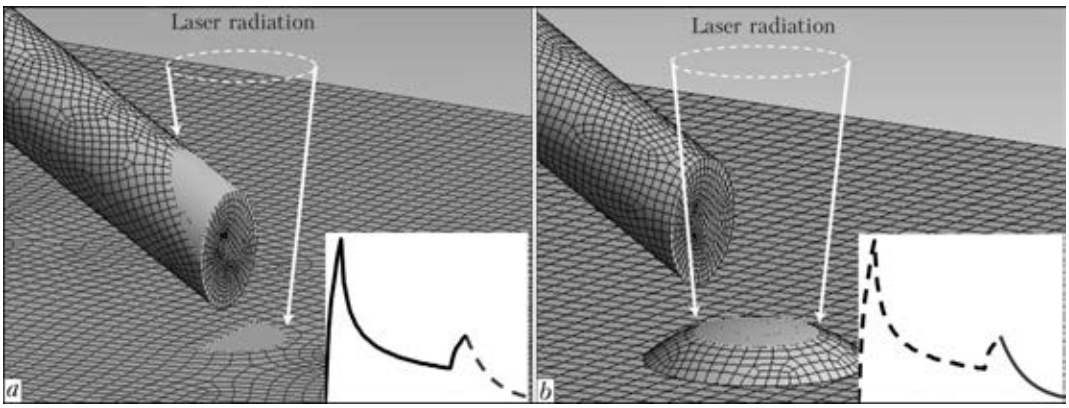

Figure 5. Finite element discretization and schematic of laser radiation impact on the surface of both filler and base (*a*) and deposited bead surface (*b*)

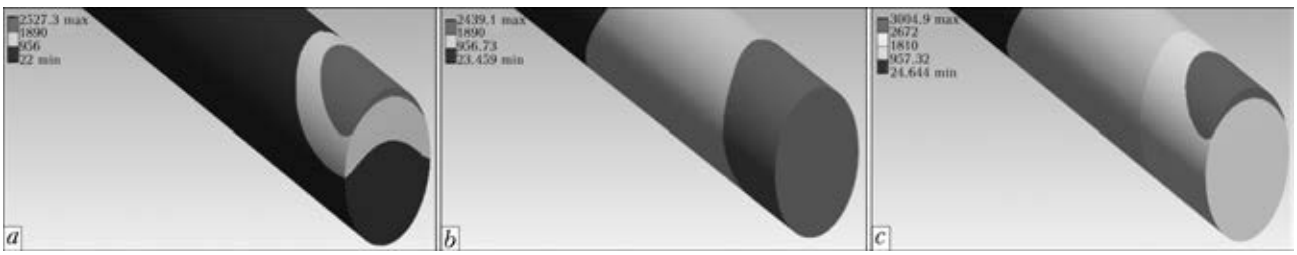

Figure 6. Temperature field distribution in chromium filler of 0.2 mm diameter: *a* — t_1 = 0.5; *b* — t_2 = 4.0; *c* — t_3 = = 4.5 ms

fields were calculated within 3D finite element model, which solved the nonlinear equation of heat conductivity [4–7]. Nonlinearity of the equation is due to temperature dependence of material thermophysical properties (Figure 4) [8]. Laser radiation power density distribution over the beam cross-section was considered to be uniform (see the expression, given above).

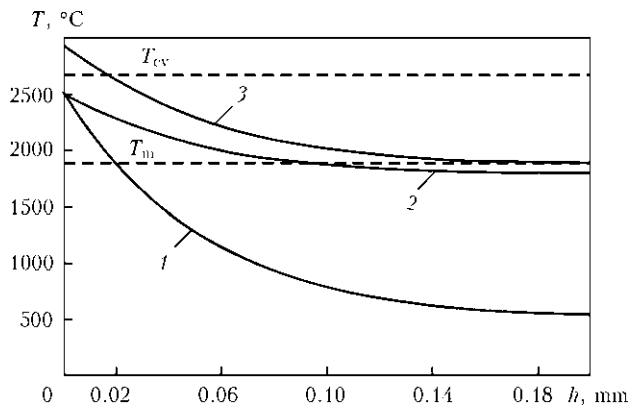

Figure 7. Temperature distribution by filler depth at specified moments of time: *1* — t_1 = 0.5; *2* — t_2 = 4.0; *3* — t_3 = 4.5 ms

Finite element discretization and schematic of laser radiation impact on the surface of the filler and base are given in Figure 5. Laser beam is focused so that 50 % of the energy is consumed by the filler, and 50 % — by base metal (Figure 5, *a*). During time $0 < t \le t_2$ the filler metal in the area of laser radiation impact is heated and melted; at moment of time t_3 melt drop under the impact of gravity and recoil force, generated at metal evaporation from the surface, separates from the filler, drops onto the base and spreads over it. Fourth front of laser pulse during time $t_3 < t \le t_4$ promotes deposited bead formation (Figure 5, *b*).

During investigations energy parameters of the first two pulse fronts, shown in the Table,

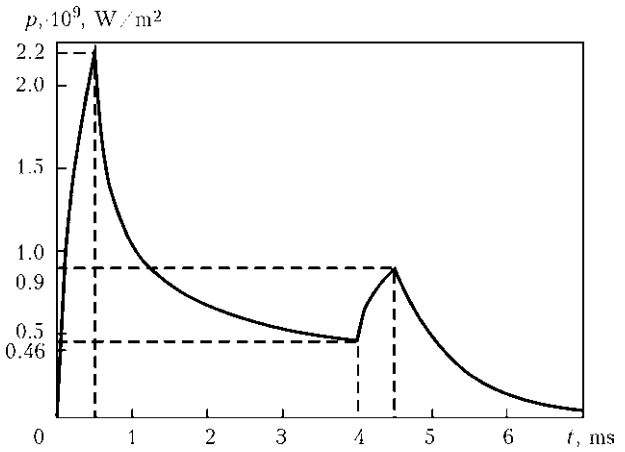

Figure 8. Pulse shape of focused laser radiation for melting 0.2 mm diameter chromium filler

have been determined, which have a significant influence on the dynamics of filler material heating up to temperature T ($T_m \le T < T_{ev}$).

As is seen from tabulated data, minimum energy consumption ($77.7 \cdot 10^{-3}$ J) for metal heating and melting in the area of impact of the first two fronts of laser radiation pulse (see Figure 3) is ensured at second front duration of $4 \cdot 10^{-3}$ s. In this case, the filler surface temperature is equal to 2500 °C.

Thus, optimization of the processes of filler material heating and melting can be implemented by changing the time and energy characteristics of the first two fronts of laser radiation pulse.

Distributions of temperature fields in 0.2 mm chromium filler wire at moments of time, corresponding to ends of pulse fronts, are shown in Figure 6. So, at the moment of time t_1 = 0.5 ms the filler is molten to the depth of 0.02 mm (Figures 6, *a* and 7), at t_2 = 4 ms the melting depth is equal to 0.09 mm (Figures 6, *b* and 7), at t_3 = = 4.5 ms the volume of filler metal in the area of laser radiation impact melts completely, and melt surface is heated up to evaporation temperature (Figures 6 *c* and 7).

Thus, conducted studies allowed establishing the shape of time and energy parameters of laser radiation pulse for melting 0.2 mm chromium filler (Figure 8). Moreover, melting of 0.2–0.4 mm filler material is ensured due to application of this pulse shape, and is implemented by

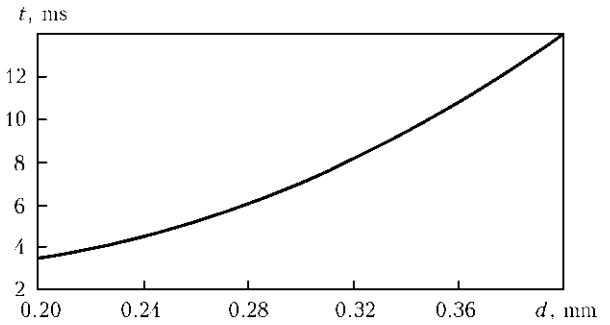

Figure 9. Dependence of second front duration of laser radiation pulse on filler diameter

selection of the pulse second front duration (Figure 9).

Conclusions

1. Laser radiation pulse shape has been established for filler material melting and transfer to the base with minimum metal evaporation.

2. Parameters of the first two pulse fronts are determined, which ensure minimum energy consumption for chromium filler heating and melting.

3. Study results can be used in development of process modes of pulsed laser welding and surfacing of metals and alloys.

1. Jeric, A., Grabec, I., Govekar, E. (2009) Laser droplet welding of zinc coated steel sheets. *Sci. and Technol. of Welding and Joining*, 14(**4**), 362–368.
2. Kayukov, S.V. (2000) Enhancement of pulsed YAG-lasers of millisecond duration range in welding technology. *Kvant. Elektronika*, 30(**11**), 941–948.
3. Grigoriants, A.G., Shiganov, I.N., Misyurov, A.I. (2006) *Technological processes of laser treatment*. Moscow: N.E. Bauman MGTU.
4. Tseng, W.C., Aoh, J.N. (2013) Simulation study on laser cladding on preplaced powder layer with a tailored laser heat source. *Opt. and Laser Technol.*, **48**, 141–152.
5. Myshkovets, V.N., Maksimenko, A.V., Baevich, G.A. (2012) Modeling of pulsed laser welding process of thin-wall structures of aluminium alloys. *Materialy. Tekhnologii. Instrumenty*, **3**, 16–20.
6. Farnia, A., Ghainia, F.M., Sabbaghzadeh, J. (2013) Effects of pulse duration and overlapping factor on melting ratio in preplaced pulsed Nd:YAG laser cladding. *Opt. and Lasers in Eng.*, **51**, 69–76.
7. Mumtaz, K.A., Hopkinson, N. (2010) Selective laser melting of thin wall parts using pulse shaping. *J. Mater. Proc. Technol.*, **210**, 279–287.
8. Zinoviev, V.E. (1989) *Thermophysical properties of metals at high temperatures*: Refer. book. Moscow: Metallurgiya.

Received 23.12.2014

THERMODYNAMIC PROPERTIES OF MELTS OF CaO_2–SiO_2 SYSTEM

I.A. GONCHAROV[1], **V.I. GALINICH**[1], **D.D. MISHCHENKO**[1] and **V.S. SUDAVTSOVA**[2]
[1]E.O. Paton Electric Welding Institute, NASU
11 Bozhenko Str., 03680, Kiev, Ukraine. E-mail: office@paton.kiev.ua
[2]I.M. Frantsevich Institute of Problems of Materials Science, NANU
3 Krzhizhanovsky Str., 03680, Kiev, Ukraine

Given is the analysis of literature data on the phase equilibriums of constitutional diagrams and thermodynamic properties of alloys of calcium oxide–silicon oxide system. It was found that data on activities of components of these melts are characterized by high scattering. The activity of calcium oxide and silicon oxide in eutectic melt were calculated from coordinates of liquidus line of constitutional diagram of calcium oxide–silicon oxide system. It was established that the calcium activity at silicon concentration of more than 0.2 shows the negative deviations from perfect solutions and correlates with experimentally established data. Activity of silicon oxide at silicon concentration of less than 0.5 in eutectic melt shows the large negative deviations from perfect solutions and correlates with experimentally established ones. At concentration of silicon oxides of 0.34 the activity of silicon oxide is 0.03, i.e. it is by one order lower than its concentration in solution that is explained by the formation of thermodynamically stable two-calcium silicate. At 725 °C α–γ transformation occurs in this compound, accompanied by change in volume. Therefore, it is recommended to keep such ratio of calcium and silicon oxides in the composition of fluxes for electroslag remelting of hollow ingots and welding, at which two-calcium silicate will be formed in the melt. These fluxes will have a poor interaction with molten metal and provide the excellent removal of solidified slag from the surface of ingot and weld metal. 17 Ref., 1 Table, 3 Figures.

Keywords: *calcium oxide, silicon oxide, constitutional diagram, activity of melt components, fluxes for welding and electroslag remelting*

In mechanized electric arc welding, surfacing, as well as in electroslag remelting (ESR) of steels the slags of $CaO–Al_2O_3–CaF_2$ are widely used. These slags provide usually requirements specified for them as to metallurgical properties, however in this case their technological properties are not rather high. Adding of SiO_2 into $CaO–Al_2O_3–CaF_2$ system improves their forming properties, but they increase their chemical activity as applied to melts on iron base. The result of interaction of SiO_2, with molten metal is the silicon reduction process, which leads to enrichment of weld metal with non-metallic silicate inclusions. The intensity of the mentioned reactions is proportional to thermodynamic activity of SiO_2 in the slag melt. Therefore, the evaluation of the latter is quite important in selection of compositions of fluxes for ESR and welding.

Taking into account the high aggressiveness and refractoriness of oxide-fluoride melts, the experimental methods of their investigations are rather complex. During recent years the theoretical methods of prediction of thermodynamic properties of these melts are developed by using similar data for solid compounds and phase equilibriums. To predict the thermodynamic properties of $CaO–Al_2O_3–CaF_2–SiO_2$ slag system and ternary systems, included into it, it is necessary to carry out the prediction of corresponding binary systems. Earlier we investigated $CaO–Al_2O_3$ system [1]. The subject of this work is the thermodynamic properties of $CaO–SiO_2$ system.

Alloys of $CaO–SiO_2$ system represent a great interest for welding and special metallurgy, as they are a base for a number of welding fluxes and refining slags. As the melts of this system have also importance for production of ferrous metals and steels, they serve as an object of many experimental and theoretical investigations [2–14].

To judge about the reactions of interaction of the slag with metallic melts in welding and during metallurgical processes, the information is necessary about their thermodynamic properties, among which the activity of alloy components, heat of formation of compounds and melts are very important. For example, in works [2–10] the activities of silicon dioxide were determined, while in works [3–5, 8–10] the activities of calcium oxide in the range of 1500–1930 °C temperatures were determined. Here the methods of electromotive forces (EMF), high-temperature calorimetry, heterogeneous equilibriums between slags and gas, as well as sulfide capacity

of slags and Knudsen effusion mass-spectrometry were used. The thermodynamic modeling was used also for melts of this system by using the quasi-chemical theory [11], modified quasi-chemical theory [12] and method CALPHAD. As these reactions of interaction between slag and steel in fusion welding proceed at 1800–2300 K, in work [2] the determination of SiO_2 activity in melts of $CaO–SiO_2$ system was made at higher temperatures than it was done earlier. The activity of SiO_2 was measured by EMF method at temperature 2200 K, and at 1960 K the heat (enthalpy) of formation of $CaO–SiO_2$ melts was studied.

To determine SiO_2 activity in above-said melts by EMF method, a concentration element with ion transfer was manufactured in work [2] in the form

$$W, Si–Sn \mid SiO_2 \parallel CaO–SiO_2 \mid Si–Sn, W. \quad (1)$$

SiO_2 activity was calculated from the obtained EMF values. Results of calculation are given in the Table and Figure 1.

In Figure 1 the obtained values of SiO_2 activities [2] were compared with data given in other sources [3–9]. These data are only qualitatively correlated between themselves showing alternate deviations from perfect melts that is correlated with their behavior in a solid state. Data [2] correlate with the main number of literature data, but have less deviation from perfect melts. It is probably caused by the higher temperature of making measurements, at the increase of which, as is known, the inter-particle interaction is decreased.

The comparison of available data on activities of components of melts of $CaO–SiO_2$ system allowed establishing that only in works [8, 10] they were determined at close temperatures (1903 and 1933 K) and have a quite good correlation between themselves (Figure 2).

To determine validity of these data and to describe mostly correctly the thermodynamic properties of molten alloys of $CaO–SiO_2$ system, the coordinates of liquidus of constitutional diagram of this system were used and using the procedure developed by us [15], the a_{CaO} was calculated in eutectic melt with $x_{CaO} = 0.295$. This value is correlated with those experimentally found in works [8, 10] (see Figure 2).

As is seen from Figure 2, the activities of silica in melts of $CaO–SiO_2$ system reveal the alternate deviations from Raoult's law. In melts of this system with $x_{SiO_2} < 0.65$ the SiO_2 activity is characterized by negative, and at $x_{SiO_2} > 0.65$ by more positive deviations form perfect solutions.

Activity of silicon dioxide in melts of $CaO–SiO_2$ system [2]

Molar fraction of SiO_2 in melt $CaO–SiO_2$	EMF, mV	a_{SiO_2}, molar fraction
0.675	11	0.786 ± 0.002
0.604	16	0.712 ± 0.002
0.503	53	0.325 ± 0.001
0.393	85	0.166 ± 0.001

This is correlated with behavior of melts in solid state. In silicate-silica alloys enriched with SiO_2 there is a large region of delamination. And vice-versa, in alloys with $x_{SiO_2} < 0.65$ in solid state two compounds are formed, one of which (Ca_2SiO_4) is very refractory and melted congruently. It is seen from Figure 2 that in melts at $x_{SiO_2} > 0.4$ the activity of SiO_2 is by one order lower than its molar fraction in perfect solution and, consequently, they will poorly interact with weld pool metal. This is explained with the formation of congruently melted compound Ca_2SiO_4, in which compound $2CaO·SiO_2$ is formed, that stipulates the significant reduction of activities of both components. According to the constitutional diagram of $CaO–SiO_2$ system this compound is melted at very high temperature (2130 °C). Thus, in fluxes on base of $CaO–SiO_2$ system the content of silica should be less than 0.4 molar fractions. This can decrease the harmful effect of silica in melts of $CaO–SiO_2$ system and

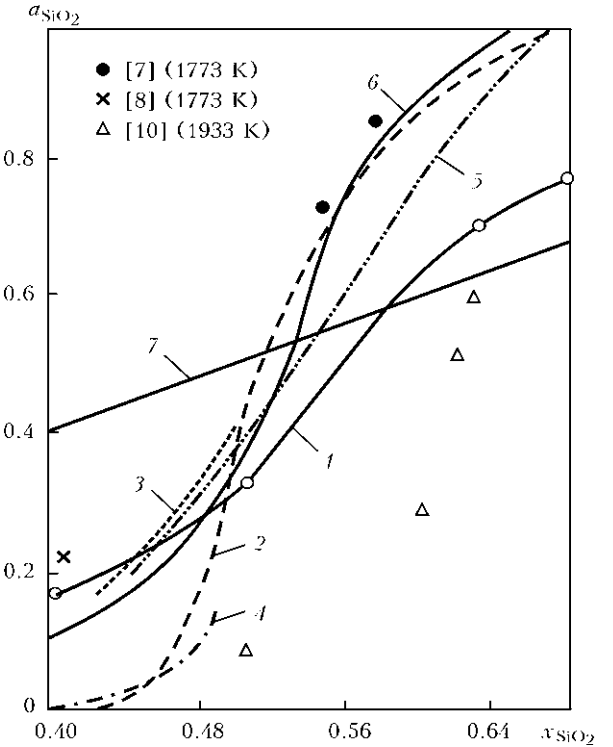

Figure 1. Activity of silicon dioxide in melts of $CaO–SiO_2$ system: *1* — data of work [2] (2200 K); *2–5* — [3–6] (1873 K); *6* — [9] (1773 K); *7* — perfect solution

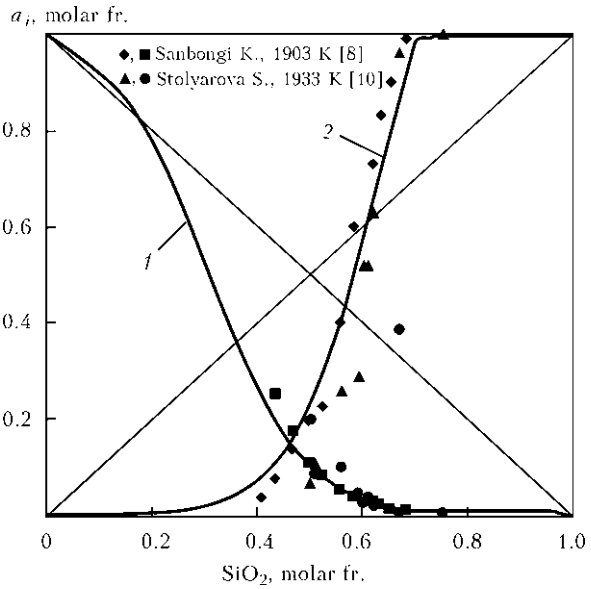

Figure 2. Activity of components in melts of $CaO–SiO_2$ system: *1* — activity of CaO, calculation by constitutional diagram, 2000 K; *2* — the same, activity of SiO_2

in multicomponent slags on metallurgical and technological properties of fluxes.

By the present time the heat of formation of melts of $CaO–SiO_2$ system was not almost studied. In work [2] the heat (enthalpy) of formation of these melts was investigated by the method of calorimetry to have a complete idea about their nature. The calorimetric cell, mixer and housing of thermocouple were manufactured of molybdenum, which did not interact with the melts being studied. The investigation was made at temperature 1960 ± 15 K. Calibration of calorimeter was made by specimens, manufactured of molybdenum, tungsten or tin (all these metals do not interact with melts of $CaO–SiO_2$ system). During experiments the alloy of required composition was place into calorimetric pool, and then the samples of SiO_2 and CaO in solid state were added to it from drum-type proportioning device. The powder-like calcium oxide was placed preliminary into ampoules, manufactured of tin or copper foils. The obtained data on partial and integral molar enthalpies of components with calculated confidence intervals are given in Figure 3.

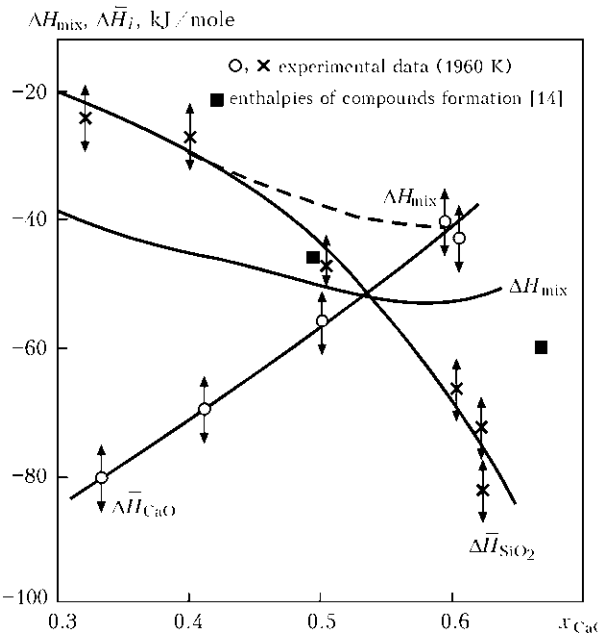

Figure 3. Partial and integral enthalpies of mixing of melts of $CaO–SiO_2$ system: solid curves — approximating curves for ΔH_i and ΔH_{mix} [2]; dashed curves — calculation [11]

The Figure gives also the values of ΔH_{mix}, calculated by the modified variant of quasi-chemical theory [14]. It is seen that between data of works [2, 11] there is a qualitative correlation. Comparison of definite thermodynamic properties of melts of $CaO–SiO_2$ system with constitutional diagram showed that they have a good correlation.

For melts containing more than 0.3 molar fractions of CaO, the enthalpies of mixing are the negative values. Minimum on the curve of dependence ΔH_{mix} on composition is 52 kJ/mole and corresponds to the melt close to the congruently melted compound $CaSiO_3$.

We compared the integral enthalpies of formation of melts and compounds of $CaO–SiO_2$ system determined in work [14] in the calorimeter of dissolution. It is seen that they have a good correlation.

So, for binary system $CaO–SiO_2$ the positive deviations from perfectness (with region of delamination of given temperatures), are typical for alloys with $x_{SiO_2} > 0.5$. At the lower content of SiO_2 these deviations become negative (that correlates with formation of stable solid compounds). The highest negative values are reached in the fields of solidification of such complex compound as $2CaO·SiO_2$. It is thermodynamically stable, i.e. it will have a poor interaction with metal in welding and ESR. This is confirmed by results of our calculations of SiO_2 activity.

Thus, it is possible to select the zone of slag melt compositions, where SiO_2 activity will be minimal and proceeding of processes of interaction with metal will be limited. This analysis was made. It was found that from the point of view of providing the best forming properties of the flux the formation of $2CaO·SiO_2$ in the melt will be most priority. Two-calcium silicate has the melting temperature 2130 °C, i.e. at this temperature the solid phase $2CaO·SiO_2$ in molten slag melt will form. The presence of the solid phase in the liquid solution will lead to the change of properties, in particular, to the increase in effective toughness that is the positive factor from the point of view of weld formation in weld-

ing at forced conditions and in ESR in a movable mould. The investigation of melts of $CaO–SiO_2–MgO–Al_2O_3–CaF_2$ system carried out by Park [16] showed that adding of CaF_2 into composition of oxide melt allows decreasing the solidus temperature of the melt, decreasing the size of solid-phase constituent in the molten slag melt. Thus, there are potentialities for control of constitution and properties of the slag melt.

In addition, the formation of $2CaO·SiO_2$ in the melt is positive from the point of view of providing the better slag removal from the metal surface. It is known [17] that at 725 °C the $\alpha–\gamma$ transformation takes place in this compound, which is accompanied by the change in volume. As a result the significant local stresses occur in the slags, which become the cause of self-disintegration of slags. This effect is very important first of all for the technology of ESR of hollow ingots, where the problem of slags removal from ingot inner surface is very acute.

Conclusions

1. The carried out critical analysis of literature data on phase equilibriums and thermodynamic properties of alloys of $CaO–SiO_2$ system made it possible to establish that the constitutional diagram is correct and activity of components of these melts are characterized by large scattering.

2. It is shown that integral enthalpies of formation of melts and compounds of $CaO–SiO_2$ systems, determined experimentally in isoperibolic calorimeter and calorimeter of dissolution, correlate between themselves.

3. From the coordinates of liquidus line of constitutional diagram of $CaO–SiO_2$ system determined by different authors were a_{CaO} calculated in eutectic melt with $x_{CaO} = 0.295$. It was found that it has large negative deviations from perfect solutions and correlates with experimentally established ones.

4. From the coordinates of liquidus line of constitutional diagram of $CaO–SiO_2$ system, determined by different authors, a_{SiO_2} were calculated. It was found that at $x_{SiO_2} < 0.5$ and in eutectic melt it shows the large negative deviations from perfect solutions and correlates with earlier experimentally established ones. At $x_{SiO_2} = 0.34 a_{SiO_2}$ it amounts to 0.03, i.e. the activity of SiO_2 is by one order lower of its concentration in solution. This is explained by the formation of thermodynamically stable compound $2CaO·SiO_2$. Taking into account that at 725 °C the $\alpha–\gamma$ transformation occurs in this compound, accompanied by changing volume, the namely such ratio of calcium oxides and silicon can be recommended in the composition of fluxes for ESR of hollow ingots and welding. These fluxes will poorly interact with molten metal and provide an excellent removal of solidified slag from the surface of ingot and weld metal.

1. Goncharov, I.A., Galinich, V.I., Mishchenko, D.D. et al. (2014) Prediction of thermodynamical properties of melts of $CaO–Al_2O_3$ system. *The Paton Welding J.*, **4**, 26–29.
2. Sudavtsova, V.S., Kiriakov, V.M., Podgaetsky, V.V. (1988) Thermodynamical properties of $CaO–SiO_2$ melts. *Avtomatich. Svarka*, **7**, 35–37.
3. Richardson, F.D., Jeffes, H.E., Withers, G. (1950) Thermodynamic data on materials which are important for steel production. *J. Iron and Steel Inst.*, 166(**2**), 213–234.
4. Fincham, C.J.B., Richardson, F.D. (1954) Behaviour of sulphur in silicate and aluminate melts. *Proc. Roy. Soc. Sec. A*, 233(**1**), 40–62.
5. Fullton, J.C., Chipman, J. (1954) Slag-metal-graphite reaction and silica activity in limestone-alumina-silicate slags. *Transact. of Amer. Inst. Min. Met. Eng.*, 200(**9**), 1136–1146.
6. Murray, P., White, K. (1948) SiO_2 activities in molten $CaO–SiO_2$ system. *Disc. Faraday Soc.*, 4(**3**), 287–296.
7. Chang, L.C., Derge, G. (1947) Sampling and analysis in determination of hydrogen in steels. *Transact. of Amer. Inst. Min. Met. Eng.*, 172(**1**), 90–120.
8. Sanbongi, K., Othani, M. (1952) Measurement of the equilibrium among silicon in molten iron, $CaO–SiO_2$ binary slag and $H_2–H_2O$ mixed gas. *Sci. Rep. Tohoku Univ.*, 4(**1**), 59–71.
9. Carter, P.T., Macfarlane, T.G. (1957) Thermodynamics of slag systems. Pt 2: Thermodynamic properties of $CaO–SiO_2$ slags. *J. Iron and Steel Inst.*, 173(**1**), 62–66.
10. Stolyarova, V.L., Shornikov, S.I., Ivanov, G.G. et al. (1991) High-temperature mass spectrometric study of thermodynamic properties of the $CaO–SiO_2$ system. *J. Electrochem. Soc.*, 138(**12**), 3710–3714.
11. Pelton, A.D., Blander, M. (1986) Thermodynamic analysis of liquid solutions by a modified quasichemical approach — Application to silicate slag. *Met. Transact. B*, **7**, 805–815.
12. Hillert, M., Sundman, Bo., Wang, X. (1990) An assessment on the $CaO–SiO_2$. *Met. Transact. B*, **4**, 303–312.
13. Ayed, F., Sorrentino, F., Castanet, R. (1994) Determination par calorimetrie de dissolution des enthalpies de formation de quelques silicates, aluminates et alumino-silicates de calcium. *J. Thermal Anal.*, **41**, 755–766.
14. Sryvalin, I.T., Esin, O.A. (1970) Application of quasichemical theory for calculation of thermodynamic properties of alloys of silicate melts. In: *Physical chemistry of molten slags*, 83–94. Kiev: Naukova Dumka.
15. Sudavtsova, V.S., Makara, V.A., Kudin, V.G. (2005) *Thermodynamics of metallurgical and welding melts*. Pt 3: Alloys on the base of nickel and tin, methods of modeling and prediction of thermodynamic properties. Kyiv: Logos.
16. Park, J.H. (2007) Solidification structure of $CaO–SiO_2–MgO–Al_2O_3$ ($–CaF_2$) systems and computational phase equilibria: Crystallization of $MgAl_2O_4$ spinel. *Computer Coupling of Phase Diagrams and Thermochemistry*, **31**, 428–437.
17. (1995) *Slag atlas*. 2nd ed. Duesseldorf: Verlag.

Received 30.10.2014

TECHNOLOGY OF MANUFACTURING HIGH-QUALITY WELDED TUBES FROM CORROSION-RESISTANT STEEL IN UKRAINE

T.N. BURYAK[1], **I.A. KATSAJ**[2], **V.G. KUZNETSOV**[2], **A.I. NOVIKOV**[2], **A.A. TARANENKO**[1] and **N.V. YAROSHENKO**[1]
[1]SE «NITI»
1a Pisarzhevsky Str., 49005, Dnepropetrovsk, Ukraine. E-mail: lab241@i.ua
[2]«ALFA-FINANS» Ltd.
4g Barrikadnaya Str., 49000, Dnepropetrovsk, Ukraine. E-mail: igor_ka68@mail.ru

Welded thin-walled tubes are widely applied in different industrial sectors owing to a number of their advantages, compared to seamless tubes. The paper describes the experience of mastering in Ukraine manufacturing of thin-walled small diameter tubes from TR 316L steel by two variants: with weld metal deformation by rolling-off and without deformation. Longitudinal welds are made by TIG welding. The paper gives the results of comprehensive testing of manufactured tube samples, which are indicative of the fact that they are not inferior to seamless tubes as to their technological and mechanical properties, corrosion resistance and metallographic characteristics, and are even superior to them by a number of parameters. They meet the requirements of the respective ASTM and EN standards. 10 Ref., 4 Tables, 4 Figures.

Keywords: *welded tube, technology, argon-arc welding, weld, quality, mechanical properties, intercrystalline corrosion, nuclear steam condensers*

Welded superthin-wall tubes from corrosion-resistant steel of TR 321/321H, TR 304/304L, TR-316L/316Ti grades to standards [1–3] are widely applied abroad in heat-exchanger equipment, in particular in turbine condensers in nuclear and heat generation, and in chemical industry. Domestic welded tubes supplied earlier to [4] were significantly inferior to them by a number of reasons: lower production standards because of unsatisfactory quality of the weld, lack of equipment for manufacturing, heat treatment and nondestructive testing of extended tubes, deficit of quality strip blank of up to 1 mm wall thickness, etc.

Historically, this resulted in lack of trust for welded tubes from corrosion-resistant steels, particularly, molybdenum-containing steels of 03Kh17N13M3 and 08Kh17N13M2T type. Therefore, in a number of cases, preference was given to other materials: seamless tubes from less expensive material (copper, copper-nickel alloys) or general purpose seamless tubes from corrosion-resistant steel of 08–12Kh18N10T type, supplied to different GOSTs. However, in NPP condensers replacement of tubes for welded ones from molybdenum-containing TR 316L/316Ti steels or of titanium was performed long ago practically all over the world [1, 5, 6]. The process of these tube manufacturing is highly efficient, and ensures lowering of welded tube cost compared to seamless tubes from similar steel by 30–35 %. Up to now, however, information on the quality of Ukrainian tubes, produced under modern conditions, remained rather limited. Therefore, in this work, comprehensive studies of welded tubes from a local manufacturer have been performed.

Under production conditions of ALFA-FINANS Ltd. (Dnepropetrovsk), a technology has been developed, by which electrically welded straight-seam tubes of 20 mm diameter with 0.8 mm wall thickness and up to 15 m length are manufactured from strip blank from corrosion-resistant steel TR 316L by two variants: with weld deformation (by rolling-off) in keeping with the requirements of ASTM A 249 standard (variant «r»), and without weld deformation (variant «n») that is allowed by local normative documents. Inert-gas nonconsumable-electrode welding (TIG), namely argon-arc welding, with weld factor $V = 1$ is applied.

Modern technology of welding fabrication by TIG process emerged at the beginning of 1940s and was used for welding aluminium and magnesium alloys [7]. This method, however, was the most profoundly perfected for welding corrosion-resistant steels and alloys. In TIG welding the electric arc is used for heating and melting metal edges, while shielding gas (argon), which is supplied from the gas nozzle, is fed into the

welding zone, as well as on the tube inner surface and protects the weld from contamination penetration from the outside that promotes good penetration of the weld root. This welding process was later on called argon-arc welding. The electrode/cathode proper, made from refractory material (tungsten), is located in the center of the gas nozzle at a certain distance from the edges of metal being welded. Under the modern conditions of electric-welded tube manufacture, welding is performed automatically by three cathodes, ensuring melting, formation and maintaining of the so-called metal «pool» with uniform filling along the entire weld depth, without feeding any filler materials into the welding zone. Application of multiarc welding of the longitudinal weld in a chamber with protective atmosphere (argon) ensures its high quality, as in this case the parent metal composition is preserved completely in the weld structure. The advantage of argon-arc (TIG) welding is very high quality of the weld, absence of spatter, practical absence of slags or impurities. This process is highly versatile and allows application of variants of different current and gas mixture settings in welding austenitic, molybdenum, as well as ferritic steel grades with 0.4 to 3.0 mm metal thickness.

Tube manufacturing technology. Tube manufacturing technology consists of the following operations:

1. In-coming inspection of the quality of fed cold-rolled coiled stock, which was pre-cut in longitudinal cutting machine that includes random visual inspection, continuous monitoring of geometrical dimensions and verification of compliance of quality certificate data.

2. Manufacturing tubes in electric-weld tube mills TESA 5-25 and TESA 10-60 (Italy) (Figure 1) includes the following sequence of operations: strip forming in the forming mill; edge welding in the welding assembly; eddy current testing of the quality of weld and HAZ; grinding outer and/or rolling-off the inner flash and tube calibration.

3. Tube heat treatment in shielding atmosphere (hydrogen).

4. Eddy current testing of tube body quality.

5. Grinding the tube outer surface as required by the user.

6. Tube marking using automatic jet printer.

7. Tube cutting up to specified length in flying shears.

8. Tube acceptance by QID, performance of testing specified by standards.

9. Tube packing.

10. Executing a quality document and required shipping documentation; tube shipping to user in keeping with the order.

The above-mentioned electric-weld tube mills allow manufacturing tubes of 5.0 up to 60.3 mm

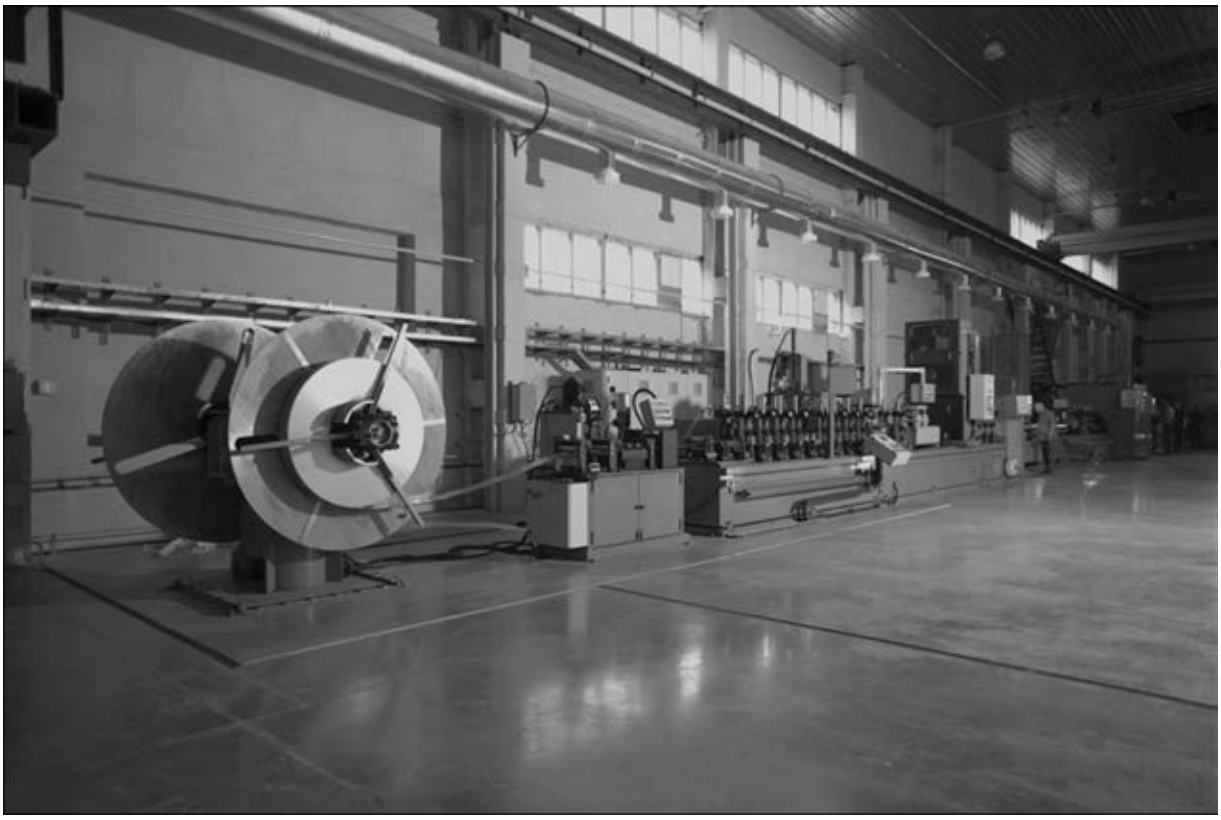

Figure 1. Appearance of electric-weld pipe line (mill 10-60) in the tube manufacturing shop

Table 1. Composition of studied samples of initial strip and ∅20 × 0.8 mm welded tubes from TR 316L steel (wt.%)

Sample	C	Cr	Mn	Mo	Ni	P	S	Si
Strip	0.011	16.79	1.18	1.91	10.05	0.042	0.0099	0.477
To certificate	0.012	16.63	1.11	2.092	10	0.043	0.001	0.51
Tube «r»	0.015	16.77	1.17	1.94	10.07	0.044	0.012	0.494
Tube «n»	0.016	16.89	1.19	1.91	9.94	0.044	0.012	0.49
Norms of EN 10217-7 (1.4404)	max 0.03	16.5–18.5	max 2	2.0–2.5	10–13	max 0.045	max 0.015	max 1
Norms of ASTM A (TR 316L)	max 0.03	16–18	max 2	2–3	10–14	max 0.045	max 0.030	max 1

Notes. 1. Measurement error by molybdenum is equal to 0.08 %; in finished products deviation by molybdenum of ±0.1 % is allowed as per EN 10217-7. 2. Measurement error by nickel is equal to 0.11 %; in finished products deviation by nickel of ±0.15 % is allowed as per EN 10217-7.

outer diameter inclusive with 0.4 to 3.0 mm wall thickness and up to 15 m length.

All over the world welded tubes for condensers are most often supplied to standard [2]. Tubes studied in this work have been manufactured and tested in keeping with the main requirements of this standard. For illustration purposes evaluation of the obtained results was performed, allowing for European norms [8], as well as other norms, currently available for this kind of tubes.

As a set of high requirements are applied to tubes, we will include them into the category of precision items. Steel TR 316L and its analogs 03Kh17N14M3 and 1.4404, by the totality of their corrosion resistance, technological and thermophysical characteristics are regarded to be optimum for condenser and heat exchanger equipment, operating in aggressive media [6, 9, 10].

Investigations were performed at the facilities of Testing Center of SE «NITI», accredited for technical competence to DSTU ISO/IEC 17025:2006, for which purpose an integrated approach was applied. First, direct in-coming inspection of the initial blank (strip) for compliance to technical requirements of ASTM A 240 standard for thin strip and sheet was performed.

Analysis of chemical composition. It was established that metal belongs to steel of TR 316L grade to ASTM and its analog 1.4004 to EN norms (Table 1). Metal has rather low carbon content that is beneficial for corrosion resistance. Here, as a result of processing, carbon content in tubes rose slightly, compared to strips. It should be noted that phosphorus content is on the upper level, and content of expensive nickel and molybdenum is on the lower limit.

Table 2. Geometrical dimensions of studied ∅20 × 0.8 mm tubes

Manufacturing variants	Outer diameter D_{out}, mm	Wall thickness S, mm
«r»	19.94–20.01 19.93–20.02	0.77–0.79 0.78–0.80
«n»	19.93–20.03 19.94–20.02	0.77–0.79 0.78–0.80
Norms of ASTM for this size	19.90–20.11	0.72–0.88

Note. Tube ovality is 0.07–0.10 mm at norms from +0.11 up to −0.10 mm.

Visual inspection of tubes. Examination without magnifying devices showed that the surface is light-coloured, clean, and no inadmissible defects of the type of cracks, deep scratches, films, sticking, cavities, delaminations, etc. have been detected. Outer surface is after fine abrasive treatment (grinding), outer flash and weld are not visualized. The following is observed on the inner surface:

- variant «r» — a thin weld with deformation trace (inner flash is absent), and a longitudinal trace on the tube diametrally opposite side, which, most probably, formed from mechanical contact with the mandrel or gage at weld rolling-off;
- variant «n» without weld deformation — thin weld with inner flash height of up to 0.1 mm, diametrally opposite side of the weld is clean, without any speciall features.

Roughness Ra on the inner (working) surface at the requirement of not more than 2 μm is equal to: variant «r» — from 0.31 up to 0.76 μm (av. 0.56 μm), variant «n» — from 0.27 up to 1.34 μm (av. 0.63 μm).

Accuracy of tube geometrical dimensions. Measurement of diameter and wall thickness confirmed the high manufacturing accuracy (Table 2).

Macro- and microstructure were studied in the base metal, near-weld HAZ and weld zone, as well as in the strips.

Blank metal is clean as to non-metallic inclusion content. Evaluation of inclusions in the strip was performed to DSTU 3295–95 — scale 3 for

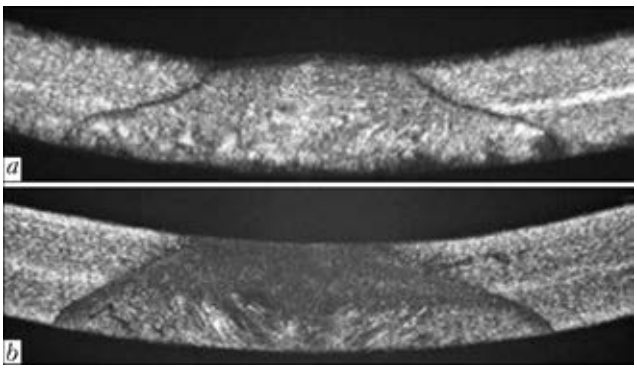

Figure 2. Macrostructure (×12) of welded joints of ∅20 × 0.8 mm tubes from TR 316L steel: *a* — undeformed weld; *b* — deformed weld

evaluation of metal with wall thickness below 2.5 mm. Content of isolated uniformly distributed globular-type inclusions is up to point 1. Strip microstructure is fine-grained, grain size is 9–10, with pronounced striation, characteristic for high-alloyed steels.

Tube macrostructure at 10-fold magnification does not have any defects in the form of pores, cracks, lacks-of-penetration, foreign inclusions, melts-through, etc. (Figure 2). Inner flash in the sample with undeformed weld is small — up to 0.1 mm (~0.08–0.09 mm, see Figure 2, *a*). Rolling-off changes weld geometry and it becomes wider (Figure 2, *b*).

The following is clearly visible in the microstructure:

- weld with the morphology of cast structure and presence of a small fraction of ferrite component;
- small (up to 200 μm) near-weld zone with slight (by 1 point) coarsening of the grain, compared to base metal;
- base metal with recrystallized grain 7–8 (grain in the base metal, coarsened only slightly, compared to initial strip, as a result of the performed heat treatment of tubes).

Tubes produced by two studied variants, passed all process testing, namely: flattening to achieve the specified distance H = 7.2 mm between the surfaces being flattened (weld located at 90° angle or in 3 o'clock position); complete flattening by ASTM procedure; static bending of tube sample (branch-pipe) through 90° around mandrel D_{man} = 60 mm; expansion up to outer diameter increase by 10 % by a mandrel with cone angle of 30°; flanging with 90° flanging angle.

After process testing there were no defects or fractures in the form of cracks, tears, lacks-of-penetration or overlaps.

Mechanical properties of initial strip and tubes were determined by tensile testing.

Results confirmed the strip compliance to ASTM A 240 standard for TR 316L steel (norm values are given in parenthesis): ultimate strength σ_t = 651–661 MPa (not less that 485), yield point $\sigma_{0.2}$ = 343 MPa (not less than 170), $\sigma_{1.0}$ = 379–381 MPa, relative elongation δ_{50} = = 42 % (not less than 40 %), δ_5 = 48–48.5 %.

Mechanical testing of tubes showed that they have a rather high level of strength and ductility properties. Compared to strip properties, the tubes showed higher values of relative elongation and lower values of ultimate strength and yield point that is due to slight coarsening of the grain as a result of tube heat treatment. Based on results of tensile mechanical testing tube metal corresponds to the norms of standards ASTM A 249 for steel of TR 316L grade and EN 10217-7 for steel-analog 1.4404 (Table 3).

For welded tubes an important criterion of their quality in terms of weld strength is their ability to withstand the above technological tests for flattening, expansion and bending. A not less important criterion is *rupture of transverse ring samples* with weld location at 90° to the axis of force application or in 3 o'clock position (Table 4).

Results confirm that tubes with a rolled-off weld have higher welded joint strength: rings fractured not through the weld, but through the base metal, i.e. they stood testing for ring rupture without anomalies.

Testing for intercrystalline corrosion (ICC) was performed by AMU GOST 6032 method by

Table 3. Mechanical properties of ∅20 × 0.8 mm tubes from TR 316L steel after tensile testing

Variant	σ_t, MPa	$\sigma_{0.2}$, MPa	$\sigma_{1.0}$, MPa	δ_{50}, %	δ_5, %
«r»	617 623	349 347	370 372	55 56.5	57.5 59.5
«n»	588 602	306 322	335 347	56 58.5	57 62
Norms of EN 10217-7	490–690	min 190	min 225	min 30	min 40
Norms of ASTM A 249	min 485	min 170	–	min 35	–

Table 4. Results of transverse rupture testing of ring samples to determine the strength of weld and near-weld zone

Sample	σ_t, MPa	Weld location	Fracture location
«r»	689 639 693	90° relative to applied force axis	Through base metal
«n»	650 642 673	Same	Through weld or in the HAZ (ductile fracture)

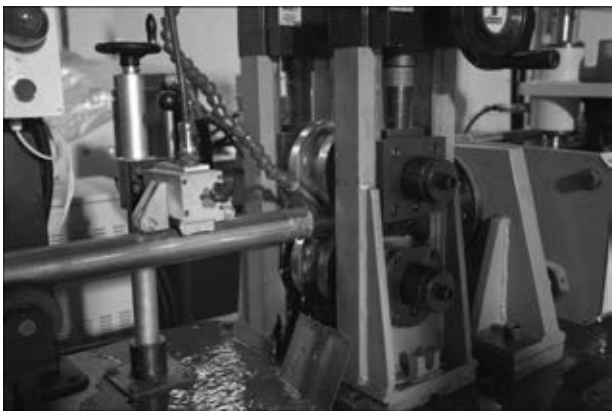

Figure 3. Eddy current flaw detector to monitor the continuity of weld and near-weld zone metal (located immediately after the welding assembly)

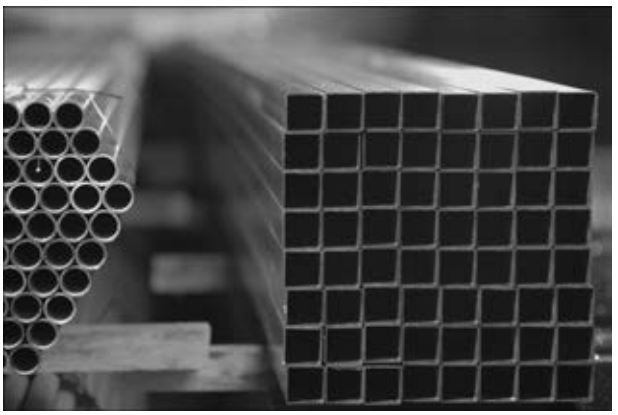

Figure 4. Kinds of standard export packing of square and round stainless steel tubes

boiling in copper sulphate solution for 8 h. According to this standard, the welded joints, deposited metal and weld metal are not subjected to provoking heating. In this case testing was performed both without the preliminary provoking heating, and in a more stringent mode with provoking preheating — 650 °C for 1 h. After that, all the samples were bent by a special method to detect possible cracks. After testing no cracks were revealed in the places of Z-shaped sample bends, either on the inner or on the outer tube surface, or in the weld and near-weld zone, or in the base metal, that is indicative of ICC resistance of tubes produced by both variants.

In this work *pitting corrosion* (PC) studies in keeping with the main postulates of GOST 9.912 and ASTM G 48 were performed as experimental ones to obtain additional comparative data on corrosion resistance of welded tube material (base metal and weld zone of the same tube). Tube samples were soaked in aggressive 10 % solution (ferrous trichloride hexahydrate ($FeCl_3 \cdot 6H_2O$)–100 g of salt per 900 cm^3 of distilled water) for 5 h at ≈20 °C (19.5 ± 0.5 °C). After soaking, the samples were washed, dried and their mass loss was assessed by weighing before and after soaking in an aggressive solution. Surface condition was also analyzed for presence, size, depth of pits and nature of their location, while paying special attention to the inner (working) surface. In keeping with the traditional concepts, it was confirmed that weld area is more prone to PC. In this case loss of mass of 0.004–0.008 g in samples with a weld is only slightly greater than loss of mass of 0.002–0.005 g in samples without a weld. However, in samples with rolled-off weld «r» mass loss of 0.006–0.008 g turned out to be greater than in samples with internal flash, i.e. without weld deformation «n» — 0.004 g. Moreover, samples with a rolled-off weld «r» demonstrated a greater susceptibility to weld pitting on the inner surface, while in samples with an unrolled weld «n» PC develops less intensively on the inner surface, but more actively over the outer surface. In base metal samples without a weld, pits are either totally absent, or are isolated shallow ones. Through-thickness pits were absent in all the cases. We can conclude that on the whole these tubes have relatively low rate of PC by the results of testing in $FeCl_3$ water solution.

NDT of welded tubes was performed with eddy current (ECT) and ultrasonic (UT) techniques.

ECT was performed in production in equipment of ALFA-FINANS, where the weld and tube body were tested in the mill line (Figure 3). Testing for longitudinal and transverse defects on the outer and inner surfaces was performed. ECT results did not reveal any defects, and 100 % of tested tubes were found to be fit.

UT was performed at NITI, for which purpose two standard samples with a rolled-off and unrolled weld were made for setting up the UT flaw detector (artificial longitudinal reflectors of «scratch» type of the depth of 10 % of nominal wall thickness). In the tested two variants of tubes «r» and «n» no defects, equivalent to artificial defects of the standard sample, were found. These tubes can be regarded as having passed UT, i.e. corresponding to specified requirements for condenser tubes.

Obtained results enable stating that welded tubes produced by ALFA-FINANS (Figure 4) are practically not inferior in any way to seamless tubes by their technological, mechanical, anticorrosion, metallographic characteristics, and they are even superior to seamless tubes in terms of accuracy of maintaining the wall thickness, both in the transverse section and longitudinally along the entire length, and geometrical dimensions simultaneously with the clean and light surface along the entire length.

Conclusions

Comprehensive testing of the metal of ∅20 × × 0.8 mm welded tubes from TR 316L steel for compliance to basic and additional requirements of standard ASTM A 249 has been performed.

Technology of manufacturing welded tubes from corrosion resistant steel in ALFA-FINANS Ltd. includes basic operations, which determine the tube quality and reliability: argon-arc (TIG) welding, manufacturing tubes with and without rolling-off the inner flash (with and without weld deformation), heat treatment in shielding atmosphere, eddy current testing of the weld and tube body with full compliance to all the procedures and recommendations of equipment manufacturer.

In terms of geometrical dimensions, the tubes correspond to manufacturer's high precision requirements with a high quality of both the inner, and the outer surfaces. Results of mechanical and technological testing revealed that mechanical properties at tube tension meet the requirements of ASTM A 249 and EN 10217-7 standards. All the samples passed flattening test (including complete back flattening), as well as flanging, expansion, static bending without formation of cracks, tears or other defects, both in the base metal, and in the weld and near-weld zone.

Metallographic examination did not reveal any inadmissible defects (lacks-of-penetration, melts-through, cracks or foreign inclusions) in the metal of weld, near-weld zone or on tube surface. Structure corresponds to requirements to precision tube grades from corrosion-resistant steel.

Tube metal is ICC-resistant. Samples from studied tubes are characterized by small mass losses as a result of testing for pitting corrosion. Tubes have passed nondestructive testing by UT and ECT techniques, and no defects were detected.

On the whole, comprehensive comparative testing demonstrated that tubes made by two variants — with and without weld rolling-off, meet the requirements of ASTM A 249 and EN 10217-7 standards. Here, tubes with rolled-off weld should be considered preferable by individual indices for critical applications.

1. Buryak, T.N., Yaroshenko, N.V., Taranenko, A.A. et al. (2014) Evaluation of quality of welded long superthin-wall tubes from corrosion-resistant steel. *Metallurg. i Gornorud. Promyshlennost*, **5**, 40–43.
2. (2010) *ASTM A 249/A249M-10a*: Standard specification for welded austenitic steel boilers, superheaters, heat-exchangers and condenser tubes.
3. *ASTM A 312/A 312M-08*: Standard specification for seamless, welded and heavily cold-worked austenitic stainless steel pipes.
4. (1982) *GOST 11068–81*: Corrosion-resistant welded pipes. Moscow: Standart.
5. Hanson, K.F. (1978) Tendencies of application of titanium in heat exchangers. In: *Proc. of 3rd Int. Conf. on Titanium. Physical Metallurgy and Technology*, 423–435. Moscow: VILS.
6. (2006) *Validation of material for replacement of condensers of nuclear plant turbosets and development of technical conditions on long tubes*: Report of researches of SE NITI. Dnepropetrovsk.
7. Horn, F. (1977) *Atlas of structures of welded joints*. Moscow: Metallurgiya.
8. *EN 10217-7.2005*: Welded steel tubes for pressure purposes — Technical delivery conditions. Pt 7: Stainless steel tubes.
9. Ulianin, E.A. (1991) *Corrosion-resistant steels and alloys*. Moscow: Metallurgiya.
10. (2000) Stainless steel. Characteristics, grades and world-wide standards of steel. *Avesta Sheffield AB*. Bul. 10100.

Received 17.12.2014

EVALUATION OF STRESS-STRAIN STATE OF GAS PIPELINE SECTION WITH LOCAL STABILITY LOSS

A.A. RYBAKOV[1], **E.F. GARF**[1], **A.V. YAKIMKIN**[1], **I.V. LOKHMAN**[2] and **I.Z. BURAK**[2]
[1]E.O. Paton Electric Welding Institute, NASU
11 Bozhenko Str., 03680, Kiev, Ukraine. E-mail: office@paton.kiev.ua
[2]Company «Ukrtransgaz»
9/1 Klovsky Spusk Str., 01021, Kiev, Ukraine. E-mail: press@utg.ua

Causes for damaging of a gas pipeline pipe, which was accompanied by significant deformations and involves local loss of stability in a short pipe section, are considered. Certain characteristic indices of damage are established, namely damage is located in direct vicinity of the circumferential weld and develops on a lower strength pipe. A set of physico-mechanical studies did not reveal any lowering of metal performance that allows looking for the cause for pipe damage in the features of pipeline stress-strain state in service. It is shown that temperature deformations in the pipeline under the most unfavourable conditions induce insignificant stresses, which cannot lead to any local loss of pipe stability. Analysis of pipeline laying route showed that it passes through mining area and the pipeline stress-strain state is influenced by earth surface deformation. Magnitude of displacements and stress levels in the pipe, caused by earth surface deformation in the mining area, allow regarding them to be the cause for gas pipeline damage. 11 Ref., 2 Tables, 10 Figures.

Keywords: *damage, pipeline, pipe, mechanical properties, stress-strain stage, stability loss, stresses, displacements, calculation, welded butt joint, undermined territories*

In October 2013, damage of 325 mm diameter pipe with 6 mm wall thickness was detected in the branch of Shebelinka–Dnepropetrovsk–Odessa main gas pipeline, leading to the town of Ternovka. It was accompanied by gas outflow from the gas pipeline. Diagnostics of the gas pipeline section allowed establishing local loss of pipe stability at large longitudinal displacements (Figure 1).

Deformations were so significant that through-thickness cracks developed in the formed corrugations. Measurements showed that displacements at corrugation formation were equal from 260 up to 320 mm. A certain break (up to 7°) of pipeline axis was observed in the location of stability loss.

Stability loss occurred in the vicinity of circumferential weld on one of the abutted pipes, designated by letter A. No indications of local stability loss were observed on the other pipe (designation B).

Such pipe damage in gas pipeline system is a quite rare phenomenon, and it was not highlighted in special literature [1, 2]. Therefore, the cause for its formation is of scientific and practical interest and is the objective of this study.

In keeping with the project, pipes from steel 20 (GOST 1050–74)* with a longitudinal weld

Table 1. Composition of studied pipe base metal

Object of control	Weight fraction of elements, %					
	C	Mn	Si	S	P	Al
Pipe A	0.097	0.43	0.225	0.025	0.018	0.051
Pipe B	0.168	0.58	0.229	0.015	0.020	0.035
Certificate data	0.19–0.20	0.54–0.57	0.20–0.23	0.003–0.007	0.013–0.020	0.30–0.50
GOST 1050–74	0.17–0.24	0.35–0.65	0.17–0.37	≤0.035	≤0.030	–

*Pipe performance was studied by T.N. Filipchuk and L.G. Goncharenko.

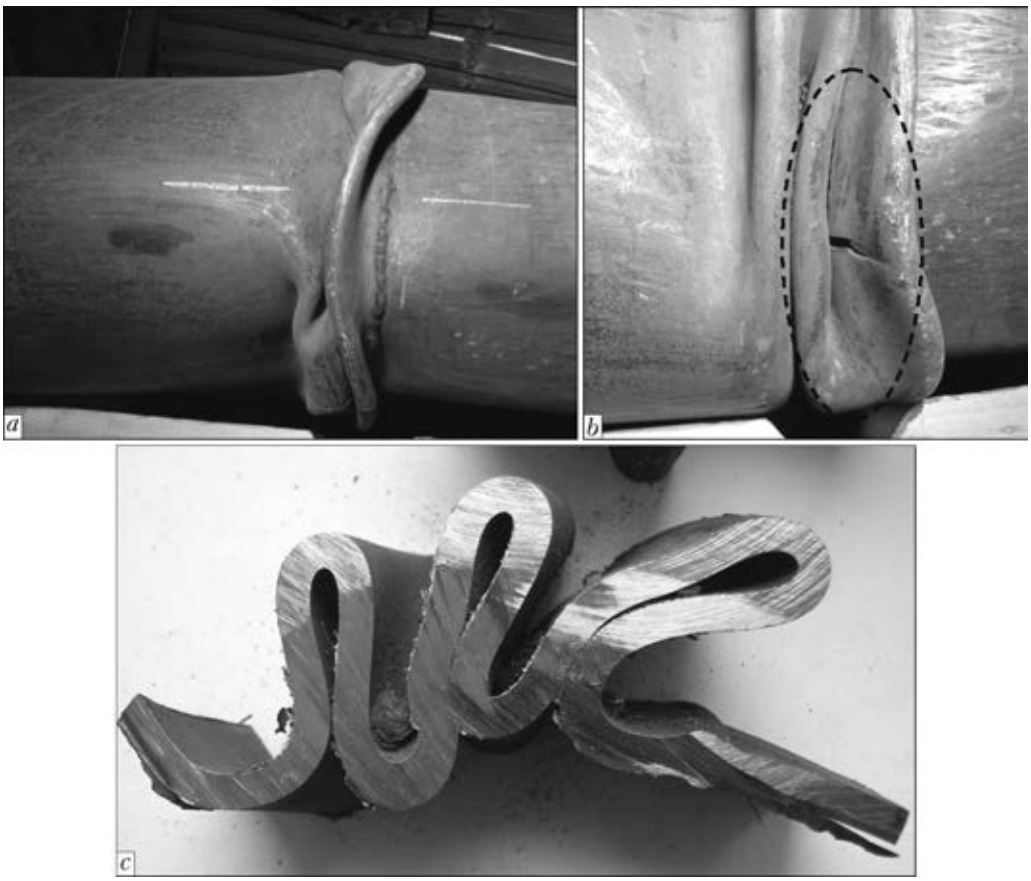

Figure 1. Damaged pipe section: *a* — general view of studied sample; *b* — damaged fragment with through-thickness crack; *c* — wall deformation

made by high-frequency welding were used in the considered pipeline section. Table 1 gives the data on pipe metal composition, in keeping with the certificates, normative requirements and results of spectral analysis performed at PWI in the Baird «Spectrovac-1000» instrument.

It follows from Table 1 that in keeping with control chemical analysis, main alloying element and impurity content, even though it is different from the certificate data, corresponds to the requirements of GOST 1050–74, except for carbon in base metal of pipe A, the weight fraction of which (0.097 %) is essentially lower than the required value (0.17 %). This gives reason to believe that pipe A is made from steel 10, and not steel 20, as indicated in the certificate. Base metal of pipe B, as to its composition, corresponds to normative requirements to steel 20, as well as to certificate data.

Mechanical properties of metal of pipes A and B were studied in the sections adjacent to stability loss zone, not subjected to deformation.

Longitudinal samples, to GOST 10006–80, drw. 2, were tested to determine the values of yield point (σ_y), ultimate strength (σ_t), relative elongation (δ_5) and reduction in area (ψ).

Impact toughness at temperature of 0 and –40 °C was determined on longitudinal samples of 5 × 10 mm section with a sharp-notch (GOST 9495–78, type 13). Bend testing of transverse samples, prepared to GOST 6996, type XXVII, was conducted to determine the deformability of longitudinal pipe welded joint. Table 2 gives the results of tensile and impact toughness testing of pipe metal.

Data of Table 2 are indicative of the fact that the values of pipe metal mechanical properties meet the requirements of GOST 20295–74 for steel 20. On the other hand, there is a significant difference in strength values (σ_y, σ_t) of base metal of the examined pipes. For pipe A yield point σ_y is lower than for pipe B by 22 %, and ultimate strength σ_t — by 11 %.

Impact toughness of pipe base metal at temperatures of 0 and –40 °C is quite high, and is considerably higher than the normative requirements. Results of welded sample bend testing also meet the normative requirements.

Structural state of pipe metal was studied in «Neophot-32» microscope. It is established that microstructure of base metal of both the pipes is typical for hot-rolled steel, and is a sufficiently fine-grained ferrite-pearlite mixture with ferritic grain, corresponding to number 8–9 to GOST 5639 (Figure 2). The fraction of pearlitic component in the structure of pipe A base metal is

Table 2. Mechanical properties of base metal of the studied pipes

Property monitoring	Tensile testing				Impact bend testing*	
	σ_y, MPa	σ_t, MPa	δ_5, %	ψ, %	KCV_0, J/cm^2	KCV_{-40}, J/cm^2
Pipe A	326.1 312.5	418 418.7	34.9 34	58.0 60.3	223.2–258.2 239.0	156.9–204.3 173.3
Pipe B	403.2 417.6	469.7 471	33.3 31	57.3 54.6	165.9–213.6 192.8	70.1–96.8 85.5
Certificate date	333–338	463–482	33.3–34.1	N/D	–	–
GOST 20295–74	≥245	≥410	≥25	≥55	29.4**	–

*The numerator gives the extreme values, and the denominator gives average values from three tests.
**Requirements to SNiP 2.05.06–85.

somewhat smaller that is due, as was noted above, to lower carbon content compared to pipe B.

The given results of examination of pipe metal performance reveal that the cause for gas pipeline damage is associated not with the quality of base metal or welded joints, but with the features of stress-strain state developing in its service.

There is no doubt that damage in the form of local stability loss with corrugation formation around the entire perimeter can be caused predominantly by compressive forces in the pipe. It should be noted that at loading by internal pressure the gas pipeline develops longitudinal tensile stresses, corresponding to half of the level of hoop stresses. Therefore, such conditions should develop in gas pipeline service, under which in the considered section the applied compressive forces would not only compensate the longitudinal tensile stresses in the pipe induced by internal working pressure, but would also induce compressive stresses, sufficient for local stability loss.

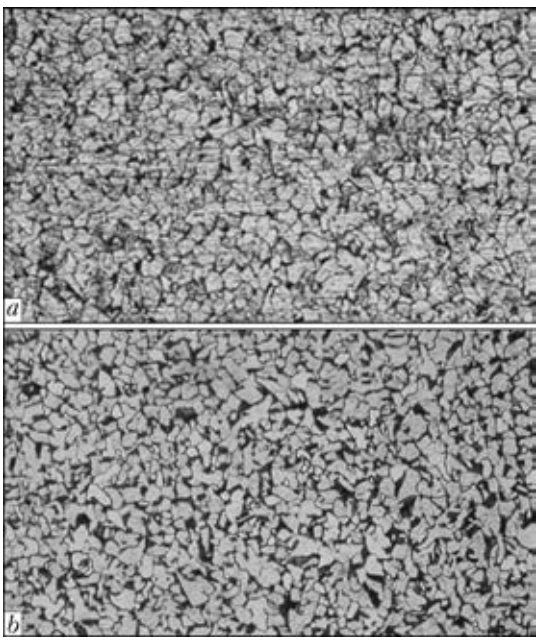

Figure 2. Base metal microstructure (×200): *a* — pipe A; *b* — pipe B

It is known [3] that critical stresses of local stability loss in a cylindrical shell (pipe) under the impact of uniform axial compression, are found from the following equation:

$$\sigma_{cr} = \frac{1}{\sqrt{3(1-\mu^2)}} E \frac{t}{R}, \quad (1)$$

where μ is the Poison's ratio, which is within 0.25–0.35; E is the modulus of elasticity taken equal to $2 \cdot 10^5$ MPa; t is the pipe wall thickness; R is the pipe radius along the median section line.

Taking $\mu = 0.3$, we obtain critical stress of local stability loss

$$\sigma_{cr} = 0.6E \frac{t}{R}. \quad (2)$$

Note that local stability loss in the pipe occurred in the immediate vicinity of the circumferential weld, while, on the other hand, the entire damage zone is located on one side of this weld, i.e. in one of the gas pipeline abutted pipes.

The fact of local loss of stability is observed near the circumferential welded joint of pipes and is attributable to the fact that when making the circumferential weld its shrinkage results in smaller pipe diameter [4, 5], and geometrical shape imperfection develops in the circumferential butt joint, which lowers critical stresses of local loss of stability, compared to an ideal pipe (Figure 3).

It was earlier shown that mechanical properties of the metal of pipes, abutted in the damage zone, differ markedly. A pipe, which has lost its stability, has the yield point approximately 100 MPa below that of the adjacent pipe. Measurements showed that the actual wall thickness of pipe A was in the range of 5.4–6.0 mm. In the other pipe the wall thickness was 6.2 to 6.4 mm.

Proceeding from expression (2), which is valid for circular shells (initial deflection amplitude should not exceed shell thickness [6]), critical stresses of local stability loss for pipe A are equal to ~4120 MPa, and for pipe B they are 4740 MPa.

Note that the derived values of critical stresses characterize local stability loss in the elastic work region. As these stresses many times exceed the yield point of steel, from which the pipes are made, then for specific pipes the values of pipe material yield point will be the critical stresses of local stability loss. It is natural that the local stability loss will occur in the pipe, requiring a smaller force, which, however, is capable of inducing yield point stresses in it. This is exactly what we see in this case. Local loss of stability is observed in a pipe with smaller wall thickness, and lower values of material yield point.

An open question still is what could have caused generation of forces in the gas pipeline, which induced compressive stresses, exceeding the steel yield point? The following factors were considered to provide an answer to this question:

- climatic temperature variations;
- wetting of soil foundation;
- earthquake;
- adjacent territory undermining by mining industry enterprises.

The latter assumption is based on the fact that operating Geroev Kosmosa and #4 mines of «Ternovskoe» Mine Management are located at a certain distance from the gas pipeline running zone. Figure 4 shows the locations of mine entrances and the route, including gas pipeline damaged section.

Considering that no earthquakes were registered in gas pipeline location areas during its service period this factor can be ignored.

Analysis of the results of engineering-geological surveys [7] allows eliminating from consideration the influence of wetting of soil foundation, as the foundation is composed of clay soils, namely loamy soils of solid and tight plastic consistency. Foundation soils do not have any subsidence properties.

Let us consider gas pipeline temperature deformations and the associated loads. Under certain conditions, temperature gradients during gas pipeline construction and service may induce compressive forces and stresses in it. Their level, however, will depend on the magnitude of temperature gradient. Compression may arise in the pipeline in the case when pipeline mounting and laying were conducted at maximum low temperatures, i.e. in winter, and in service pipe temperature reached its maximum.

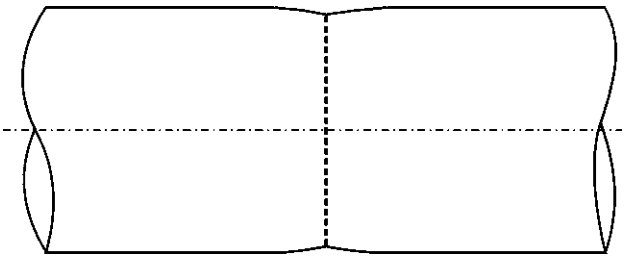

Figure 3. Geometrical imperfection in butt joint zone, caused by making the circumferential weld

Taking as the initial prerequisite the most unfavourable conditions of pipeline construction, i.e. in winter at ambient temperature of –20 °C, and considering that pipeline depth is equal to 0.8–1.0 m, and, therefore, its temperature will not be higher than 20 °C in the hottest months, the maximum possible temperature gradient will not be higher than 40 °C.

The coefficient of linear expansion for carbon steel, depending on chemical composition, varies in the range from $(11–15)\cdot10^{-6}$ deg^{-1}. At temperature gradient of 40 °C maximum relative elongation will be equal to $\varepsilon = 6\cdot10^{-4}$ mm.

Note that the connection between stresses and temperature elongation is given by the following expression:

$$\sigma = \varepsilon E. \qquad (3)$$

According to expression (3), temperature stresses in gas pipeline do not exceed 120 MPa.

Considering that thermal stresses are relatively uniformly distributed along the pipeline length, and their magnitude is much lower than pipe metal yield point, it is quite clear that they could not have caused local stability loss in the gas pipeline.

Deformations of soil foundations, arising during mining operations, have a significant influ-

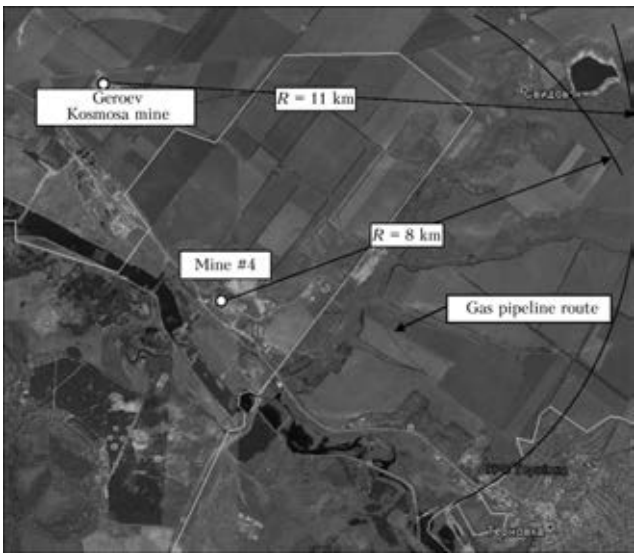

Figure 4. Gas pipeline location on the ground

ence on the strength and service characteristics of underground pipeline structures.

Relative location of gas pipeline calculated section and the mines (see Figure 4) leads to the assumption of mining operations influence on the gas pipeline, as in keeping with Table 1 of the Standard [8], the considered section pertains to group III of undermined territories.

At formation of the calculation procedure, pipeline section of length L = 7.5 m was taken, which consists of two pipes of ∅325 × 6 mm size, connected to each other by a circumferential weld. Calculated section length is due to the distance between the cantledges (cantledge spacing is 3.7 m).

Impact of internal service pressure p = = 5 MPa and impact of friction forces, arising on the pipe outer surface as a result of soil shifting, was taken into account as the main loads.

Force of friction of pipeline outer surface against the soil depends on the perimeter of the pipe proper and on soil shear resistance in the form of tangential stresses τ. Nature of underground pipeline interaction with the soil can be conditionally divided into two sections, namely elastic and limit (Figure 5). In section I the bond between the soil and the pipe is elastic, characterized by the dependence proposed in [5]:

$$\tau(x) = k_u u(x), \qquad (4)$$

where k_u is the soil resistance coefficient at pipeline longitudinal displacement; $u(x)$ are the displacements.

This region is characterized by relatively small displacement of soil (up to $u < 100$ mm). In point «k» tangential stresses reach their maximum value and in section II the soil goes into the limit stressed state (pipe slipping relative to the soil occurs).

Visual inspection of gas pipeline fragment in its fracture zone revealed that the magnitudes of pipe wall deformation in the direction of pipeline longitudinal axis Uz are much greater than

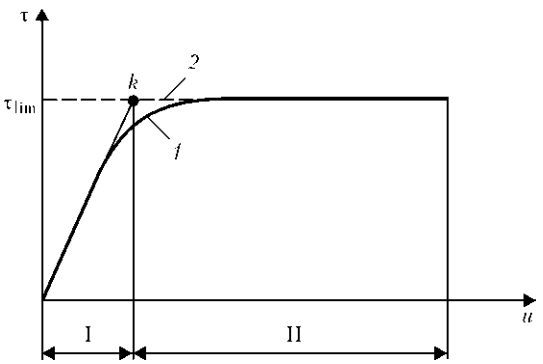

Figure 5. Nature of interaction of underground pipeline with the soil: *1* — actual curve; *2* — calculated

100 mm. Thus, it can be assumed that in the actual case considered the soil interaction with the pipe wall corresponds to the limit stressed state.

In keeping with [9], soil shear resistance for the limit stressed state is equal to

$$\tau_{lim} = q_{pr} \operatorname{tg} \varphi_s + 2\gamma_s c_h \pi D_{out}^2 \operatorname{tg} \varphi_s + 0.6\pi D_{out} c_s = 537.2 \cdot 0.344 + 2 \cdot 1800 \cdot 0.685 \cdot 3.14159 \times \times 0.325^2 \cdot 0.344 + + 0.6 \cdot 3.14159 \cdot 0.325 \cdot 2000 = 1691.51 \text{ kg/m}^2, \qquad (5)$$

where q_{pr} — weight of pipeline with the product is

$$q_{pr} = q_p + q_{gas} = 47.2 + 490 = 537.2 \text{ kg/rm};$$

q_p — weight of 1 rm of pipe of 325 × 6 mm size is equal to 47.2 kg/rm; q_{gas} — weight of natural gas per 1 rm of pipeline, which is allowed to be taken equal to [10]

$$q_{gas} = 10^{-2} p \cdot D_{in}^2 = 10^{-2} \cdot 5 \cdot (0.313)^2 = 0.0049 \text{ MN} = 490 \text{ kg/rm},$$

where p = 5 MPa is the working pressure; D_{in} = = 0.313 m is the pipeline inner diameter; φ_s = = 19° is the angle of soil internal friction; γ_s = = 1800 kg/m^3 is the specific soil weight; c_h is the dimensionless coefficient equal for clay soils to

$$c_h = 0.367(h/D_{out}) - 0.046(h^2/D_{out}^2) + 0.06 = 0.367(0.8/0.325) - 0.046(0.8^2/0.325^2) + + 0.06 = 0.685,$$

where h = 0.8 m is the backfill height; D_{out} = = 0.325 m is the gas pipeline outer diameter; c_s = = 2000 kg/m^2 is the specific adhesion of soil around the pipe.

Proceeding from that, the limit value of tangential stresses on the surface of soil contact with pipeline wall, induced by soil shifting, does not exceed τ = 0.0169 MPa.

In connection with the complexity of the process of the considered pipeline structure deformation, calculation was performed allowing for physical nonlinearity of pipe material properties. Change of physico-mechanical properties of pipe material was simulated in calculations by stress-strain diagram, derived by the results of testing the longitudinal samples cut out of the pipe (see Table 2). The accepted stress-strain diagram has the form given in Figure 6.

Finite element model of the pipeline is made in 3D formulation, using shell finite elements of general position. Numerical model includes two pipes (A and B) connected to each other by a circumferential weld. Initial geometrical imperfection was allowed for in the zone of pipe abut-

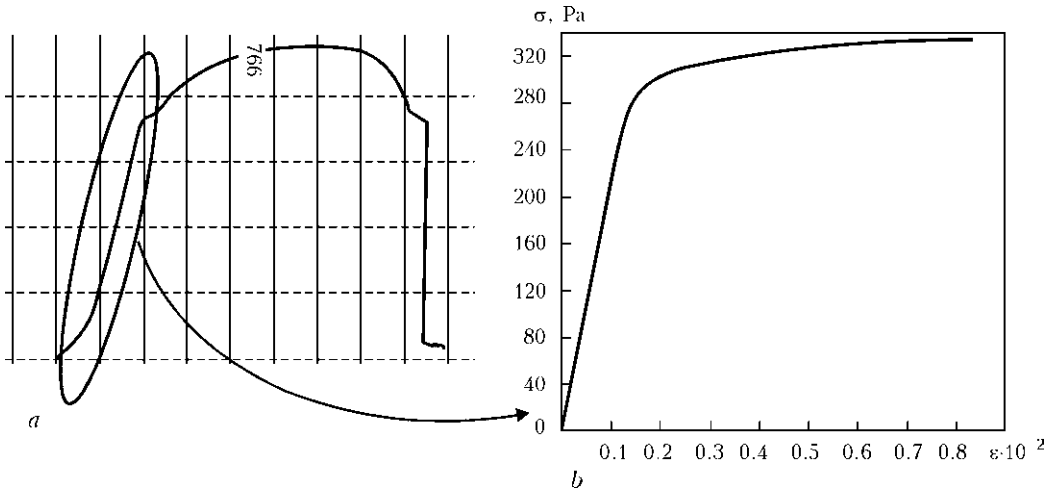

Figure 6. Stress-strain diagrams for tested sample of studied pipe base metal (*a*) and for numerical calculation model (*b*)

ment. General view of the geometrical and FE models of the gas pipeline is shown in Figure 7.

To ensure geometrical stability of the model, linear and angular displacements in the plane normal to longitudinal axis, are limited along the edges of calculation area. Linear displacements along gas pipeline axis are allowed.

At formation of calculation procedure, it was taken into account that from calculation point of view, the pipeline buried into the soil is a rod in an elastic medium [7, 11]. Here, the rigidity of this medium — the soil surrounding the pipe — is non-uniform. In particular, backfilling soil, located above the pipe body, has lower rigidity than soil located from the pipe sides or the underlayer.

Development of longitudinal compressive load in the pipeline under certain conditions can result in loss of stability, which is accompanied by pipeline section buckling in the direction of day surface (direction with the lowest rigidity of elastic medium). Here, one of the important parameters affecting the magnitude of critical force and form of stability loss is the value of free length of calculated pipeline fragment.

Mounting cantledges along the gas pipeline greatly lowers the possibility of pipe transverse displacement and changes the free length of calculated pipeline sections. Reduction of free length, in its turn, leads to increase of critical load, capable of leading to overall loss of pipeline stability. The required critical load force can exceed the axial load magnitude, which causes formation of plastic hinges in the pipe wall. This results in formation of the zone of local loss of pipe wall stability. Thus, cantledges can be a factor, influencing both the type and form of stability loss, and critical force values.

Influence of saddle-like concrete cantledges was simulated by limiting linear displacements of pipeline individual sections in the directions normal to gas pipeline longitudinal axis. It is assumed that cantledges are equidistant from the weld (for 1.85 m on each side).

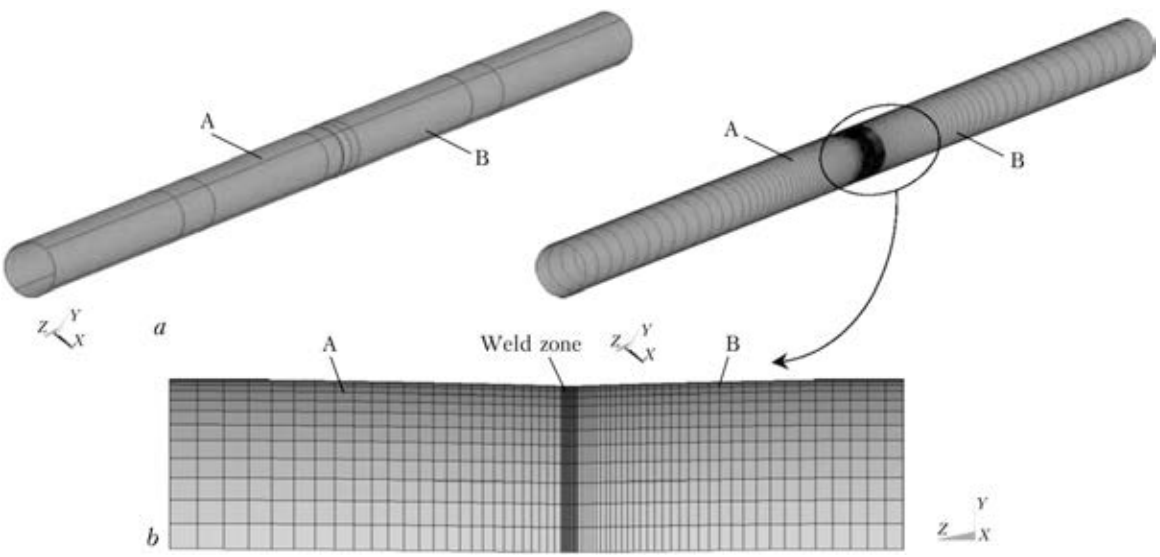

Figure 7. Geometrical (*a*) and finite-element (*b*) numerical models

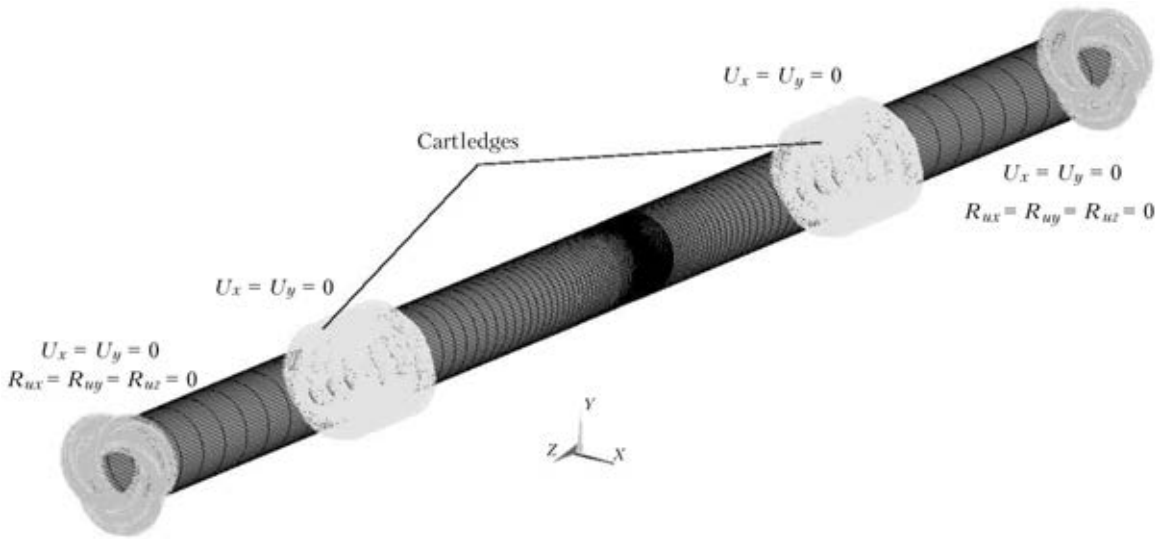

Figure 8. Boundary conditions: U_y, U_x — linear displacements; R_{ux}, R_{uy}, R_{uz} — angles of pipe axis rotation

Boundary conditions taken in calculation procedure are given in Figure 8.

The following assumptions and simplifications were taken, when plotting the FE model of gas pipeline calculated section:

• circumferential weld in the section of abutting two pipe edges was taken to be equivalent to pipeline base material;

• pipeline numerical model was formed for pipe wall median surface.

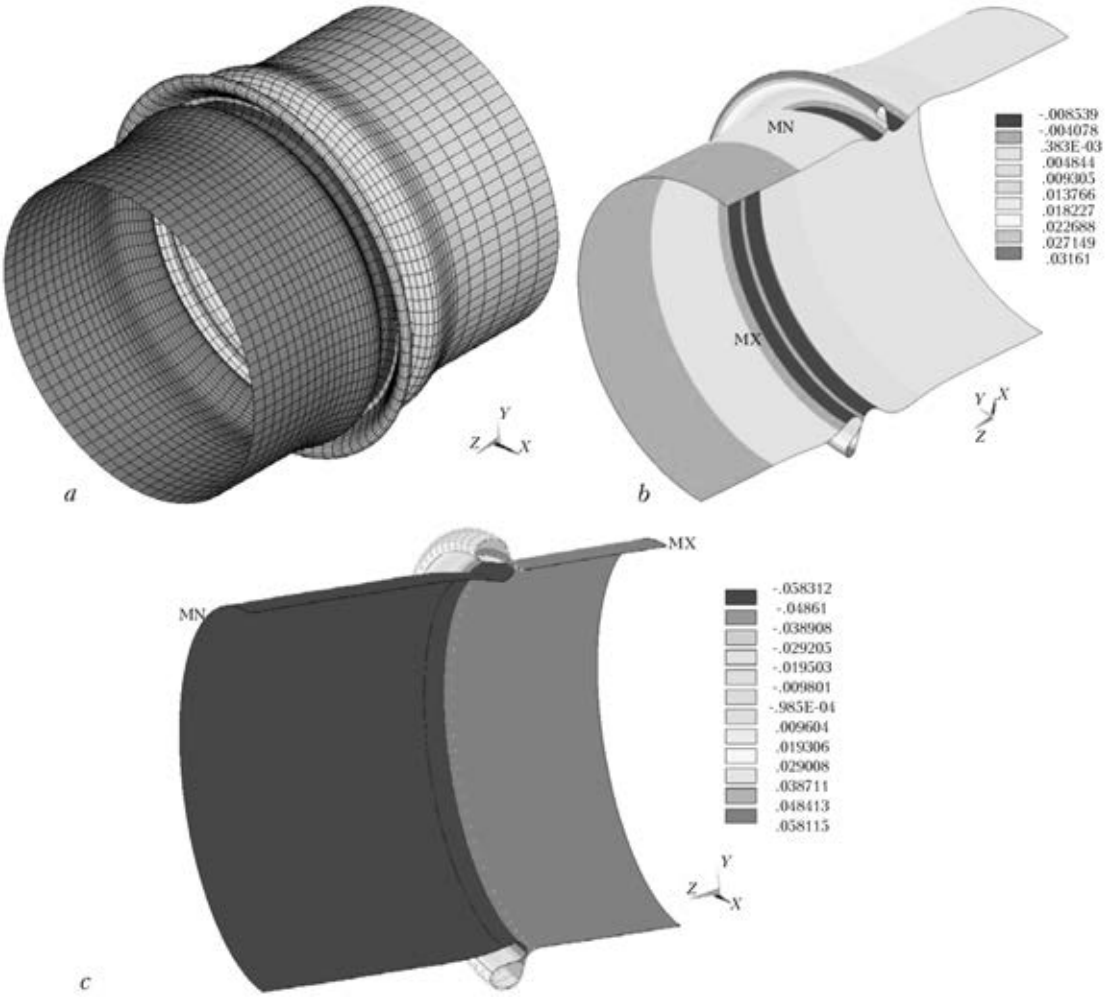

Figure 9. Calculation results: *a* — deformed schematic fragment; *b* — radial displacements U_r (m); *c* — displacements along *OZ* axis (m)

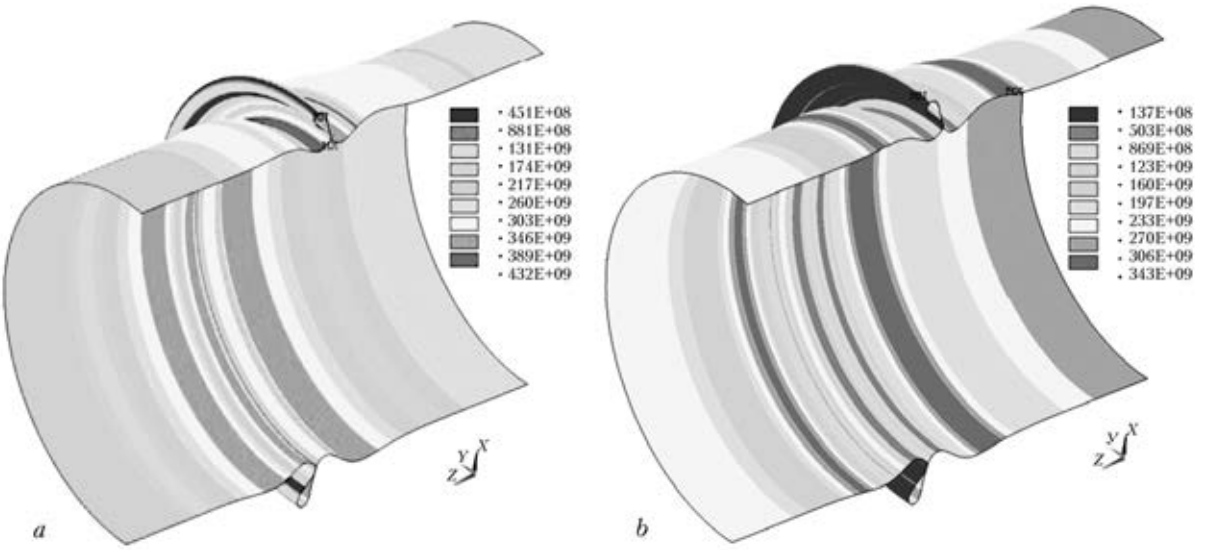

Figure 10. Equivalent stresses S_{mises} on face (*a*) and median (*b*) surfaces, MPa

Analysis of obtained results showed that under the impact of loads, the wall develops considerable deformations, and stress magnitudes exceed pipe material yield point.

Figure 9, *a* gives the deformed pipeline schematic. Deformed section of pipeline wall is characterized by buckling of pipe wall section in the radial direction (along axes U_y and U_x). At summary axial pipe displacements U_z = 116 mm in pipeline wall, closing of pipe walls and formation of the first wave of buckling is observed. Displacements in pipe wall reach $U_x = U_y$ = 30 mm in the radial direction. Isofields of linear displacements in the radial (along axes U_y and U_x) and axial (along axis U_z) directions are given in Figure 9.

Considerable deformations of gas pipeline wall are accompanied by formation of local zones with higher stress magnitudes. In the zones of pipe wall bending the magnitudes of equivalent stresses exceed the yield point value. On median surface stress values are equal to S_{mises} = = 342 MPa, and on face surfaces they reach values S_{mises} = 430 MPa. Isofields of equivalent stresses on median and face surfaces of gas pipeline wall are given in Figure 10.

Thus, it is established that soil shifting in territories undermined by mine working, results in pipe displacements in the axial direction, and is the cause for local loss of stability of the pipeline. Level of equivalent stresses arising in the wall exceeds the pipe material yield point. Cartledges have an additional influence on the form of stability loss and magnitude of critical load.

1. Mazur, I.I., Ivantsov, O.M. (2004) *Safety of pipeline systems*. Moscow: Elima.
2. Ivantsov, O.M. (1985) *Reliability of structural units of main pipelines*. Moscow: Nedra.
3. Volmir, A.S. (1956) *Flexible plates and shells*. Moscow: Tekhteorizdat.
4. Vinokurov, V.A. (1968) *Welding strains and stresses*. Moscow: Mashinostroenie.
5. Kuznetsov, S.A. (1974) *Welding strains of ship hull structures*. Leningrad: Sudostroenie.
6. (1962) *Designer reference book. Design and theory*. Ed. by A.A. Umansky. Moscow: Strojizdat.
7. Ajnbinder, A.B., Kamershtejn, A.G. (1982) *Design of main pipelines for strength and stability*. Moscow: Nedra.
8. *DBN V.1.1-5–2000*: Buildings and constructions in undermined territories and subsiding soils. Pt 1: Buildings and constructions in undermined territories. Kyiv: State Committee on building, architecture and housing policy of Ukraine.
9. Florin, V.A. (1954) *Principles of soil mechanics*. Vol. 1. Leningrad: Gosstrojizdat.
10. (1997) *SNiP 2.05.06–85*: Main pipelines. Moscow.
11. Ajnbinder, A.B. (1991) *Design of main and field pipelines. Strength and stability*: Refer. Book. Moscow: Nedra.

Received 26.11.2014

MANUFACTURE OF RODS OF SINTERED TITANIUM ALLOYS BY USING DIFFERENT METHODS OF WELDING (Review)

A.V. OVCHINNIKOV
Zaporozhie National Technical University
64 Zhukovsky Str., 69063, Zaporozhie, Ukraine. E-mail: glotka87@ukr.net

Presented is the state-of-the-art of production of semi-products and products of titanium and its alloys in Ukraine. The rod of titanium and its alloy is one of the mostly demanded semi-products. In Ukraine the titanium rods are not manufactured in principle. For its mass production it is necessary to reduce the cost of technology for their production. The production of rod semi-products by using methods of powder metallurgy in applying of powders with the developed surface and welding was grounded. Peculiarities of application of different methods of welding were considered, the application of pressure welding was shown as challenging. The optimum one is the rotation friction welding for production of rod semi-products. The main problems, which may occur in friction welding of sintered semi-products, were considered, the need in further investigations of weldability of the given semi-products was shown. 51 Ref.

Keywords: *titanium, powder metallurgy, pressing, sintering, welding, semi-product, rod*

One of the largest consumers of titanium is the aerospace industry in manufacture of civil and military aircrafts, and this tendency is more increased. The world application of titanium in aerospace industry in 2013 was 46 % [1], while in 2006 it did not exceed 40 % [2]. Moreover, up to 70 % of parts in aerospace engineering structures have up to 30 mm section and up to 25 % of parts have up to 50 mm section [3].

The rod is the main semi-product for manufacture of blade pieces [4] and fastening parts (screws, bolts, nuts, plugs) [5], as well as springs [6]. Rods of unalloyed titanium are used for manufacture of naildrawers and crow bars for the Ministry of Emergency Situations medical instruments, implants, casings and membranes of tensoresistor transducers, stop valves and other products.

To produce the semi-products of such sections of titanium alloys, having high values of strength, it is necessary to perform deformation at high values of specific upsetting forces and at high temperatures, thus causing application of high-power and expensive equipment, and also leading to losses of metal in removal of surface layers [7]. This is partially explaining the fact that at concentration in Ukraine of about 20 % of world resources of titanium the casting and rolling productions are not enough developed, only tubes and hot-deformed rods of 10–90 mm diameter are produced [8]).

In Ukraine, the metallic titanium in ingots is produced by Zaporozhie Titanium-Magnesium Works, PWI Research & Production Centre «Titan», International Company «ANTARES» and «Strategy BM» Ltd. in billets of section: round ingots of diameter from 200 up to 1100 mm and slabs from 150 × 500 up to 400 × × 1350 mm [9, 10]. The main part of titanium resources is exported in the form of raw material [11], and the national industry is mainly oriented to import, that puts Ukraine into dependence on foreign suppliers of semi-products and ready products of titanium and its alloys [9], thus reducing the financial stability and compatibility of the national manufacturers. At the same time, the tendency to concentration of production and consumption of titanium inside the country is observed in other countries [12].

The production of semi-products and products includes, except the cost of material, the cost of technology of their producing and cost of subsequent treatments: thermal, mechanical, deformational [13]. High cost of titanium rods is predetermined by the complicated technology of their production [14]. Thus, the search of ways for reducing the costs at all the stages of production is necessary.

Application of inexpensive material can reduce the cost of the product to 20 % [15]. Up to 14 % of cost of semi-products of titanium alloys fall to melting and up to 52 % — for producing rolled metal [16], i.e. more than 65 % of cost of semi-products can fall to technologies of producing. Therefore, the main way of reducing the cost

of semi-products of titanium alloys is making cheaper the technology of their producing, but not deteriorating quality of semi-products [17].

The powder technologies are the most challenging methods for processing the titanium raw material [18–20]. In applying of these technologies the number of required operations is reduced and high-efficient equipment is used [21], the parts during pressing into the required shapes are manufactured more quickly at a little machining and less wastes [22], it is possible to produce new materials with characteristics, which are often impossible to obtain by other methods [18, 23].

The reducing of costs and improving the manufacturability of producing semi-products can be provided by using granular metallurgy [21, 24–26] or even more economical methods of powder metallurgy by using powders with a developed surface [27–29]. These technologies are successfully used for manufacture of parts in different branches of industry: automobile- and avia engine construction [30]. However, the manufacture of long semi-products, to which the rods are referred, is rather problematic by powder technologies.

One of the most effective and widely spread methods of titanium alloy joining is welding [31]. Therefore, the problem of producing rods from sintered titanium can be solved by applying the advanced technologies of welding production [32], moreover, the manufacture of parts of medical purpose also admits the application of welding [33]. Technological potentials of welding process and level of mechanical properties of welded joints have a great influence on the volume of industrial application of titanium.

The proper selection of welding method predetermines the quality and efficiency of the welded joint fulfillment [34, 35]. One of the main requirements to the advanced structural titanium alloys is the assurance of ratio of the weld strength to the base metal strength of not lower than 0.9 [34]. It was earlier considered that the fusion welding even at additional effect is not capable to provide the strength factor of the welded joint of more than 0.9 [36]. The recent investigations show that the strength factor in argon arc welding makes 0.93–0.97 [31], and in argon arc welding into narrow and traditional gaps with reinforcement [37] the full strength of titanium alloy welded joints is provided. The full strength is also provided in fusion welding by the concentrated power sources: electron beam [37–39], laser [40, 41] and plasma [41]. However, these methods have a number of technological and economic drawbacks, typical of all the methods of liquid-phase welding. Methods of pressure welding can join the semi-products in solid phase for relatively short period of time, that allows minimizing the above-said effect and retaining the physical-chemical characteristics of weld metal close to the base metal [42].

In particular, the friction welding allows making the quality welded joints of titanium alloys, the mechanical properties of which are at the level of the base metal [36, 43, 44], simplifies greatly the technology of preparation for welding of titanium and its alloys as compared with the fusion welding, reduces effect of edge preparation of parts for welding, eliminates the negative effect of filler wire on the welded joint quality [35, 45, 46], and admits the absence of gas shielding of welded joint and the part [47]. In addition, the problems of noticeable shrinkage and feasibility of initiation and propagation of cracks in HAZ metal of sintered material, subjected to fusion welding, are leveled [47].

At the same time, the application of as-sintered alloys in welding can lead to the presence of inadmissible inherited defects in weld and near-weld zone caused by imperfection of the initial semi-product [46, 48]. Control of content of impurities entered from the environment is required to prevent the degradation of properties [49], the additional saturation of weld with oxygen, nitrogen and hydrogen as compared with that of base metal is inadmissible [48].

The porosity can also change the mechanism of heat transfer and, finally, the welding parameters [50]. In particular, the fraction, size, distribution and morphology of porosity have a great influence on weldability [47]. It is known that the porous titanium products can be successfully welded by the argon arc welding and some methods of pressure welding [23], but there are no almost similar investigations on friction welding, in particular, on conventional one which is especially urgent for welding of semi-products in the form of bodies of rotation. In this connection, it is necessary to carry out the investigation of weldability for the wider application of titanium, as it has a special importance in manufacture of long semi-products [39], sintered titanium semi-products, produced by the friction welding.

Actuality of works in this direction predetermined by the national and world strategies and tendencies of progress of aircraft, space, nuclear, chemical, medical and other industry branches, actively consuming the products of titanium and its alloys [51].

Thus, the analysis of the state-of-the-art of production of rod semi-products of up to 50 mm section and products of its alloys in Ukraine showed the dependence of the country on foreign suppliers. The effective method of reducing the cost of rod semi-products of titanium alloys by updating the technology of their producing was grounded. The actuality of producing rods of titanium in Ukraine from sintered titanium semi-products by using methods of powder metallurgy and welding was outlined. The need was defined for the further investigations on determination of weldability of the sintered titanium alloys.

1. Leder, O.O., Kurochkin, D.A., Alabusheva, M.O. (2014) State-of-the-art of titanium market in 2013 and tendencies of its development. In: *Proc. of Int. Conf. on Ti-2014 in CIS* (Nizhny Novgorod, 25–28 May, 2014).
2. Teslevich, S.M., Shvartsman, L.Ya., Zhigunov, N.N. (2007) Main trends in strategy of development of researches on improvement of technology for production of titanium semi-products and products on ZTMK. In: *Proc. of Int. Conf. on Ti-2007 in CIS* (Yalta, 15–18 April, 2007), 25–33.
3. Khorev, A.I. (2011) Fundamental and applied researches on thermal and thermomechanical treatment of titanium alloys for aviation and rocket-space engineering. In: *Proc. of Int. Conf. on Ti-2011 in CIS* (Lvov, 25–28 April, 2011), 314–321.
4. Nochovnaya, N.A., Izotova, A.Yu., Moiseev, N.V. et al. (2011) Formation of structure during isothermal stamping of blade billets from ($\alpha + \beta$) heat-resistant titanium alloys. *Ibid*., 38–40.
5. Ivanova, L.A., Kudryavtsev, A.S., Travin, V.V. (2009) Experience of application of high-strength titanium alloys in power equipment. In: *Proc. of Int. Conf. on Ti-2009 in CIS* (Odessa, 17–20 May, 2009), 46–60.
6. Kalienko, M.S., Savvateeva, G.V., Petren, M.G. (2013) Study of possibility for application of cold deformation and its influence on structure and mechanical properties of TS6 alloy rods. In: *Proc. of Int. Conf. on Ti-2013 in CIS* (Donetsk, 26–29 May, 2013), 189–193.
7. Skvortsova, S.V., Dzunovich, D.A., Shalin, A.V. et al. (2011) Deformability of titanium alloys at normal and elevated temperatures. In: *Proc. of Int. Conf. on Ti-2011 in CIS*, 361–363.
8. Site of production association OSCAR. *http://oscar-tube.com*
9. Galetsky, L.S., Remezova, E.A. (2011) Role of mineral-resource base of titanium of Ukraine in world. In: *Proc. of Int. Conf. on Ti-2011 in CIS*, 22–27.
10. Site of International company ANTARES. *http://www.antares.com.ua/ru/index.html*
11. Galetsky, L.S., Remezova, E.A., Kogon, E.Sh. et al. (2013) New stage in development of mineral-raw materials base and titanium industry of Ukraine. In: *Proc. of Int. Conf. on Ti-2013 in CIS*, 7–11.
12. Ivashchenko, V.I., Chervonny, I.F. (2009) Trends of reduction in prime cost of titanium. In: *Proc. of Int. Conf. on Ti-2009 in CIS*, 87–91.
13. Shiryaev, A.A., Nochovnaya, N.A., Burkhanova, A.A. et al. (2013) Prospects and possibilities in development of scarcely-alloyed beta-titanium alloys. In: *Proc. of Int. Conf. on Ti-2013 in CIS*, 14–18.
14. Kovalenko, T.A., Ovchinnikov, A.V. (2010) Influence of initial structure on fracture mechanisms and mechanical properties of submicrosrystalline titanium. *Novi Materialy i Tekhnol. v Metalurgii ta Mashynobud.*, **1**, 72–80.
15. Kolobov, G.A., Pecheritsa, K.A., Pavlov, V.V. et al. (2013) Secondary raw titanium: Efficiency of application and refining. In: *Proc. of Int. Conf. on Ti-2013 in CIS*, 119–121.
16. Telin, V.V., Ivashchenko, V.I., Chervonny, I.F. et al. (2005) Analysis of tendencies in development of technologies, manufacturing and consumption of titanium. *Titan*, 17(**2**), 62–68.
17. Antashev, V.G., Kashapov, O.S., Pavlova, T.V. et al. (2007) State-of-the-art, problems and prospects in development of heat-resistant titanium alloys for compressor parts. In: *Proc. of Int. Conf. on Ti-2007 in CIS*, 22–24.
18. Galetsky, L.S., Remezova, E.A., Kogon, E.Sh. et al. (2007) Problems and prospects of mineral-raw materials base of titanium in Ukraine. *Ibid*., 34–38.
19. Stavitsky, Yu.L. (2007) Approval of hydrogenated titanium powder of ZTMK production in technological processes of powder metallurgy. *Ibid*., 73–77.
20. Zyakhor, I.V., Kuchuk-Yatsenko, S.I. (2012) Friction welding of PIM heat-resistant steel to steel 40Kh. *The Paton Welding J*., **9**, 2–11.
21. Telin, V.V., Teslevich, S.M., Shvartsman, L.Ya. (2007) Development of novel economical processes and equipment at ZTMK in technological processes of powder metallurgy. In: *Proc. of Int. Conf. on Ti-2007 in CIS*, 60–64.
22. Selcuk, C., Bond, S., Woolin, P. (2010) Joining processes for powder metallurgy parts: A review. *Powder Metallurgy*, 53(**1**), 7–11.
23. Drozdenko, V.A., Pavlov, V.A., Ter-Pogosiants, E.D. et al. (2007) Experience of production of titanium powders, powder titanium items and materials. In: *Proc. of Int. Conf. on Ti-2007 in CIS*, 149–155.
24. Ternovoj, Yu.F., Pashetneva, N.N., Vodennikov, S.A. (2010) *Semi-products and products from pulverized metallic powders*. Zaporozhie: Zaporozh. GIA.
25. Moskvichev, Yu.P., Panin, V.I., Ageev, S.V. (2013) Granular composites and efficiency of their application. In: *Proc. of Int. Conf. on Ti-2007 in CIS*, 41–47.
26. Spektor, V.S., Runova, Yu.E., Zanetdinova, G.T. et al. (2013) Effect of thermohydrogen processing on formation of structure of titanium alloy powder materials. In: *Proc. of Int. Conf. on Ti-2013 in CIS*, 345–347.
27. Ivasishin, O.M., Savvakin, D.G., Matvijchuk, M.V. (2011) Approval of hydrogenated titanium powder of ZTMK production in technological processes of powder metallurgy. In: *Proc. of Int. Conf. on Ti-2011 in CIS*, 322–328.
28. Bykov, I.O., Ovchinnikov, A.V., Davydov, S.I. et al. (2011) Application of hydrogenated titanium with predetermined oxygen content for manufacturing of products by powder metallurgy method. *Teoriya i Praktika Metallurgii*, 80/81(**1/2**), 65–69.
29. Ivasishin, O.M., Markovsky, P.E., Savvakin, D.G. et al. (2013) Effect of structure of structural titanium alloys on change of deformation strengthening in zone of local plastic deformation. In: *Proc. of Int. Conf. on Ti-2013 in CIS*, 287–296.
30. Yakovlev, M.G., Zhuplov, M.V. (2014) Increase in production and quality of processing of gas-turbine engine discs from granular materials due to the application of optimal cutting conditions. In: *Proc. of Int. Sci.-Techn. Conf. on Prospects of Development Trends of Aircraft Engine Building*, Vol. 1, 281–291. St.-Petersburg: Skifiya-Print.
31. Antonyuk, S.L., Korol, V.N., Molyar, A.G. et al. (2004) Fatigue resistance of welded joints of experimental titanium alloy T-110. *The Paton Welding J*., **2**, 25–28.
32. Hamill, J. (2007) Weld techniques give powder metal a different dimension. *Metal Powder Report*, 62(**5**), 22–31.
33. Topolsky, V.F., Akhonin, S.V., Grigorenko, G.M. (2011) New titanium biocompatible alloys in orthopedy and stomatology. In: *Proc. of Int. Conf. on Ti-2011 in CIS*,173–176.

34. Khorev, A.I. (2007) Influence of complex alloying on mechanical properties of welded joints and base metal (α″ + β)- and β-titanium alloys. *Tekhnologiya Mashinostroeniya*, **2**, 29–34.
35. Blashchuk, V.E., Shelenkov, G.M. (2005) Fusion welding of titanium and its alloys (Review). *The Paton Welding J.*, **2**, 35–42.
36. Seliverstov, A.G., Tkachenko, Yu.M., Kulikovsky, R.A. et al. (2013) Effect of friction welding parameters on structure and mechanical properties of joints on titanium alloy VT3-1. *Ibid.*, **1**, 28–33.
37. Kuznetsov, S.V., Leonov, V.P., Mikhajlov, V.I. (2013) Resistance to deformation and fracture of welded joint zones of titanium pseudo-alloys at higher temperature conditions. In: *Proc. of Int. Conf. on Ti-2013 in CIS*, 180–188.
38. Saenko, V.Ya., Polishko, A.A., Ryabinin, V.A. et al. (2014) Electron beam welding of sheet commercial titanium VT1-0, hardened by nitrogen in the process of arc-slag remelting, and properties of produced joints. *The Paton Welding J.*, **11**, 46–49.
39. Markashova, L.I., Akhonin, S.V., Grigorenko, G.M. et al. (2012) Structure and properties of welded joints on titanium alloys containing silicon additions. *Ibid.*, **11**, 6–15.
40. Shelyagin, V.D., Khaskin, V.Yu., Akhonin, S.V. et al. (2012) Peculiarities of laser-arc welding of titanium alloys. *Ibid.*, **12**, 32–36.
41. Shabdinov, M.L., Izmailova, G.M., Dzhemilov, E.Sh. (2011) Advanced aspects in application of laser thermal technology for welding and cutting of titanium alloys. *Visnyk Khmelnyts. NU*, **5**, 31–34.
42. Taranova, T.G., Grigorenko, G.M., Akhonin, S.V. et al. (2013) Peculiarities of formation of structural and chemical heterogeneity in pressure-welded joints of experimental titanium alloys of Ti–Si–X system. In: *Proc. of Int. Conf. on Ti-2013 in CIS*, 214–220.
43. Seliverstov, A.G., Petrik, I.A., Tkachenko, Yu.M. et al. (2011) Examination of mechanical properties of VT3-1 alloy friction-welded joints. *Kompres. i Energet. Mashinostroenie*, 26(**4**), 41–44.
44. Petrik, I.A., Seliverstov, A.G., Ovchinnikov, A.V. (2014) Increase of properties of titanium alloy welded joints of rotor parts. *Aviats.-Kosmich. Tekhnika i Tekhnologiya*, **8**, 25–29.
45. Blashchuk, V.E. (2004) Titanium: Alloys, welding, application. *The Paton Welding J.*, **3**, 30–37.
46. Golub, T.V., Kashevskaya, O.N., Zamkov, V.N. et al. (1990) Density of weld metal produced by different methods of welding on VT1-0 commercial titanium. *Avtomatich. Svarka*, **11**, 31–33.
47. Edmilson Otoni Correa (2011) Weldability of iron based powder metal alloys using pulsed GTAW process, arc welding. *http*://www.intechopen.com/books/arc-welding/weldabilityof-iron-based-powder-metal-alloys-using-pulsed
48. Pichugin, A.T., Fedirko, V.N., Lukianenko, A.G. et al. (2007) Influence of annealing factors on fatigue service life of welded joints of VT1-0 and PT7M titanium alloys. In: *Proc. of Int. Conf. on Ti-2007 in CIS*, 431–440.
49. Savvakin, D.G., Matvijchuk, M.V., Gumenyak, N.M. et al. (2011) Prospects of application of alloys produced by hybrid technology for medicine demand. In: *Proc. of Int. Conf. on Ti-2011 in CIS*, 183–186.
50. Talas, S., Dogan, M., Cakmakkaya, M. et al. (2014) The effect of voltage on the arc stud welding of microwave sintered Fe + Al powder mixture. *Materials Research*, 17(**3**).
51. Khrushchov, D.P., Lobasov, A.P., Remezova, E.A. et al. (2013) Information-prediction structural-lithologic numerical models of titanium-zirconium gravel deposits. In: *Proc. of Int. Conf. on Ti-2013 in CIS*, 83–91.

Received 15.12.2014

MULTILAYER STRUCTURES OF INCREASED CRACK RESISTANCE FORMED BY EXPLOSION WELDING

R.P. DIDYK and **V.A. KOZECHKO**
National Mining University
19 Karl Marks Ave., 49027, Dnepropetrovsk, Ukraine. E-mail: didyk@nmu.org.ua

Application of laminar structural materials is challenging in the solution of problem of increasing the reliability and life of heavy-loaded machines and equipment. The work deals with the possibility of application of explosion welding for producing myltilayer structures with a high reserve of crack resistance, achieved by control of composition and properties of the joining zone by adding barrier layers. As a barrier layer it was suggested to apply metals, not interacting in solid state or those, forming interstitial solid solutions (vanadium, copper, nickel). The analysis of test results of laminar specimens for low-cycle fatigue under conditions of pulsaring tensile cycle allowed establishing the kinetics of fatigue fracture, depending on structural state of interlayer interface of metal composition. It is shown that adding of an intermediate metal layer, characterized by greatly different properties and increased ductility, to the structure of composition leads to increase in crack resistance of material as compared to the similar equivalent. 5 Ref., 3 Figures.

Keywords: *explosion welding, laminar composite materials, multilayer structures, crack resistance of compositions, barrier layers, copper, zone of plastic deformation*

One of the main ways of solution of problems of increasing the reliability and service life of structures of machine parts, operating under severe conditions of loading, can be the development of laminar composite materials, allowing formation of structure and interfaces of layers in accordance with the conditions of the parts service.

Manufacture of laminar composite materials is realized by hot and cold plastic deformation of semi-products using rolling or pressing, thermodiffusion welding, casting, different types of deposition of one or several components on the surface or by combination of these methods. However, the significant drawbacks of the abovementioned methods are their selectivity, associated with a problem of producing a strong physical binding of metals and alloys, greatly differed by a complex of physical-mechanical and chemical characteristics [1]. In this connection, the actuality of technological processes based on feasibility of producing strong metallic compositions almost of any combinations and control of structure and properties of the joining interface does not raise any doubts. Explosion welding can be referred to these processes [2].

The explosion welding has a number of peculiarities, which are due to high intensity of plastic yielding and short-time action of high gradients of pressures and temperatures in near-contact layers of the collided plates. Under the specific conditions of explosion welding as one of the most profitable forms of conversion of kinetic energy of collided bodies into the energy of plastic deformation is the process of wave formation, which greatly influences the structure of contact zone and, respectively, the joint properties [3]. It should be noted that the unique potentialities of the explosion welding were mainly realized as effective means in the technology of manufacture of bimetal products to save the deficit non-ferrous metals and alloys.

In the present work the feasibility of application of explosion welding for the producing multilayer structures, characterized by high reserve of crack resistance, are considered for the first time.

During explosion welding of multilayer compositions both the successive joining of plates and also simultaneous joining of the whole packet for one operation are possible for producing the flat multilayer structures and also spatial ones with symmetric and conical symmetry. The simultaneous multilayer joining at a parallel scheme of orientation of elements being welded found the widest spreading. In this case, firstly the collision of upper plate with an intermediate one is occurred and then the intermediate plate acquires the speed of the upper plate and the combined flying of two plates is realized, and so on.

However, in explosion welding of multisheet compositions the problems are encountered, connected with the change of the process parameters: decrease in angle of collision, decrease in pressure during transition from upper to lower sheet, that

in its turn causes the change of layers joining interface: from continuous layer of melts along the entire boundary of contacting to the sinusoidal boundary with the presence of eddy zones or rectilinear boundary without formation of regions of cast structure and, consequently, to the change of adhesion strength of layers. This drawback can be prevented by applying the guiding element of a proper mass. In this case the angle of collision is preset by guiding plate, the pulse of which is not almost changed during interaction with the first sheet, the flying speed of which is equal also to the speed of the guiding plate, that is repeated also for next sheets almost without changing the parameters of collision, i.e. explosion technology allows producing the quality joints both of double-layer and also multilayer compositions (Figure 1).

Figure 1. Explosion-welded two- and three-layer pipes

Development of new laminar compositions with a preset level of properties and rational structure of the material requires the well-grounded selection of components and technology of their manufacture. The selection of material of layers is realized coming from the conditions of the product service, as well as from chemical (thermodynamic and kinetic) and mechanical compatibility of components. The thermodynamically compatible components are those, which are not dissolved in each other and do not form chemical compounds of metals (for example, Mo–Cu, Nb–Cu). The majority of thermodynamically compatible components under definite temperature-time conditions can be compatible kinetically (metastable equilibrium) and provide the reliable operation of the structure. Mechanical compatibility, consisting in conformity of elastic constants, coefficients of thermal expansion and values of ductility of composing materials, predetermine the stress-strain state of the laminar materials.

The serviceability of composite products is determined by the joining zone, non-homogeneous in composition, the structure and properties of which are formed during the explosion welding process by melting the near-surface layers, their mixing and diffusion of the elements. In the zone of joining the producing of transition layers with lower or increased microhardness, as compared to initial materials, formation of brittle intermetallics and so on are possible. Depending on this, the nature of fracture of transition zone is changed: from tough-plastic to cleavage with regions of surface of tough fracture or brittle cleavage [3]. If follows from the above-said that it is necessary to produce the combination of strength of material of transition layers at its rather high ductility that can be provided by technological parameters of the explosion welding.

During development of crack-resistant laminar compositions the feasibility of control of composition and properties of the joining zone is considered by introducing of barrier layers. The application of these layers in development of laminar materials for chemically-interacting components is a quite well-known method [4, 5]. The barrier layer plays a role of inert interlayer, not allowing interaction between the layers being welded. The task of the investigation was the evaluation of possibility of using tough interlayer as a barrier layer, preventing the crack developing, study of crack interaction with interlayer and creation of a rational structure of composite material, capable to reduce the rate of crack propagation, to change its direction and arrest. As a barrier layer it was suggested to use metals, not interacting in solid state or forming the interstitial solid solutions (vanadium, copper, nickel). The most challenging material is copper, which eliminates the possibility of formation of intermetallic and carbide compounds.

To study the crack resistance of laminar composite materials, produced by explosion welding, the investigations of composites on steel 45 base: steel–steel bimetal and steel–copper–steel trimetal were carried out for multi-cyclic fatigue in machine UPM-2000 by scheme of pulsating tension with maximum force of cycle of 250 MPa, coefficient of cycle asymmetry 0.2 and loading frequency of 400 cycle/min. Type and shape of specimen are given in Figure 2.

The tests were carried out at constant loading, i.e. with fatigue crack developing the stresses were increasing in the rest part of the section. The process of fatigue crack growth was investi-

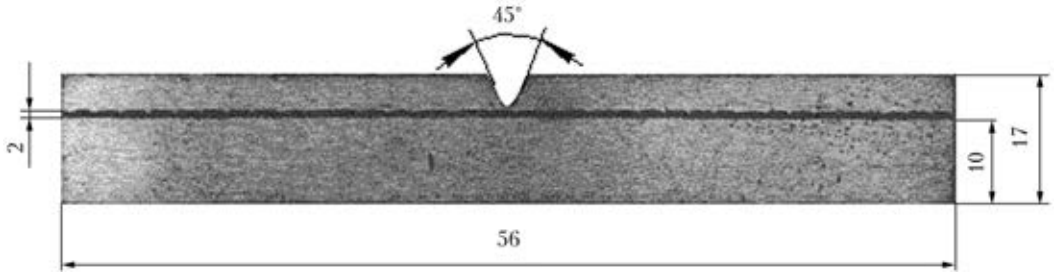

Figure 2. Appearance of trimetal specimen of steel–copper–steel for low-cycle fatigue test

gated on flat rectilinear specimens with a side notch. The presence of sharp side notch predetermined the initiation and propagation of crack in the transverse direction. The notch was made in steel 45, the notch bottom in bimetals was located at the distance of 3 mm from the interface of layers joining, in trimetals it was located at 2.5 mm distance. Under the same conditions not less than 6 specimens were tested. Face surfaces of specimens were polished from the apex of initiating notch into the direction of the future fatigue crack (roughness in the places of polishing was 0.05–0.08 μm), and then the measuring scale with 1 mm factor was applied on the way of crack growth.

Observation of the fatigue crack growth was made by the type MVT microscope, mounted on a special bracket on the machine frame. The crack length obtained for definite number of cycles of specimen loading was measured after the machine stop, moving the microscope objective in horizontal and vertical by means of micrometric screws. The measurement of crack length was made by the microscope limb at 0.01 mm accuracy.

The analysis of obtained results showed that the initial fatigue crack in steel 45 was initiated during $9 \cdot 10^{-4}$ cycles. The period of fatigue crack propagation from the steel–steel interface in bimetal and steel–copper (interface *A*) in trimetal was similar in principle and amounted to 140,700 cycles. After transition of the fatigue crack through the interface into the second layer in bimetal the final fracture of specimen quickly occurred, and the trimetal withstood even next 122,262 cycles, 18,962 cycles from which the crack was simply propagating in the copper interlayer and 103,300 cycles was required for delamination at the copper–steel interface (interface *B*) and for initiation of the fatigue crack in the second steel layer. The fatigue life of three-layer specimens was 348,000 cycles, and two-layer ones — 237,700 cycles.

Results of experiments, given in Figure 3, allowed establishing the kinetics of growth of the fatigue cracks. The obtained dependence of fatigue crack length on number of loading cycles shows that the change in rate of crack propagation in bimetal up to the joining interface coincides with the change in rate in trimetal up to the steel–copper interface. In bimetal, in which both the base metal and cladding layer are made of the same material, the strong joining of layers, excluding the possibility of delamination at the interface, predetermined the crack transition from one layer into another one at some delay. At the same time, in the three-layer composition the rate of fatigue crack, transferred into copper interlayer, drops immediately. The rate of crack, reached to the interlayer middle, is decreased by 40 % as compared with the crack rate at the steel–copper interface. At crack approaching the copper–steel interface its rate is continuously dropped, the crack is arrested and corresponds to the beginning of the crack growth in the base steel layer.

Having transferred into copper interlayer the crack changes the direction of its propagation, deviates from the plane of effect of maximum tensile stresses and develops in the direction of effect of maximum tangential stresses. Change in direction of the fatigue crack propagation in copper interlayer was caused by change in type of the fatigue crack formation. Copper is the metal with high energy of packing defects, in which transverse sliding is provided due to high capability of sliding of screw dislocations from one crystallographic plane into another one. In the copper interlayer a large number of microcracks is observed at cyclic loading, crack branching is occurred, most of which interrupt their growth, however, a part of microcracks continues their development with joining between themselves and forming an avalanche macrocrack.

With approach to the copper–steel interface, the fatigue crack is deviated from the initial direction of movement and propagated into both sides along the interface. In this case the growth of the avalanche crack is interrupted, and the crack itself is remained in the tough interlayer (horizontal area of curve *2* in Figure 3). Delay in crack movement during transition from copper

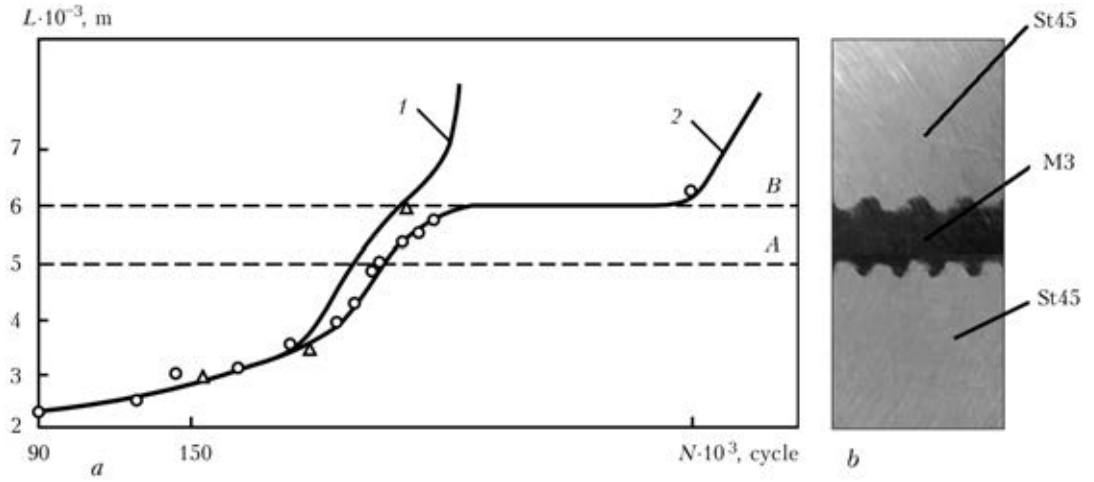

Figure 3. Kinetics of growth of fatigue crack in laminar specimens of steel 45 base in testing under conditions of pulsating tension (*a*): *1* — steel; *2* — steel–copper–steel; *A* — interface in steel–steel bimetal; *B* — copper interlayer in steel–copper–steel trimetal; *b* — appearance of interface of steel 45– copper M3–steel 45 joining

layer into steel one is connected with the crack movement along copper–steel interface and with mechanism of its initiation in the steel layer. Copper–steel interface became a barrier, which arrested the growth of fatigue crack and increased significantly the fatigue life of the metal composition. The process of fracture of the second layer of steel is occurred similarly to the fracture in the first steel layer.

Physical nature of metal fracture at cyclic loading is connected with accumulated plastic deformation [5]. The formation of zones of the local plastic deformation at the notch apex during testing of specimens under conditions of pulsating tension was studied by the visual observation of polished surface. The zone of deformation and fracture surface were investigated additionally by using the optic microscope.

Thus, the following regularities of formation of zones of local plastic deformation and crack movement were established. During the process of loading at notch apex under 45° angle relative to axis of load applying the two symmetric zones of local plastic deformation are formed in the form of pellets, representing the concentration of front of plastic deformation, the sizes of which are increased with load growth. Developing of these zones up to the moment of reaching the value of loading, close to maximum one, is occurred symmetrically, then the growth of one of them is delayed, while that of the second one is increased intensively and the avalanche crack is beginning to be formed in it. Local plastic deformation during explosion welding is developed in surface layers with the formation of hump of deformation and depression. Crack initiation is observed at the specimen surface near the notch edge within the region of maximum metal yielding (transition from deformation hump to depression). Fracture has a discrete nature and represents a joining of pores and tears in the region of the local plastic deformations. Trajectory of crack movement has an intricate configuration and depends on number and properties of the layers. At transition of crack from the material with close values of elasticity modulus into another material, its crossing through interface is observed without changing the propagation direction. Transition of crack from the material with lower modulus of elasticity to material with the higher modulus is difficult, the long time crack movement is observed along the interface. Adding of intermediate metal layer, characterized by greatly different physical-mechanical properties and increased ductility, to the composition structure leads to the increase of crack resistance of material as compared to the similar equivalent.

1. Chepurko, M.I., Reznikov, E.A., Bujnovsky, A.M. et al. (1974) *Bimetallic pipes*. Moscow: Metallurgizdat.
2. Didyk, R.P. (2006) High-energy treatment of materials — Technology of 21st century. *Tyazh. Mashinostroenie*, 17–20.
3. Mali, V.I. (2010) *Structural features of wave formation in explosive welding*, 42–43. Moscow.
4. Bataev, I.A., Bataev, A.A., Mali V.I. (2010) Increase in impact strength of lamellar composites, produced by explosion welding method of steel plates. In: *Zababakhin. Sci. Lectures* (Snezhinsk), 24–28.
5. Kovalevsky, V.N. (1999) Assessment of working capacity of lamellar materials produced by explosion welding. In: *Welding and related technologies*: Transact., Issue 2.

Received 02.09.2014

WELDING UNITS A1569M(M1) FOR AUTOMATIC SUBMERGED-ARC WELDING OF CIRCUMFERENTIAL ROTATABLE JOINTS IN DEEP GROOVE

In April 2014, new welding (surfacing) units A1569M and 1569M1, were implemented at OJSC «Turboatom» (Kharkov) by the specialists of the PWI Experimental Design-Technological Bureau (Kiev).

The equipment is designed for multi-pass automatic and semi-automatic submerged-arc welding of circumferential welds of turbine rotors in deep groove as well as surfacing of outer surfaces of cylindrical products.

A1569M unit with SU415 control system is installed at «Shumakher» shop bench. Welding of rotors of steam turbines and water turbine shafts with groove achieving 400 mm is carried out at the bench. It can be also used for surfacing of blade journals of guide vanes and other cylindrical surfaces of 250–1500 mm diameter.

Two-head unit A1569M1 with SU410 control system is installed at the shop portal. Welding of rotors of stream turbines of 1000 MW power and more, water turbine shafts as well as surfacing of bodies of water turbine wheels and surfaces on water turbine shafts is carried out on the portal unit. Maximum length of parts makes 10 m, outer diameter is 3450 mm and groove depth achieves 400 mm.

Welding is carried out at strong inductive heating of part up to 350 °C. Welding equipment was developed for operation in high-temperature zone up to 120 °C. Application of water-cooled shield allowed reducing temperature over shield to 65 °C.

The works on project were carried out by two departments, namely «Welding equipment», and «Control systems», based on performance specification of «Turboatom». Spare parts of foreign and domestic producers were used in the equipment. The units are carried out in to versions: single A1569M and coupled A1569M1.

Both units consist of:

- mechanisms of horizontal and vertical movement, based on rack-and-gear drive;
- mechanism of wire feeding with changeable feeding gear rollers for different wire diameters;
- mechanism of nozzle turn, which includes overtime clutch in its structure for prevention of nozzle failure due to groove wall being welded.

All the mechanisms are actuated with the help of the NORD worm gear gear-motors (German production), selected and equipped with additional functions based on equipment service peculiarities.

There is a system for flux feeding with manual sliding shutter. The units are delivered with changeable nozzles, current-conducting nozzles and spirals for different groove depth and various diameter of welding wire.

Structure of A1569M1 differs from A1569M by the fact that coupled unit has two heads installed at one horizontal beam. Each of the heads has own movement mechanism. Coupled variant is designed for increase of

efficiency by means of welding of two rotatable joints, simultaneously.

Electric equipment of control system (SU415) of A1569M unit is located in separate control cabinet standing close to machine. Controls are included into main stationary panel, located at cabinet door and in manual panel of the unit.

Electric equipment of control system (SU410) of A1569M1 unit is located in separate control cabinet standing far from the unit. Controls are in two main panels, located close to the unit as well as in manual panels of the unit. SU410 system provides for complex regulation of all equipment, namely welding unit, drives of portal carrier movement as well as control of power drive (37 kW) of part rotation bench.

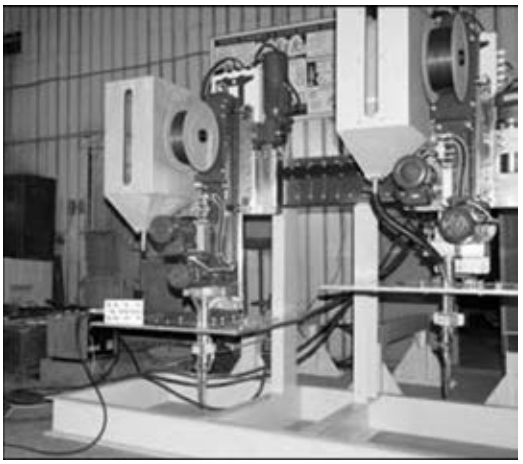

The control systems also carry out remote switching and regulation of voltage of welding current sources of VDU-1250 type.

The control system provides for entering of all necessary process parameters, indication of measured welding parameters, displaying of emergency and technological messages as well as sound and light alarm at the emergency situations.

There are three possible modes of electric equipment operation, namely Setting, Semi-Automatic, and Automatic. Setting mode is designed for verification of operation of all mechanisms of the unit and performance of setting movements before welding. Semi-automatic mode is designed for regulation of welding process by manual (by operator decision) turning of the nozzle for beads positioning and lifting-up of the unit to further weld layer. Automatic mode is designed for regulation of technological process of multi-pass welding with automatic positioning of beads and lifting-up of the unit to next layer.

Specific attention during system development was given to ergonomics and ease of operator work. Operator enters the process parameters in real units. The system automatically maintains set linear speed of welding at part diameter change. Control of process as well as diagnostics of system faults with displaying of alarm messages is provided.

At present the equipment is operated in three-shift mode. It is proved to be safe and reliable in course of operation. Process of welding (surfacing) of some parts is carried out continuously during 3 or more days.

In course of last months number of standard parts — rotors of low and average pressure as well as water turbine wheels were welded and surfaced using our equipment.

Specification

Groove depth, mm	not more 400
Groove width, mm	24–36
Welding current, A (100 % duty cycle)	500
Welding wire diameter, mm	1.2–3.2
Wire feed rate, m/h	30–350
Value of head lifting-up	not more 500
Displacement of head along part axis, mm	not more ±75 (A1569M); ±170 (A1569M1)
Rate of head lifting-up, m/min:	
operating	0.05
cruising	1.5
Rate of displacement along part axis, m/min:	
operating	0.05
cruising	1.5
Groove filling by beads (in automatic mode), pcs	1–3
Temperature of preheating of part to be welded (surfaced), °C	not more 350
Voltage and frequency of power main	3 × 380 V, 50 Hz

V.S. Romanyuk, S.I. Veliky, A.V. Semenenko, A.K. Polishchuk, M.I. Dubovoj, PWI EDTB

PATON PUBLISHING HOUSE

www.patonpublishinghouse.com

SUBSCRIPTION

«The Paton Welding Journal» is Published Monthly Since 2000 in English, ISSN 0957-798X.

«Avtomaticheskaya Svarka» Journal (Automatic Welding) is Published Monthly Since 1948 in Russian, ISSN 005-111X.

«The Paton Welding Journal» is Cover-to-Cover Translation of Avtomaticheskaya Svarka» Journal into English.

If You are interested in making subscription directly via Editorial Board, fill, please, the coupon and send application by Fax or E-mail.

The cost of annual subscription via Editorial Board is $348 for «The Paton Welding Journal» and $180 for «Avtomaticheskaya Svarka» Journal.

«The Paton Welding Journal» can be also subscribed worldwide from catalogues subscription agency EBSO.

SUBSCRIPTION COUPON

Address for journal delivery _____

Term of subscription since _____ **20** **till** **20**

Name, initials _____

Affiliation _____

Position _____

Tel., Fax, E-mail _____

We offer the subscription all issues of the Journal in pdf format, starting from 2009.

The archives for 2009–2012 are free of charge on *www.patonpublishinghouse.com* site.

ADVERTISEMENT

in «Avtomaticheskaya Svarka» and «The Paton Welding Journal»

External cover, fully-colored:
First page of cover (190×190 mm) — $700
Second page of cover (200×290 mm) — $550
Third page of cover (200×290 mm) — $500
Fourth page of cover (200×290 mm) — $600

Internal cover, fully-colored:
First/second/third/fourth page of cover (200×290 mm) — $400

Internal insert:
Fully-colored (200×290 mm) — $340
Fully-colored (double page A3) (400×290 mm) — $500

- Article in the form of advertising is 50 % of the cost of advertising area
- When the sum of advertising contracts exceeds $1001, a flexible system of discounts is envisaged

Size of journal after cutting is 200×290 mm

Editorial Board of Journal «Avtomaticheskaya Svarka» and «The Paton Welding Journal»
E.O. Paton Electric Welding Institute of the NAS of Ukraine
International Association «Welding»
11, Bozhenko Str., 03680, Kyiv, Ukraine
Tel.: (38044) 200 60 16, 200 82 77; Fax: (38044) 200 82 77, 200 81 45
E-mail: journal@paton.kiev.ua; www.patonpublishinghouse.com